Redox Chemistry Of Iron In Multiphase Atmosphere

Thesis by Simo Olavi Pehkonen

In Partial Fulfillment of the Requirements

for the Degree of

Doctor of Philosophy

California Institute of Technology

Pasadena, California

1995

(Defended September 13, 1994)

Acknowledgments

I would like to thank all the people who have provided help and friendship to me over the years here at Caltech. First of all, I thank my parents, who have supported my study far away from home in Finland. I am extremely grateful to my advisor, Michael Hoffmann, for his support and help and for encouraging me to carry out independent research throughout the four years here at Caltech. I am also very grateful to Yigal Erel, who helped me extensively at the beginning of my study and taught me the necessary clean-lab techniques to carry out trace metal research. I also want to thank Prof. Jim Morgan for several enlightening discussions about various aspects of aquatic chemistry.

I am also grateful to Elaine Granger, Linda Scott, Rayma Harrison, Joe Fontana, Jennifer Packman and Dian Buchness who have helped me with a variety of problems during my study.

I also want to thank a number of fellow students who have provided scientific ideas and insight and also personal friendship. They include Ronald Siefert, Amy Hoffman, Patrick Lang, Anastassia Kotronarou, Ralf Hochemer, Inez Hua, Scot Martin, Ken Klewicki, Wonyong Choi and Axel Kratel.

Lastly, I am most grateful to my wife, Laura, for the love and support during my study here at Caltech. She has been very helpful and understanding during the many weekends and nights that I have spent working in the laboratory.

Abstract

Iron redox chemistry was investigated in fog and stratus clouds in urban and remote locations in California, Delaware and New York. It was observed that iron(II) contributed from 20 to 70 % of the total iron in the samples and that iron(III) was bound mostly as oxalato complexes in most samples. The iron(II) oxidation state seemed to correlate best with organic compounds, i.e., carboxylic acids and TOC (total organic carbon), indicating the important role of organic compounds to the redox state of iron.

The applicability of a new spectrophotometric technique for measuring simultaneously iron(II) and iron(III) in atmospheric water samples real time in the field was studied. DPKBH (Di-2-pyridyl ketone benzoylhydrazone) forms complexes with both iron(II) and iron(III) with an absorption maximum at 375 nm for both iron(II)-DPKBH and iron(III)-DPKBH and an absorption maximum at 660 nm for iron(II)-DPKBH. The detection limit of this method is 4 nM of iron with chloroform-water extraction and 0.1 μM without the extraction. DPKBH forms bis complexes with iron and binds via the oxygen and two nitrogen atoms of the enol form of DPKBH as indicated by a FTIR study of the iron(III)-DPKBH complex.

In addition to field observations, complementary laboratory photoreduction experiments were carried out with a variety of iron oxides and a variety of important atmospheric organic compounds such as oxalate, formate, acetate and formaldehyde. Photoreduction of am-$Fe(OH)_3$ with formate yielded the highest rates of photoreduction. Stability of the iron oxide and the strength of Fe-O bonds in the lattice played a more important role in the rate of iron photoreduction than the reactive surface area. Hydrogen peroxide was produced in the case of oxalate as the electron donor. Additional iron photoreduction experiments were carried out with halogenated acetic acids (the end

products of tropospheric HCFC degradation) as electron donors and it was observed that monohalo acetic acids reduce iron oxides faster and get photooxidized faster compared to acetic acid.

Table of Contents

Chapter 1

Prologue

Iron derives its name from the Anglo Saxons. The atomic symbol for iron is Fe, this and words such as "ferrous" and "ferric" are derived from the latin ferrum, iron. Iron is the most important metal of human technology. We use it to build our civilization and produce more of it than all other metals combined.

Iron plays an important role in the chemistry of living organisms being found at the active center of many biological molecules. Iron is also known to catalyze a variety of important reactions in the hydrosphere.

Iron makes up 1.5% of the lithosphere and is the eighth most abundant element in it. In 1983, 1.1 x 10^{13} moles of atoms of iron were consumed by the world manufacturing industries; only hydrogen, carbon, oxygen and calcium were used in greater quantities.

The two most common oxidation states of iron found in natural waters are +2 and +3. The redox potential of transformation from one oxidation to the other is such that iron can oxidize and reduce a variety of other species that are in contact with it. For example iron(III) can oxidize S(IV) to S(VI) in water to make sulfuric acid, a major constituent of acid precipitation. Because of its importance in reactions such as the above, it is important to know what controls the redox state of iron in natural waters.

Very little is known about the speciation of iron in natural waters. Most measurements of iron have been the total concentrations in rain, fog, in lake and ocean water. Behra and Sigg showed that iron(II) can be present at appreciable concentrations in fogwater. Although their results indicated that sulfur was important in determining the redox state of iron, the overall redox behavior of iron seems to involve a variety of other constituents. The overall goal of this thesis is to explore the factors that control the redox

state of iron in atmospheric water and to study and quantify the effects that iron has on other important atmospheric constituents.

This thesis is organized into eight chapters. This chapter introduces the importance of iron in nature and in particular in natural waters. The second chapter provides background information regarding the known redox chemistry of iron, measurements of total iron in a variety of natural water systems and the possible role of iron as an important nutrient of the phytoplankton in the open oceans. The third chapter describes an iron chelating agent, DPKBH, which has been used to measure iron(II) and iron(III) in atmospheric water. The fourth chapter details the determination of stability constants and structure of iron(II)-DPKBH and iron(III)-DPKBH complexes. The fifth chapter describes the field observations of iron redox state in fog and cloudwater. The sixth chapter details the investigation of the rates and mechanism of photoreduction of iron oxyhydroxides in the presence of important atmospheric organic compounds. The seventh chapter describes the studies of the rates and mechanism of photoreduction of iron oxyhydroxides and the concomitant photooxidation of halogenated acetic acids. The eighth chapter summarizes the results of this research.

Chapter 2

Background

Iron is prevalent in the global environment. It is the fourth most abundant element in the earth's crust with an atomic weight of 55.85 (5.8% ^{54}Fe + 91.7% ^{56}Fe + 2.2% ^{57}Fe + 0.3% ^{58}Fe). In rocks and soils, iron is found in a wide variety of minerals and clays as Fe(II) or Fe(III), and because of its abundance it is often found as an impurity in many materials. Iron is also ubiquitous in living systems. It is at the active center of proteins responsible for O_2 and electron transport and it is a critical component of metalloenzymes such as oxidases, reductases, dehydrogenases, deoxygenases and dehydrases (1). Recent research by Martin and co-workers (2, 3) has shown that Fe can be a growth-limiting nutrient for phytoplankton in the open ocean.

Iron is found at variable levels in the atmosphere in both the aqueous-phase (i.e., clouds and rain) and the solid phase (i.e., aerosol). Ferric iron has been shown by a number of investigators (4, 5) to be an extremely important catalyst for the autoxidation of SO_2 and concomitant generation of acidity in atmospheric water. In the following sections I will review aspects of the atmospheric chemistry of iron and examine some important reasons for acquiring a better understanding of atmospheric iron chemistry.

Occurrence of Iron in Aerosol, Cloud, Fog and Rain

1. Aerosol Concentrations of Iron Urban, Non-Urban and Remote

Iron constitutes approximately 4.1% of the earth's crust and 3.2% of soil (6). The major source of iron-containing aerosol is from windblown dust with secondary sources coming from natural emissions (e.g., volcanic dust) and anthropogenic emissions (e.g., coal-fired power plants). The iron content of fly ash can be as high as 2-15% by weight (7-9) with higher concentrations near the particle surfaces.

Representative values of total iron in aerosol samples collected in remote rural and urban locations are summarized in Table 1. Aerosol concentrations of Fe range from 0.21 ng m^{-3} on American Somoa to 4200 ng m^{-3} in Boston. In marine environments, Fe concentrations range from 0.21 ng m^{-3} in the tropical South Pacific to 50 ng m^{-3} in the tropical North Pacific, and from 94 ng m^{-3} in the Atlantic to 740 ng m^{-3} in the North Sea. In rural areas, Fe concentrations range from 32 ng m^{-3} in the Sierra Nevada to 360 ng m^{-3} in Glacier National Park; while in urban locations concentrations can range as high as 4200 ng m^{-3}.

Location	$[Fe]_T$ (ng m^{-3})	Reference
Arctic, Greenland	2.7-53.1	10
Dye3, Greenland	5.1+-2.6	11
Ny-Alesund, Norway	2-65	12
Tropospheric Arctic Haze	45 +- 37	13
Stratospheric Arctic Haze	17 +- 4	13
Marine Boundary Layer Arctic Haze	19 +- 5	13
Antarctic	0.12-0.92	14
Antarctic, South Pole	0.62	14
Enewetak Atoll, N. Pacific (Mar.-Jun.)	50.0	15
Enewetak Atoll, N. Pacific (Jul.-Feb.)	2.0	15
Bermuda, Open Atlantic	94-100	16
Bermuda, Open Atlantic	109	17
American Somoa, S. Pacific	0.21	18

Table 1a: Total aerosol iron concentrations in remote locations.

Location	$[Fe]_T$ (ng m^{-3})	Reference
Wraymires, UK	118	19
Jungfrau, Switzerland	35	19
Great Smoky Mtns (fine)	28	20
Great Smoky Mtns (coarse)	118	20
Northwestern Mediterranean	114	21
North Sea	300-700	22
Great Smoky Mountains	250	11
Olympic National Park, WA	310	11
Glacier National Park, MT	360	11
Sequoia National Park, CA	6-235	23
Emerald Lake, Sierra Nev.	32	23
Shenandoah Valley, VA	53	24

Table 1b: Total aerosol iron concentrations in non-urban locations.

Location	$[Fe]_T$ (ng m^{-3})	Reference
Swansea, UK	1152	19
UK Urban Average	834	19
Los Angeles, CA	2050	25
Pasadena, CA	1770	25
San Francisco, CA	610-3900	26
Portland, OR	3300	27
Houston, TX (fine)	170	28
Houston, TX (coarse)	730	28
Chicago, IL	686	29
Venice, Italy	790-2620	30
Boston, MA	260-4200	31

Table 1c: Total aerosol iron concentrations in urban locations.

Location	$[Fe]_T$ (μM)	Reference
Petten, Holland	10.7	32
Sotra, Norway	1.9	32
Flamborough, UK	17.7	32
Collfirth, UK	3.0	32
Northern Minnesota	0.7-3.0	33
Big Bear, CA	0.6	34
Los Angeles, CA	0.46	34
Mt. Wilson, CA	0.17	34
Holland	5.9-129	35
England	2.3-56	35
Sudbury, Canada	0.1-143	36
Zürich, Switzerland	0.3-2.0	37
Leeds, UK	0.3-23	38

Table 2a: Typical concentrations of total iron in rain in continental locations.

Location	$[Fe]_T$ (nM)	Reference
Open Atlantic, Bermuda	52-86	39
Coastal Atlantic, DE	276	40
American Somoa	16-25	18
Enewetak Atoll	6	41
Indian Ocean	297-1558	42

Table 2b: Typical concentrations of total iron in rain in oceanic locations.

Location	$[Fe]_T$ (μM)	Reference
Los Angeles, CA	25.8	43
Santa Barbara, CA	0.4	44
San Nicholas Is., Coastal Pacific	7.7	44
San Francisco, CA	2.8	44
Lennox, CA	6.3-424	45
Bakersfield, CA	4.3-115	45
Zürich, Switzerland	0.3-91	46
Dübendorf, Switzerland	50-200	47
San Gabriel Mts., CA	3.5-123	48
Po Valley, Italy	1.0-29	49

Table 3: Typical concentrations of total iron in clouds and fogs.

Iron-containing aerosols have been found to be transported over great distances. For example dust from central China is transported eastward across the Pacific (50-53), while Saharan dust (54) is transported westward across the Atlantic (54, 55). Schütz et al. (56) estimated the annual mass transport of particles in the Saharan dust plumes to be 260 Tg yr^{-1}; of this amount, 80% is deposited in the Atlantic Ocean and the remaining 50 Tg yr^{-1} reaches the Caribbean. Chester and Stoner (57) reported that soil-sized particulates collected on a ship cruise from England to Japan had iron concentrations ranging from 3.0 to 7.3 % by weight.

2. Cloud-, Fog-, and Rainwater Concentrations of Iron

Typical concentrations of total iron in rainwater vary from 0.016 μM in American Somoa (18) to 143 μM in the Sudbury Region of Canada (Table 2); while in fogwater (Table 3) the reported concentrations of total iron vary from 0.3 μM in rural Switzerland to 424 μM in the Los Angeles area. Using the concentrations of Fe_T given in Table Ic for urban aerosol and assuming that the aerosol containing iron is activated as cloud condensation nuclei in a fog/cloud with a liquid water content of 0.2 g m^{-3}, we can predict the cloud-/fogwater concentrations in urban areas to have variations in $[Fe]_T$ from 61 μM in Chicago to 376 μM in Boston. Similar calculations carried out on the aerosol data in Table 1b show that the rural cloud-/fogwater concentrations should range from 0.57 μM to 32.2 μM while the remote cloud-/fogwater concentrations (Table 1a) should vary from 19 nM to in American Somoa to 9.0 μM in Bermuda. Rainwater concentrations of Fe_T in American Somoa have been reported to vary from 16-25 nM (18), while Fe_T concentrations between 52 and 86 nM have been reported by Church et al. (40) for rainwater collected in Bermuda. The rainwater concentrations in Bermuda are substantially less than those predicted by the complete scavenging of the measured aerosol. This may be due to a complex meteorology in the vicinity of Bermuda preceding and during rainfall events.

The Possible Role of Iron In Global Climate Change

Global climate change due to the rise in "Greenhouse" gases such as CO_2, CH_4, $C_2Cl_xF_y$, etc. and depletion of the stratospheric ozone layer are subjects of current global concern and substantial scientific interest. The rise in CO_2 and other "Greenhouse" gases coupled with an enhanced flux of sunlight due to depletion of stratospheric ozone is predicted to result in a corresponding rise in the mean global temperature by several degrees. The extent of global warming and its consequences have been hotly debated (58-60). Some investigators (61) have proposed biological feedback mechanisms involving enhanced production of dimethyl sulfide (DMS) by oceanic phytoplankton. This production would in turn result in an increase in cloud condensation nuclei (CCN) from the oxidation of DMS via a hydroxyl radical to sulfate and methane sulfonate aerosol. The increased production of CCN is predicted to result in a concomitant increase in cloud cover which, as a consequence, would deflect a portion of the incident solar radiation flux (61).

Martin and co-workers (2, 3, 62) have presented strong evidence that Fe derived from atmospheric deposition is a limiting growth nutrient for various species of phytoplankton in some regions of the open ocean. Martin and colleagues postulated that the atmospheric deposition of iron in various forms may be a critical factor that may control Southern Ocean phytoplankton production, which in turn may affect atmospheric CO_2 levels (2). They argue that "low phytoplankton growth rates, which are exemplified by excess, unused major nutrients in the Southern Ocean, result from low atmospheric dust (i.e., Fe-containing aerosol) input occurring in the present and past interglacials." When the major growth nutrients (e.g., NO_3^-, $HPO_4^{2-}/H_2PO_4^-$) are under utilized, atmospheric CO_2 levels should be relatively high. This claim appears to be supported by an anti-correlation between CO_2 and Fe in the Antarctic Vostok ice core over 160,000 years. Very low levels of Fe were found in ice cores during the present and last (~ 127,000 years

before present) interglacials (63), while high levels of CO_2 were found for the same periods (64). In contrast, large amounts of iron and low concentrations of CO_2 were observed during the last glacial maxima (~18,000 years BP). During this glacial maxima, Fe-enriched atmospheric aerosol levels were 10-20 times the levels during the interglacial period (65, 2).

The recent eruption of Mount Pinatubo released a large amount of Fe into the atmosphere (~ 500 x 10^6 tons). The recent decrease of CO_2 concentrations observed after the eruption can be due to the fertilization of the oceans by the volcanic iron. Furthermore, the removal of 2.5 Pg of carbon (equivalent to the observed decrease of 1.5 ppm in atmospheric CO_2) would require only about 0.1 x 10^6 tons of iron, only a fraction of the emitted amount.

Anderson and Morel (66), Morel and Hudson (67) and Brand et al. (68) have shown that the particular chemical form (i.e., species) of iron, which is presented to marine phytoplankton, is critical to the organism's ability to assimilate iron for nutritional needs. Despite its abundance within the earth's crust, iron is essentially unavailable to biota in aquatic environments. Thus iron assimilation can limit biological productivity as indicated by Gran (69), Goldberg (70), Barber and Ryther (71), Lewin and Chen (72), Glover (73) and Rueter and Ades (74). Duce (75) has reviewed several aspects of the impact of atmospheric iron and its effects on biological productivity.

The major reason for the limited availability of iron is the extreme insolubility of iron as Fe(III) in neutral and high pH regimes. In the presence of O_2 (high oxidation potential), the dominant form of iron will be amorphous Fe(III) hydroxide {am-Fe$(OH)_3$} or one of its oxyhydroxide companion phases such as γ-FeOOH (76). Because of the low solubility product for am-Fe$(OH)_3$ (log K_{so} = -38.7; (77)), the concentration of total

soluble iron (III) at pH 7 is predicted to be extremely low based on equilibrium considerations (e.g., $[Fe^{3+}] \sim 10^{-18}$ M). Between pH 6 and 8 the total solubility of iron in its various hydroxy forms is ≤ 5.0 nM. In the presence of the more stable iron oxides such as α-Fe_2O_3 or α-FeOOH the predicted equilibrium concentrations are even lower. However, the total solubility of Fe(III) can be enhanced substantially by complexation with organic ligands such as nitrilotriacetic acid {NTA} (78). Jackson and Morgan (79) have presented a theoretical analysis of the role of Fe(III) complexation and phytoplankton growth, while Arnold et al. (80) have shown that the dissimilative Fe(III) reduction rates of α-Fe_2O_3, am-$Fe(OH)_3$, α-FeOOH, and γ-FeOOH in the presence of bacteria are enhanced dramatically by organic complexing agents.

The Role of Iron in Cloudwater Chemistry

Iron as Fe(II) and Fe(III) has been shown to play an important role in the multiphase atmospheric chemistry of S(IV) (81-86, 4). Graedel and co-workers (84, 85) have stressed the importance of iron speciation as a major factor controlling the reactivity of Fe(III) as a catalyst, as an oxidant and as a photolytic source of •OH (87). Weschler et al. (84) calculated that the major soluble species of Fe(III) in atmospheric water droplets should be $Fe(H_2O)_5OH^{2+}$, $Fe(H_2O)_4(OH)_2^{+}$ and $Fe(H_2O)_5SO_3^{+}$ as controlled by iron hydroxide solubility.

Fe(III) in its various solid and aqueous-phase forms is an effective catalyst for the autoxidation of S(IV) to S(VI) {82, 83, 88-90}. The catalytic autoxidation of SO_2 in deliquescent haze aerosol, clouds, fogs and hydrometeors appears to be a viable pathway for the rapid formation of sulfuric acid in humid atmospheres. Jacob and Hoffmann (81) have shown that Fe(III) and Mn(II) are the most effective catalysts at ambient concentrations for the autoxidation of S(IV) to S(VI) in cloud- and fogwater.

$$HSO_3^- + 0.5\,O_2 \xrightarrow{Fe^{3+}} SO_4^{2-} + H^+ \qquad (1)$$

Pandis and Seinfeld (91) have recently carried out a sensitivity analysis on a comprehensive chemical mechanism for aqueous-phase atmospheric chemistry and have shown that the principal pathways for the oxidation of S(IV) in clouds and fogs involve H_2O_2, •OH, O_2 (as catalyzed by Fe^{3+} and Mn^{2+}) and HSO_5^-. Pandis and Seinfeld (5) then coupled their chemical model to a Langrangian trajectory model to study the time-dependent chemistry during an extended period of radiation fog. Their calculations showed that the Fe^{3+} catalyzed oxidation of S(IV) by O_2 contributed almost the same amount to total sulfate production as did the pathway involving oxidation by H_2O_2. The latter pathway is often thought to be the main contributor to sulfate production in clouds. In a similar study, Jacob et al. (4) used a simple equilibrium scheme to account for the speciation of Fe(III) in solution and found for the same event modeled by Pandis and Seinfeld (5) that only the S(IV)/Fe(III)-catalyzed pathway was able to account for the observed (92, 93) sulfate accumulation pattern. Jacob et al. (4) also noted that only the non-radical mechanisms as proposed by Conklin and Hoffmann (86) and Kraft and van Eldik (89) are consistent with field observations. A free-radical mechanism as proposed by Martin and Hill (94) was found to quench the overall production of sulfate because of the reduction of Fe(III) to Fe(II) and the absence of a pathway for the rapid oxidation of Fe(II) back to Fe(III) at low pH.

A frequently postulated initiation step for the free radical autoxidation of S(IV) catalyzed by Fe(III) is as follows (94):

$$Fe(H_2O)_6^{3+} + SO_3^{2-} \rightarrow Fe(H_2O)_6^{2+} + SO_3^{\bullet -} \qquad (2)$$

Most researchers have assumed that electron transfer between $Fe(H_2O)_6^{3+}$ and SO_3^{2-} is an outersphere process. However, a formation of an inner-sphere complex appears to be a necessary reaction step when open coordination sites are available in the octahedral coordination sphere of Fe(III) (86, 89, 90). On the other hand, Fe(2, 2'-bipyridine)$_3^{3+}$ which has a fully occupied coordination sphere oxidizes SO_3^{2-} via a bimolecular outer-sphere electron transfer to give $SO_3^{-\bullet}$ with a second-order rate constant of 2.1×10^8 M^{-1} s^{-1} (95). When O_2 is introduced to this system, the consumption of SO_3^{2-} is enhanced; this enhanced reaction can be attributed to the involvement of free-radical chain reactions involving $SO_3^{-\bullet}$, $SO_5^{-\bullet}$, $SO_4^{-\bullet}$, and SO_5^{2-} as chain carriers and intermediates (96, 83, 97).

However, when several open coordination sites (sites normally occupied by water) on the aquated Fe(III) are available for coordination, a mechanism involving inner-sphere complexation of S(IV) as SO_3^{2-} by $Fe(H_2O)_5(OH)^{2+}$ appears to be operative (83, 86, 89). One possible structure for the active catalytic intermediate, which takes into account the known geometry and mode of Fe(III)-S(IV) bonding is as follows (86):

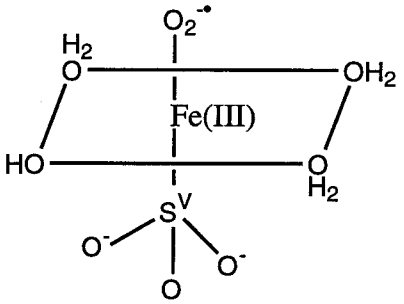

(3)

Kraft and van Eldik (89, 90) have proposed a mechanism similar to that proposed by Conklin and Hoffmann (86) with the inclusion of pathways involving the formation of two additional Fe(III)-S(IV) complexes, $Fe(H_2O)_4(SO_3)_2^-$ and $Fe(H_2O)_3(SO_3)_3^{3-}$.

Photochemistry of Fe(III) and Fe(III)-Oxides

The kinetics and mechanism of the photo-assisted oxidation of S(IV) in the presence of suspensions of α-Fe_2O_3 have been studied over the pH range of 2 to 10.5 (88). Quantum yields, ϕ, ranged from 0.08 to 0.3 with a maximum yield at pH 5.7. The photoassisted heterogeneous oxidation of S(IV) appears to proceed via the rapid formation of Fe(III)-S(IV) surface complexes by ligand exchange with the surface hydroxyl groups as follows:

$$>FeOH + HSO_3^- \xleftrightarrow{K_4^s} >FeOSO_2^- + H_2O \qquad (4)$$

Light absorption with photon energies exceeding the bandgap energy of α-Fe_2O_3 leads to the formation of electron-hole pairs followed by the one electron oxidation of adsorbed sulfite yielding the $SO_3^{-\bullet}$ radical anion.

$$>FeOSO_2^- \xrightarrow{h\nu} \overset{h^+_{vb}}{\underset{e^-_{cb}}{>}} Fe\overset{\leftarrow}{O}S(\overset{e^-}{V})O_2^- \rightarrow \underset{e^-_{cb}}{>} FeOS(V)O_2^{\bullet} \qquad (5)$$

In the absence of a suitable electron acceptor bound to the surface, the e_{cb}^- reacts with a -Fe(III)OH surface site to produce -Fe(II)OH. This reaction leads to the subsequent release of $Fe(H_2O)_6^{2+}$ to the solution phase and the progressive dissolution of the iron oxide particle. Even though the trapping of the conduction band electron is rapid, the subsequent dissolution steps are relatively slow (98, 99).

In the presence of oxygen the $SO_3^{-\bullet}$ reacts quickly with adsorbed O_2 on the surface of the catalyst particle to form $SO_5^{-\bullet}$. For small particles both the $SO_3^{-\bullet}$ and $SO_5^{-\bullet}$ remain bound to surface sites where they undergo further transformations to yield SO_4^{2-}, SO_5^{2-}, and $S_2O_6^{2-}$ (88).

Leland and Bard (100) found that the rate of photooxidation of S(IV) in the presence of iron oxide polymorphs varied by 2 orders of magnitude with the relative order of γ-FeOOH > α-Fe_2O_3 > γ-Fe_2O_3 > δ-FeOOH > β-FeOOH > α-FeOOH. They attributed this order in the S(IV) oxidation to differences in crystal structure rather than to differences in reactive surface area or the energy of the band gap. Faust and Hoigne (87) have recently determined that the photolysis of $Fe(H_2O)_5OH^{2+}$ leads to the production of •OH via

$$Fe(III)(H_2O)_5OH^{2+} \xrightarrow[H_2O]{h\nu} Fe(H_2O)_6^{2+} + \bullet OH \qquad (6)$$

with quantum efficiencies of $\phi = 0.14$ at $\lambda = 313$ nm and $\phi = 0.017$ at $\lambda = 360$ nm. Their results provide further motivation to determine Fe speciation in ambient atmospheric samples.

Photoreduction of Fe(III) to Fe(II)

Although Fe(III) has been found in high (~ 1 mM) concentrations in atmospheric water droplets (45, 44), much of the total measured iron is predicted to be in the form of solid particles or colloids based on thermodynamic considerations (77). Ferric oxides and oxyhydroxides (α-Fe_2O_3, Fe_3O_4, α-FeOOH and γ-FeOOH) have been identified as components of airborne particles (101). When these iron(III)-containing aerosols serve as cloud and fog condensation nuclei, the resulting water droplets should retain most of the total iron in the suspended particulate form. However, recent research on the speciation of iron in fog collected with the Caltech Active Strand Collector in Zürich has shown that a significant fraction of the total iron (20 to 90 %) is present as soluble Fe(II) (up to 200 μM) over the pH range of 3-7 (47) and that Fe(II) was the predominant oxidation state in solution (dissolved iron is operationally defined by filtration through either a 0.45 or 0.05 μm membrane filter). This result is very surprising in light of the thermodynamic

instability of Fe(II) in water in the presence of O_2, O_3 and H_2O_2. Behra and Sigg (47) found that the fraction of Fe(II) increased with a decreasing pH and increasing exposure to light. They postulated that Fe(III) in its various chemical forms is reduced by sulfite, organic compounds and free radicals formed photochemically during the day. At night, the reduction of Fe(III) by HSO_3^- is thought to be the main source of Fe(II). The actual steady-state Fe(II) concentration for a particular time increment appears to be the result of a balance between the reduction of Fe(III) by S(IV), HO_2, H_2O_2, and Cu(I) and the oxidation of Fe(II) by O_2, O_3, H_2O_2, and HO_2 (47).

Faust and Hoffmann (102) have shown that α-Fe_2O_3 is effectively reduced by HSO_3^- in the presence of light with quantum yields for Fe(II) production ranging from 0.006 at 676 nm to 0.39 at 350 nm. Stramel and Thomas (103), Waite and co-workers (104, 105), Cunningham and co-workers (106, 107) and Stumm and co-workers (108) have shown that other Fe(III) oxyhydroxide solids are photoreduced readily in the presence of oxygen and a wide variety of organic electron donors such as carboxylic acids, thiols, and alcohols.

Reactivity of Iron as a Function of Oxidation State

The Fe(II)/Fe(III) redox system also has a chemical/catalytic effect on other chemical species of interest in cloud, fog, haze aerosol and rain. For example, in atmospheric water droplets Fe(II) can react with H_2O_2 to form •OH as follows:

$$Fe^{2+} + H_2O_2 \xrightarrow{k_7} Fe^{3+} + {}^{\bullet}OH + OH^- \qquad (7)$$

$$FeOH^+ + H_2O_2 \xrightarrow{k_8} Fe(OH)_2^+ + {}^{\bullet}OH \qquad (8)$$

The species-dependent reactivity of Fe(II) toward H_2O_2 is seen clearly by a comparison of k_7 (76 $M^{-1}s^{-1}$; (109)) and k_8 (1.9 x 10^6 M^{-1} s^{-1}; (110)). Fe(II) also reacts with a hydroperoxyl radical to form H_2O_2,

$$Fe^{2+} + HO_2^{\bullet} + H_3O^+ \xrightarrow{k_9} Fe^{3+} + H_2O_2 + H_2O \qquad (9)$$

and with a peroxymonosulfate (111) to yield Fe(III) and S(V) as $SO_4^{-\bullet}$:

$$Fe^{2+} + HSO_5^- \xrightarrow{k_{10}} FeOH^{2+} + SO_4^{\bullet} \qquad (10)$$

In atmospheric water droplets the principal pathways for Fe(II) oxidation would be oxidation by O_2 (77, 112), H_2O_2 and O_3 (113).

Fe(III) hydroxy complexes and other mixed-ligand complexes Fe(III) can serve as effective oxidants for a variety of reductants such as HCHO, CH_3CHO, $CH_3COCOCH_3$, CH_3COCO_2H, and HOOCCOOH (114). For example, formaldehyde as its gem-diol can be oxidized to formic acid as follows:

$$2Fe(III)L_6^{3+} + H_2C(OH)_2 \longrightarrow Fe(II)L_6^{2+} + HCO_2H + H_2O \qquad (11)$$

In many cases, the actual rate of oxidation of reductants is strongly dependent on the speciation of Fe(III) (115).

Atmospheric Speciation of Fe: Solid and Liquid Phases

Jacob and Hoffmann (81), Hoffmann and Jacob (83), Weschler et al. (84) and Faust and Hoigne (87) have stressed the importance of knowing the speciation of transition

metals in atmospheric water droplets. A knowledge of the exact Fe(III)/Fe(II) species present as a function of important variables such as pH, organic ligands and ionic strength is critical to the computational assessment of *in situ* reaction pathways involving S(IV), O_2, RHCO, NO_x, ROOH, and H_2O_2. Likewise, a knowledge of the speciation of Fe in wet and dry atmospheric deposition and the subsequent speciation changes upon introduction to marine waters is important to the assessment of the ability of marine biota to utilize iron derived from the atmosphere for nutritional needs (66, 79, 75, 116).

Weschler et al. (84) determined from inorganic equilibrium models (i.e., without organic ligands) that the major soluble-phase Fe(III) species in atmospheric water droplets should be $Fe(H_2O)_5OH^{2+}$, $Fe(H_2O)_4(OH)_4^{+}$, and $Fe(H_2O)_5SO_3^{+}$ and that the distribution of total Fe(III) is pH dependent. However, in light of the work of Conklin and Hoffmann (86) and Kraft and van Eldik (89, 90) on the Fe(III)-S(IV) complexes, the redox instability of $Fe(H_2O)_5SO_3^{+}$ would preclude its accumulation at appreciable concentrations in atmospheric water droplets over the pH range of 2 to 7.

Over the pH range of 2 to 4, Faust and Hoigne (87) have computed that the soluble Fe(III) species in equilibrium with am-$Fe(OH)_3$ would be $Fe(H_2O)_6^{3+}$, $Fe(H_2O)_5OH^{2+}$, and $Fe(H_2O)_4(OH)^{+}$ with $Fe(H_2O)_5OH^{2+}$ as the predominant species over the pH range of 3 to 5. Similar calculations have been reported by Sigg (37), who also includes $Fe(H_2O)_2(OH)_4^{-}$ as an important species at higher pH. In spite of the numerous measurements of total iron in the solid and liquid phases in the atmosphere, very little information about the speciation of iron is available except for the work of Behra and Sigg (47) *(vide supra).* Dlugi et al. (8) reported that significant fractions of the total iron (12-56 %) present in fly ash were dissolved in water at pH 2 within 5 to 20 min.; similar results were reported by Williams et al. (9). In the former case, some of the soluble iron was found to precipitate as am-$Fe(OH)_3$ with time after the initial dissolution. Brimblecombe

and Spedding (117) examined the dissolution of iron from fly ash and noted that the high solubility of Fe may have been due to the presence of calcium ferrite ($5CaO \cdot 3Fe_2O_3$), calcium oxymetaferrite ($2CaO \cdot Fe_2O_3$) and calcium aluminoferrite ($4CaO \cdot Al_2O_3 \cdot Fe_2O_3$), which are more readily soluble in water than hematite (Fe_2O_3).

Experimental Approaches to Speciation

Several different approaches have been taken to ascertain the speciation of dissolved metals in water (6). Among these approaches are 1) speciation modeling using computer-generated chemical equilibrium models (77), 2) physical separation according to size (i.e., particulate, colloidal, dissolved) by techniques such as ultrafiltration with membrane filters (118) or dialysis, 3) physicochemical methods such as selective chelation, direct electrochemical determination of free (hexaquo) metals (e.g., ion specific electrodes) or free and labile metals (e.g., anodic stripping voltammetry), and 4) direct chemical methods such as ion-pairing chromatography or HPLC/AAS (119).

The goal of the study of iron speciation in atmospheric water was accomplished by the use of a specific chelating agent for iron(II) and iron(III), kinetic and mechanistic studies of reductive photodissolution of iron oxides by ligands that likely exist in atmospheric water and the application of speciation modeling (SURFEQL) to ambient atmospheric water samples. In addition, the particulate phase chemistry of iron was studied in detail by a fellow graduate student, Ron Siefert.

References

1. Cotton, F. A.; Wilkinson, G. "Advanced Inorganic Chemistry," Wiley-Interscience: New York, 3rd ed., **1972**, 868.

2. Martin, J. H.; Gordon, R. M.; Fitzwater, S. E.; Broenkow, W. W. "VERTEX: Phytoplankton/Iron Studies in the Gulf of Alaska," **1989**, *36*, 649.

3. Martin, J. H.; Fitzwater, S. E.; Gordon, R. M. *Nature,* **1988**, *321*, 341.

4. Jacob, D. J.; Gottlieb, E. W.; Prather, M. J. *J. Geophys. Res.,* **1989**, *94*, 12975.

5. Pandis, S. N.; Seinfeld, J. H. *J. Geophys. Res.,* **1989**, *94*, 12911.

6. Salomons, W.; Förstner, U. "Metals in the Hydrocycle," Springer-Verlag: Berlin Heidelberg, **1984**, 234.

7. Hansen, L. D.; Silberman, D.; Fisher, G. L.; Eatough, D. J. *Environ. Sci. Technol.,* **1984**, *18*, 181.

8. Dlugi, R.; Jordan, S.; Manegold, S. "Chemische Reaktionen und Aerosolverhalten in Rauchgahnen mit Kondensierender Atmosphare," Kernforschungszentrum Karlsruhe: FRG, **1985**, 202.

9. Williams, P. T.; Radojevic, J. L.; Morel, F. M. M. *Atmos. Environ.,* **1988**, *22*, 1433.

10. Heidam, N. Z. *Atmos. Environ.,* **1984**, *18*, 329.

11. Davidson, C. I.; Goold, W. D.; Mathison, T. P.; Wiersma, G. B.; Brown, K. W.; Reilly, M. T. *Environ. Sci. Technol.,* **1985**, *19*, 27.

12. Pacyna, J. M.; Ottar, B. *Atmos. Environ.,* **1985**, *12*, 2109.

13. Sheridan, P. J.; Zoller, W. H. *J. Atmos. Chem.,* **1989**, *9*, 363.

14. Maenhaut, W.; Zoller, W. H.; Duce, R. A.; Hoffmann, G. I. *J. Geophys. Res.,* **1979**, *84*, 2421.

15. Merrill, J. T.; Duce, R. A. "The Meteorology and Atmospheric Chemistry of Enewetak Atoll," U. S. Department of Energy, Oak Ridge, TN, **1982**, 34.

16. Duce, R. A.; Hoffman, G. L.; Ray, B. J.; Fletcher, I. S.; Wallace, G. T.; Fasching, J. L.; Piotrowicz, S. R.; Walsh, P. R.; Hoffman, E. J.; Miller, J. M.; Heffter, J. L. "Trace Metals in the Marine Atmosphere: Sources and Fluxes," in "Marine Pollutant Transfer" **1976**, 77.

17. Wolff, G. T.; Ruthkowsky, M. S.; Stroup, D. P.; Korsog, P. E.; Ferman, M. A.; Wendel, G. J.; Stedman, D. H. *Atmos. Environ.,* **1986**, *20*, 1229.

18. Arimoto, R.; Duce, R. A.; Ray, B. J.; Hewitt, A. D.; Williams, J. *J. Geophys. Res.,* **1987**, *92*, 8465.

19. Cawse, P. A., Eds. "Inorganic Particulate Matter in the Atmosphere," Royal Society London: London, **1982**, 1.

20. Stevens, R. K.; Dzubay, T. G.; Russwurm, G.; Rickel, D. *Environ. Sci. Technol.,* **1980**, *14*, 1491.

21. Berametti, G.; Dutot, A.; Buat-Menard, P.; Losno, R.; Remoudaki, E. *Tellus B,* **1989**, *41*, 353.

22. Bruynseels, F.; Storms, H.; Van Grieken, R.; Van der Auwera, L. *Atmos. Environ.,* **1988**, *22*, 2593.

23. Cahill, T. A. "Monitoring of Atmospheric Particles and Ozone in Sequoia National Park: 1985-1987," Final Report, California Air Resources Board, **1989**, A5-180-32, 63.

24. Tuncel, S. G.; Olmez, I.; Parrington, J. R.; Gordon, G. E.; Stevens, R. K. *Environ. Sci. Technol.,* **1985**, *19*, 529.

25. Cass, G. R.; McRae, G. J. *Environ. Sci. Technol.,* **1983**, *17*, 129.

26. John, W.; Kaifer, R.; Rahn, K.; Wesolowski, J. J. *Atmos. Environ.,* **1973**, *7*, 107.

27. Junge, C. E. "Air Chemistry and Radioactivity," Academic Press: New York, **1963**, 382.

28. Dzubay, T. G.; Stevens, R. K.; Lewis, C. W.; Hern, D. H.; Courtney, W. J.; Tesch, J. W.; Mason, M. A. *Environ. Sci. Technol.,* **1982**, *16*, 514.

29. Sievering, H.; Dave, M.; Dolske, D.; McCoy, P. "Transport and Dry Deposition of Trace Metals over Southern Lake Michigan," in "Atmospheric Pollutants in Natural Waters" Ann Arbor Science: Ann Arbor, MI, **1981**, 285.

30. Bertolaccini, M. A.; Gucci, P. M. B. *Sci. Tot. Environ.,* **1986**, *57*, 7.

31. Hopke, P. K.; Gladney, E. S.; Gordon, G. E.; Zoller, W. H.; Jones, A. G. *Atmos. Environ.,* **1976**, *10*, 1015.

32. Cambray, R. S.; Jeffries, D. F.; Topping, G. *Mar. Sci. Comm.,* **1979**, *5*, 175.

33. Thornton, J. D.; Eisenreich, S. J.; Munger, J. W.; Gorham, E. "Trace Metal and Acid Composition of Rain and Snow in Northern Minnesota," in "Atmospheric Pollutants in Natural Waters" Ann Arbor Science: Ann Arbor, MI, **1981**, 261.

34. Liljestrand, H. M.; Morgan, J. J. *Environ. Sci. Technol.,* **1981**, *15*, 333.

35. Slanina, J.; Van Raaphorst, J. G.; Zijp, W. L.; Vermulen, A. J.; Roet, C. A. *Int. J. Environ. Anal. Chem.,* **1979**, *6*, 67.

36. Chan, W. H.; Vet, R. J.; Ro, C. U.; Tang, A. J. S.; Lusis, M. A. *Atmos. Environ.,* **1984**, *18*, 1175.

37. Sigg, L. "Surface Chemical Aspects of the Distribution and Fate of Metal Ions in Lakes," in "Aquatic Surface Chemistry" John Wiley & Sons: New York, **1987**, 319.

38. Clark, A. G.; Radojevic, M. *Atmos. Environ.,* **1987**, *21*, 1115.

39. Jickells, T. D.; Knap, A. H.; Church, T. M. *J. Geophys. Res.,* **1984**, *89*, 1423.

40. Church, T. M.; Tramontano, J. M.; Scudlark, J. R.; Jickells, T. D.; Tolos, J. J. J.; Knap, A. H.; Galloway, J. N. *Atmos. Environ.,* **1984**, *18*, 2657.

41. Arimoto, R.; Duce, R. A.; Ray, B. J.; Unni, C. K. *J. Geophys. Res.,* **1985**, *90*, 2391.

42. Mahadevan, T. N.; Sadasivan, S.; Mishra, U. C. *Sci. Tot. Environ.,* **1982**, *24*, 275.

43. Waldman, J. M.; Munger, J. W.; Jacob, D. J.; Flagan, R. C.; Morgan, J. J.; Hoffmann, M. R. *Science,* **1982**, *218*, 677.

44. Jacob, D. J.; Waldman, J. M.; Munger, J. W.; Hoffmann, M. R. *Environ. Sci. Technol.,* **1985**, *19*, 730.

45. Munger, J. W.; Waldman, J. M.; Jacob, D. J.; Hoffmann, M. R. *J. Geophys. Res.,* **1983**, *88*, 5109.

46. Joos, F.; Baltensperger, U. *Atmos. Environ. A.,* **1991**, *25*, 217.

47. Behra, P.; Sigg, L. *Nature,* **1990**, *344*, 419.

48. Waldman, J. M. "Depositional Aspects of Pollutant Behavior in Fog," doctoral thesis, California Institute of Technology, **1986**, 121.

49. Fuzzi, S.; Orsi, G.; Nardini, G.; Facchini, M. C.; McLaren, E.; Mariotti, M. *J. Geophys. Res.,* **1988**, *93*, 11141.

50. Betzer, P. R.; Carder, K. L.; Duce, R. A.; Merrill, J. T.; Tindale, N. W.; Uematsu, M.; Costello, D. K.; Young, R. W.; Feely, R. A. *Nature,* **1988**, *336*, 568.

51. Merrill, J. T.; Uematsu, M.; Bleck, R. *J. Geophys. Res. A.,* **1989**, *94*, 8584.

52. Maring, H.; Patterson, C. C.; Settle, D. M. "Atmospheric Input Fluxes of Industrial and Natural Pb from the Westerlies to the Mid-North Pacific," in "Chemical Oceanography," Academic Press: New York, **1989**, 84.

53. Patterson, C. C.; Settle, D. M. *Mar. Chem.,* **1987**, *22*, 137.

54. Morales, C. "Saharan Dust - Mobilization, Transport, Deposition," Wiley: New York, **1979**, 320.

55. Glaccum, R. A.; Prospero, J. M. *Mar. Geol.,* **1980**, *37*, 295.

56. Schütz, L.; Jaenicke, R.; Peitrek, H. *Geol. Soc. Amer.,* **1981**, *Special Paper 186*, 87.

57. Chester, R.; Stoner, J. H. *Mar. Chem.,* **1974**, *2*, 157.

58. Trabalka, J. R.; Reichle, D. E., Eds. "The Changing Carbon Cycle - A Global Analysis," Springer-Verlag: New York, **1986**, 592.

59. Bolin, B.; Döös, B. R.; Jäger, J.; Warrick, R. A. "Scope 29, The Greenhouse Effect, Climate Change and Ecosystems," Wiley: New York, **1986**, 541.

60. Hansen, J.; Fung, I.; Lacis, A.; Rind, D.; Lebedeff, S.; Ruedy, R.; Russell, G.; Stone, P. *J. Geophys. Res.,* **1988**, *93*, 9341.

61. Charlson, R. J.; Lovelock, J. E.; Andreae, M. O.; Warren, S. G. *Nature,* **1987**, *326*, 655.

62. Martin, J. H.; Gordon, R. M. *Deep Sea Res. A.,* **1988**, *35*, 177.

63. DeAngelis, M.; Barkov, N. I.; Petrov, V. N. *Nature,* **1987**, *325*, 318.

64. Barnola, J. M.; Raynaud, D.; Korotkevich, Y. S.; Lorius, C. *Nature,* **1987**, *329*, 408.

65. Petit, J. R.; Briat, M.; Royer, A. *Nature,* **1981**, *293*, 391.

66. Anderson, M. A.; Morel, F. M. M. *Limnol. Oceanogr.,* **1982**, *27*, 789.

67. Morel, F. M. M.; Hudson, R. J. M. "The Geobiological Cycle of Trace Elements in Aquatic Systems: Redfield Revisited," in "Chemical Processes in Lakes," Wiley-Interscience: New York, **1985**, 251.

68. Brand, L. E.; Sunda, W. G.; Guillard, R. R. L. *Limnol. Oceanogr.,* **1983**, *28*, 1182.

69. Gran, H. H. *Biol. Bull.,* **1933**, *64*, 159.

70. Goldberg, E. D. *Biol. Bull.,* **1952**, *102*, 243.

71. Barber, R. T.; Ryther, J. H. *J. Exp. Mar. Biol. Ecol.,* **1969**, *3*, 191.

72. Lewin, J.; Chen, C. H. *Limnol. Oceanogr.,* **1971**, *16*, 670.

73. Glover, H. E. *Limnol. Oceanogr.,* **1978**, *23*, 534.

74. Rueter, J. G.; Ades, D. R. *J. Phycol.,* **1987**, *23*, 452.

75. Duce, R. A. "The Impact of Atmospheric Nitrogen, Phosphorous and Iron Species on Marine Biological Productivity," in "The Role of Air-Sea Exchange in Geochemical Cycling," D. Reudel Publishing: Dordrecht, **1986**, 497.

76. Sung, W.; Morgan, J. J. *Geochim. Cosmochim. Acta,* **1981**,*45*, 2377.

77. Stumm, W.; Morgan, J. J. "Aquatic Chemistry," Wiley: New York, **1981**, 356.

78. Arnold, R. G.; DiChristina, T. J.; Hoffmann, M. R. *Biotech. Bioeng.,* **1988**, *32*, 1081.

79. Jackson, G. A.; Morgan, J. J. *Limnol. Oceanog.,* **1978**, *230*, 268.

80. Arnold, R. G.; Hoffmann, M. R.; Dichristina, T. J.; Picardal, F. W. *Appl. Environ. Microb.,* **1990**, *56*, 2811.

81. Jacob, D. J.; Hoffmann, M. R. *J. Geophys. Res.,* **1983**, *88*, 6611.

82. Martin, L. R. "Kinetic Studies of Sulfite Oxidation in Aqueous Solution," in "Acid Precipitation: SO_2, NO, NO_x Oxidation Mechanisms: Atmospheric Considerations," Butterworth Publishers: Boston-London, **1984**, 63.

83. Hoffmann, M. R.; Jacob, D. J. "Kinetics and Mechanism of the Catalytic Oxidation of Dissolved SO_2 in Atmospheric Droplets: Free Radical, Polar and Photoassisted Pathways," in "SO_2, NO, NO_2 Oxidation Mechanisms: Atmospheric Considerations," Butterworth Publishers: Boston, **1984**, 101.

84. Weschler, C. J.; Mandich, M. L.; Graedel, T. E. *J. Geophys. Res.,* **1986**, *91*, 5189.

85. Graedel, T. E.; Mandich, M. L.; Weschler, C. J. *J. Geophys. Res.,* **1986**, *91*, 5205.

86. Conklin, M. H.; Hoffmann, M. R. *Environ. Sci. Technol.,* **1988**, *22*, 899.

87. Faust, B. C.; Hoigne, J. *Atmos. Environ.,* **1990**, *24*, 79.

88. Faust, B. C.; Hoffmann, M. R.; Bahnemann, D. W. *J. Phys. Chem.,* **1989**, *93*, 6371.

89. Kraft, J.; vanEldik, R. *Inorg. Chem.,* **1989**, *28*, 2297.

90. Kraft, J.; vanEldik, R. *Inorg. Chem.,* **1989**, *28*, 2306.

91. Pandis, S. N.; Seinfeld, J. H. *J. Geophys. Res.,* **1989**, *94*, 1105.

92. Jacob, D. J.; Munger, J. W.; Waldman, J. M.; Hoffmann, M. R. *J. Geophys. Res. A,* **1986**, *91*, 1073.

93. Jacob, D. J.; Shair, F. H.; Waldman, J. M.; Munger, J. W.; Hoffmann, M. R. *Atmos. Environ.,* **1987**, *21*, 1305.

94. Martin, L. R.; Hill, M. W. *Atmos. Environ.,* **1987**, *21*, 1487.

95. Wilmarth, W. K.; Stanbury, D. M.; Byrd, J. E.; Po, H. N.; Chua, C.-P. *Coord. Chem. Rev.,* **1983**, *51*, 155.

96. Hoffmann, M. R.; Boyce, S. D. "Catalytic Autooxidation of Aqueous Sulfur Dioxide in Relationship to Atmospheric Systems," in "Trace Atmospheric Constituents: Properties, Transformations, and Fates," Wiley: New York, **1983**, 147.

97. Betterton, E. A.; Erel, Y.; Hoffmann, M. R. *Environ. Sci. Technol.,* **1988**, *22*, 92.

98. Mulvaney, P.; Swayambunathan, V.; Grieser, F.; Meisel, D. *J. Phys. Chem.,* **1988**, *92*, 6732.

99. Mulvaney, P.; Cooper, R.; Grieser, F.; Meisel, D. *Langmuir,* **1988**, *4*, 1206.

100. Leland, J. K.; Bard, A. J. *J. Phys. Chem.,* **1987**, *91*, 5076.

101. Fukasawa, T.; Iwatsuki, M.; Kawakubo, S.; Miyazaki, K. *Anal. Chem.,* **1980**, *52*, 1784.

102. Faust, B. C.; Hoffmann, M. R. *Environ. Sci. Technol.,* **1986**, *20*, 943.

103. Stramel, R. D.; Thomas, J. K. *J. Colloid. Interface Sci.,* **1986**, *110*, 121.

104. Waite, T. D.; Morel, F. M. M. *Environ. Sci. Technol.,* **1984**, *18*, 860.

105. Waite, T. D.; Torikov, A. *J. Coll. I. Sc.,* **1987**, *119*, 228.

106. Cunningham, K. M.; Goldberg, M. C.; Weiner, E. R. *Photochem. Photobiol.,* **1985**, *41*, 409.

107. Cunningham, K. M.; Goldberg, M. C.; Weiner, E. R. *Environ. Sci. Technol.,* **1988**, *22*, 1090.

108. Sulzberger, B.; Suter, D.; Siffert, C.; Banwart, S.; Stumm, W. *Mar. Chem.,* **1989**, *28*, 127.

109. Walling, C. *Acct. Chem. Res.,* **1975**, *8*, 125.

110. Moffett, J. W.; Zika, R. G. *Environ. Sci. Technol.,* **1987**, *21*, 804.

111. Sato, T.; Gotto, T.; Okabe, T.; Lawson, F. *Bull. Chem. Soc. Jpn.,* **1984**, *57*, 2082.

112. Millero, F. J.; Sotolongo, S.; Izaguirre, M. *Geochim. Cosmochim Acta,* **1987**, *51*, 793.

113. Hoigne, J.; Bader, H.; Haag, W. R.; Staehelin, F. *Water Res.,* **1985**, *19*, 993.

114. Littler, J. S.; Sayce, I. G. *J. Chem. Soc.,* **1964**, *96*, 2445.

115. Basolo, F.; Pearson, R. G. "Mechanisms of Inorganic Reactions," Wiley-Interscience: New York, **1967**, 701.

116. Murphy, K.; Dymond, J. *Nature,* **1984**, *307*, 444.

117. Brimbecombe, P.; Spedding, D. J. *Atmos. Environ.,* **1975**, *9*, 835.

118. Hoffmann, M. R.; Yost, E. C.; Eisenreich, S. J.; Maier, W. J. *Environ. Sci. Technol.,* **1981**, *15*, 655.

119. Chau, Y. K.; Wong, P. T. S. "Direct Speciation Analysis of Molecular and Ionic Organometals," in "Trace Elements Speciation in Surface Waters and its Ecological Implications," Plenum: New York, **1983**, 87.

Chapter 3

Simultaneous Spectrophotometric Measurement of Fe(II) and Fe(III) in Atmospheric Water

[The text of this chapter appeared in S. O. Pehkonen, Y. Erel, and M. R. Hoffmann, Environmental Science and Technology, 1992, 26, 1731.]

Abstract

A new analytical method employing di-2-pyridyl ketone benzoylhydrazone (DPKBH) as a colorimetric chelating agent for the simultaneous determination of iron(II) and iron(III) in cloudwater has been developed. A spectrophotometric detection limit of 4 nM for both Fe(III) and Fe(II) with a linear response from 4 nM up to 0.1 μM was established for samples extracted with $CHCl_3$-H_2O. DPKBH chelation without $CHCl_3$ extraction showed a linear response from 0.1 μM to 30 μM. The molar extinction coefficients of the bis-Fe(II)-DPKBH (ε_2) and bis-Fe(III)-DPKBH (ε_1) complexes are ε_1 & $\varepsilon_2 = 3.6 \times 10^4$ L mol^{-1} cm^{-1} at 370 nm and $\varepsilon_2 = 1.1 \times 10^4$ L mol^{-1} cm^{-1} at 660 nm. Analytical interference studies on the possible changes in the oxidation state of iron with S(IV), oxalate and other potential electron donors have also been carried out. This analytical method has been used to determine iron(II) and iron(III) simultaneously in cloudwater samples collected within the Los Angeles basin airshed. The concentration of Fe(II) varied from 0.3 to 5 μM and the concentration of Fe(III) varied from 0.6 to 1.4 μM during several stratus cloud events.

Introduction

Iron is the fourth most abundant element in the earth's crust; it is present in a variety of rock and soil minerals both as Fe(II) and Fe(III) (1). Iron also plays a central role in the biosphere serving as the active center of proteins responsible for O_2 and electron transfer and of metallo-enzymes such as oxidases, reductases and dehydrases (2). The observed concentrations of total dissolved iron in natural water systems vary from 0.2 nM in mid-ocean surface water (3) up to 400 μM in polluted urban clouds (4).

Determination of the oxidation state of iron in atmospheric water is important in light of recent studies that iron may be the limiting nutrient for phytoplankton growth in the open ocean (5, 6). Moreover, Fe(II) is probably the preferred nutrient for phytoplankton (7). In addition, Fe(III) serves as an effective catalyst for the autoxidation of SO_2 to SO_4^{2-} in clouds (8, 9). In urban atmospheres, where S(IV) and oxidizable organic compounds are abundant, oxidation of S(IV) and organic compounds by Fe(III) via direct electron transfer can take place. Laboratory experiments have shown that iron(III) is an important oxidant of S(IV) (8, 9, 10) and organic pollutants (e.g., formaldehyde to formic acid) (11). Most investigations of iron in atmospheric water have been limited to the determination of its total dissolved concentration; very little is known about its oxidation state (12, 13). However, measurements of Fe(II) in sea water (14) and in stream water (15) have shown that it is present at significant levels in oxic environments.

The determination of the oxidation state of iron in a variety of samples can be conventionally achieved by complexation with specific chelating agents followed by spectrophotometric measurement. Several chelating agents have been developed specifically for iron(II) determination. Tsuchiya and Iwanami (16) used 2-diethylamino-4-hydroxy-5-nitroso-6-amino-pyrimidine for the determination of iron(II) in leaded brass,

copper-nickel, and magnesium-aluminum alloys, while Zhang et al.(17) used 2-[2-(5-bromobenzothiazolyl)azo]-5-dimethylaminobenzoic acid for the determination of iron(II) in aluminum alloys. Wang et al. (18) utilized 4-(2-benzothiazolylazo)pyrocatechol for the determination of iron(II) in water, and 2-(6'-bromo-2'-benzothiazolylazo)-5-carboxyphenol was used by Sun et al.(19) for the determination of iron(II) in graphite. Ferrozine {3-(2-pyridyl)-5,6-diphenyl-1,2,4-triazine-p,p'-disulfonic acid, monosodium salt monohydrate} as used originally by Stookey (20) and Carter (21) is the most common chelating agent used for Fe(II) determination in water and blood serum samples. Several specific chelating agents for iron(III) have also been developed, such as meso-tetrakis(4-sulfophenyl)porphyrin used by Xu et al. (22) for the simultaneous determination of iron(III), Cu(II) and Zn(II), while Vijayakumar et al. (23) used hydroxy-1-acetonaphthoneoxime for the determination of iron(III) and indirectly for fluoride.

Methods that involve the preconcentration of water samples followed by a spectrophotometric measurement using some of the above reagents have been used in the determination of very low iron concentrations in environmental samples. These methods include the pressure-filtration through a silica-gel immobilized 8-hydroxyquinoline cartridge followed by elution and complexation with Ferrozine (24), the trapping of Fe(III) with chelating resins that are analogous to naturally occurring siderophores (25) and flow injection analysis with chemiluminescence detection for the determination of low iron(II) concentrations in seawater (26). While these methods can be used effectively in the case of low iron concentrations, they are, however, quite laborious and are limited to the determination of either Fe(II) or Fe(III). In addition, many of these techniques are unable to determine iron concentrations typically found in cloudwater in pristine environments, because of their relatively high detection limits (20-60 nM).

Di-2-pyridyl ketone benzoylhydrazone (DPKBH) was selected in this study as a chelating agent for iron, because it is known to complex both iron(II) and iron(III) (27, 28). In addition to iron, DPKBH will also complex other metal ions such as cobalt, copper, nickel and zinc (27). However, the concentrations of these metals in most atmospheric water systems are several orders of magnitude lower than Fe and thus are unlikely to cause interferences (29, 30).

We investigated the use of DPKBH both with and without a preconcentration procedure in order to cover a wide range of Fe concentrations. In order to test our procedures with atmospheric water samples, cloudwater samples from the Los Angeles basin were collected and iron(II) and labile iron(III) {iron(III) that is not complexed strongly (stability constant < 10^{10}) with any ligands present in cloudwater and iron(III) that is not in particulate form} concentrations were measured using the DPKBH reagent in real time.

Experimental

Cloudwater samples were collected from San Pedro Hill, which is the easternmost hill (elevation 450 m) of the ridge that forms the Palos Verdes Peninsula (31). The samples were collected using the Caltech Active Strand Cloudwater Collector (CASCC) (32). The sampling time was usually between 10-25 minutes and the iron(II) and iron(III) analysis was performed within 2 minutes of collection. "Short cut" samples were also taken. "Short cut" refers to sampling in the middle of the longer sampling, in which case sampling lasted for 2-3 minutes to collect enough water only for the iron analysis by DPKBH.

The synthesis of DPKBH was performed according to the procedure outlined by Garcia-Vargas et al. (27). Equimolar amounts of di-2-pyridyl ketone and benzoylhydrazide

were mixed in ethanol and a few drops of concentrated hydrochloric acid were added. The mixture was refluxed for one hour and after cooling distilled water was added to 1:3 volume ratio (volume organic : volume water). Several drops of sodium hydroxide solution were added to the refluxed solution to increase the pH up to ~ 5. The resulting precipitate was collected on a Büchner funnel and recrystallized twice from an ethanol-water solution. After synthesis, the melting point of the product (130-132 °C), and the absorption spectrum of its complex with iron were checked and compared with the reported values. The absorption spectrum of DPKBH is shown in Figure 1. The maximum absorbance of the Fe(II)-DPKBH complex was measured at 390 nm and at 680 nm (Figure 2a) and the maximum absorbance of the Fe(III)-DPKBH complex was measured at 390 nm (Figure 2b).

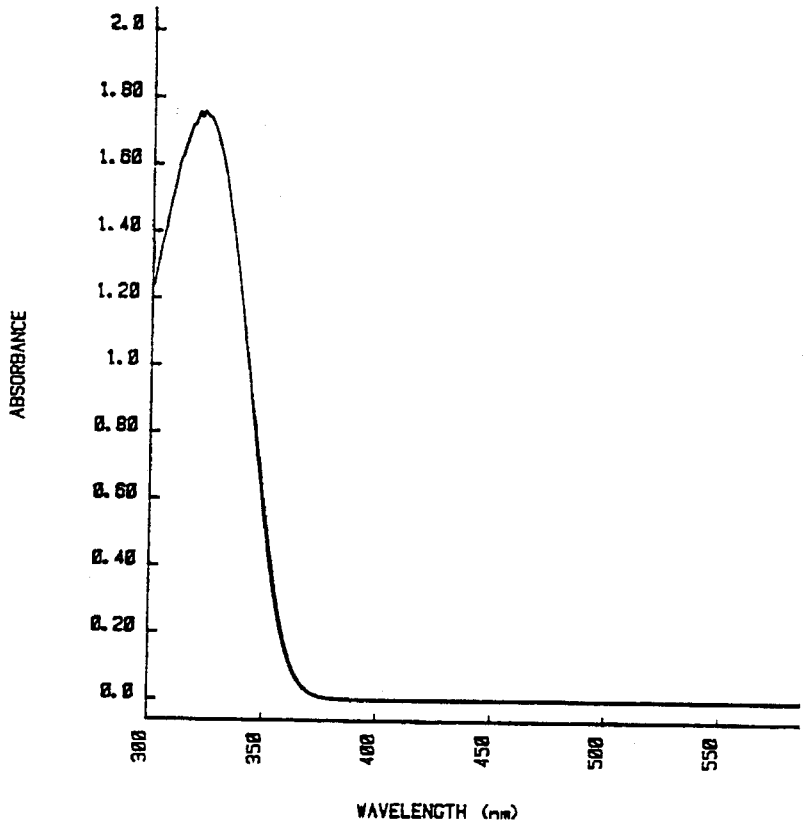

Figure 1: Absorption spectrum of 7.5 mM of DPKBH in 50 % ethanol using a 1 cm cell at pH 5.

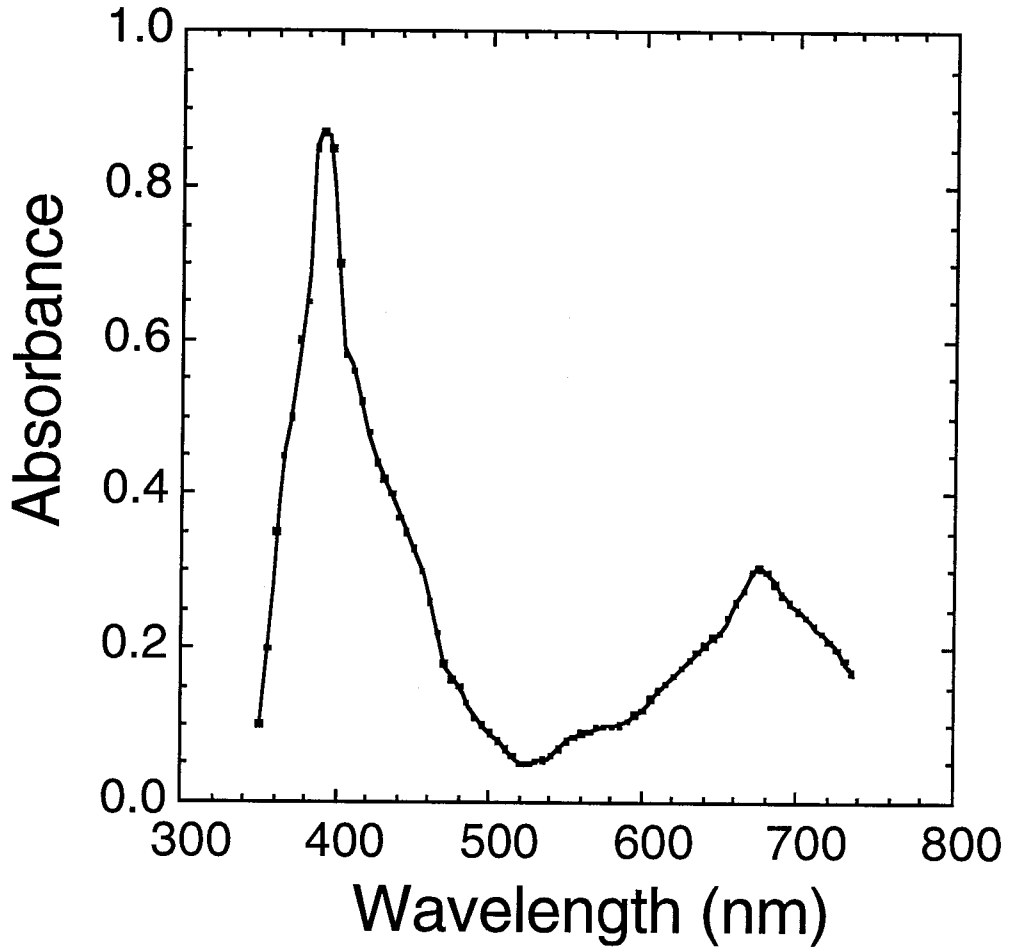

Figure 2a: Absorption spectrum of Fe(II)-DPKBH in $CHCl_3$ at pH=5 and 1-cm cell with a [Fe(II)] = 25 μM, ε(390 nm) = 3.6 x 10^4 M^{-1} cm^{-1}.

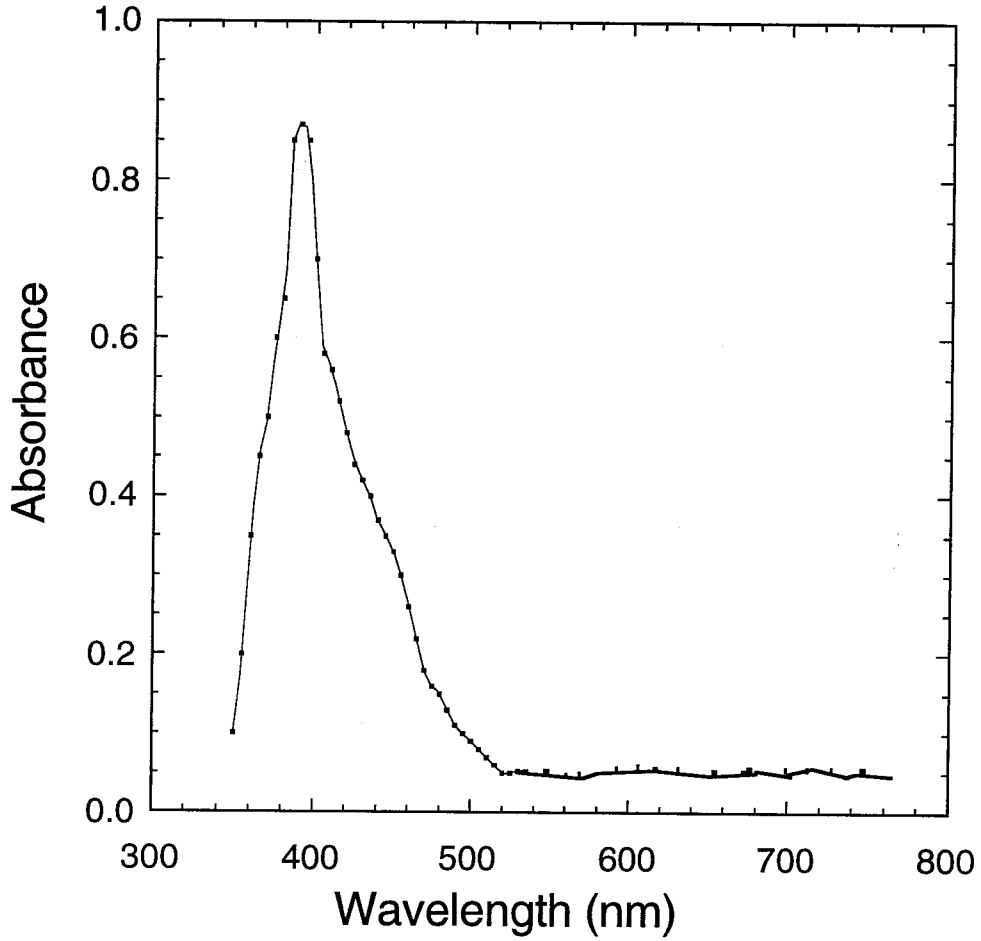

Figure 2b: Absorption spectrum of Fe(III)-DPKBH in $CHCl_3$ at pH=5 and 1-cm cell with a [Fe(III)] = 25 μM, ε(390 nm) = 3.6 x 10^4 M^{-1} cm^{-1}.

The preconcentration step is based on a liquid-liquid extraction using chloroform and water. This step relies upon the higher solubility of iron-DPKBH complexes in chloroform (50 g L^{-1}) than in water (0.2 g L^{-1}) (27). The ratio of water to chloroform in the extraction procedure was 35. This ratio was a compromise between the need for the highest ratio possible (most effective preconcentration), and the solubility of chloroform in water. The ratio was determined by several experiments with differing ratios. The actual volumes of water and chloroform used were 400 ml and 11.5 ml, respectively. The volume of chloroform must be large enough to account for the solubility of chloroform in water and also to allow enough solution for the measurement of absorbance (approximately 8 ml of solution in a 5-cm cell). In the extraction procedure, 400 ml of iron(II) solutions (using a ferrous ammonium sulfate salt) at different concentrations were prepared with deoxygenated water and immediately following this preparation, 11.5 ml of chloroform solution containing 0.08 g of DPKBH per 100 ml was added to each iron solution. After this step, the bottles containing the above solutions were shaken for two minutes to ensure a complete chelation of iron, the water was decanted and the remaining water-chloroform mixture was separated using a separatory funnel. The water phase was discarded and the chloroform phase was saved for the spectrophotometric analysis. In order to reduce contamination, only CPE (conventional polyethylene) and Teflon® ware, cleaned according to the procedures outlined by Patterson and Settle (33), were used in this process. The determination of Fe using DPKBH complexation without a preconcentration procedure was done by mixing the aqueous sample with a known amount of ethanol to ensure complete dissolution of the Fe-DPKBH complexes (28).

According to Zatar et al. (28) the maximum absorbance of Fe-DPKBH complexes occurs in the pH range 4 to 7. No buffer was used in the liquid-liquid extraction of both standards and field samples, since the pH of the chloroform phase was always ~ 5.5. However, in the case of the ethanol-water mixture (both in standards and field samples) a

small amount of a 10% solution of ammonium acetate was added in order to increase the pH of the samples from 2-4 (urban fog samples (4)) to approximately 6.5. The amount of iron contamination from ammonium acetate salt was such that addition of 0.25 ml of the 10% NH_4OAc solution to 12 ml of solution resulted in an iron concentration of 10^{-7} M.

The wavelengths that were used in the ethanol-water solution {6 ml EtOH, 5 ml of sample, 0.75 ml of 22 mM DPKBH (0.15 g in 25 ml EtOH), 0.25 ml buffer} were 370 nm for both Fe(II)-DPKBH and Fe(III)-DPKBH and 660 nm for Fe(II)-DPKBH only. These wavelengths are in agreement with previous results (27, 28). In chloroform (pH ~ 5), the wavelengths of maximum absorbance shifted to 390 and 680 nm, respectively, since the less polar chloroform caused a bathochromic shift in the wavelengths of maximum absorbance (Figure 2). The detection limit was defined as three times the standard deviation of the reagent blank reading at both wavelengths. The iron(III) concentration was found by subtracting the iron(II) concentration measured at λ = 660 or 680 nm from the $iron_{total}$ concentration measured at λ = 370 or 390 nm. The complexation of Fe with DPKBH is complete within one minute of addition of DPKBH. The ratio of Fe(III)/Fe(II) does not affect the response for Fe(II) or Fe(III) as long as DPKBH is in excess, which is confirmed by a few experiments in our laboratory using solutions containing ferric chloride and ferrous ammonium sulfate and by experiments by Zatar et al. (28). The reason for the relatively high concentration of DPKBH in the samples and standards (1.4 or 2.9 mM) is to minimize the effect of potential natural organic chelators that may be present and bind some of the iron in cloudwater. As discussed below, S(IV) and oxalate, which are present in cloudwater, are possible reductants of iron(III) and therefore the absorbance readings of iron-DPKBH complex should be taken between two to five minutes after collection. A Shimadzu UV-1201 portable spectrophotometer with a 5-cm cell was used in the liquid-liquid extraction procedure and a Hewlett-Packard 8451A diode array spectrophotometer with a 1-cm cell was used in the ethanol-water procedure.

Results and Discussion

Calibration curves

With a 5-cm cell and the liquid-liquid extraction procedure, the detection limit is 4 nM (three times STD of blank) of iron(III) and iron(II) at λ = 390 and 680 nm and the range of linear response is from 4 nM up to 0.1 μM, as can be seen in Figure 3. Above 0.1 μM, the DPKBH-iron in ethanol-water solution has a linear response up to 30 μM (Figure 4), thus making the DPKBH chelation method capable of measuring iron(II) and labile iron(III) concentrations from 4 nM to 30 μM. In chloroform the effective extinction coefficients of both Fe(III)-DPKBH and Fe(II)-DPKBH at 390 nm are 3.3×10^4 L mol^{-1} cm^{-1} and the effective extinction coefficient of Fe(II)-DPKBH at 680 nm is 1.1×10^4 L mol^{-1} cm^{-1} in the range of 4×10^{-9} to 1×10^{-7} M (Figure 3a, b). The extinction coefficients in Figure 3a, b (the value of the slopes of the best-fit lines) involving liquid-liquid extraction are 175 times larger than the above values due to the preconcentration factor of 35 and the use of a 5-cm cell. In ethanol-water the effective extinction coefficients of both Fe(III)-DPKBH and Fe(II)-DPKBH at 370 nm are 3.6×10^4 L mol^{-1} cm^{-1} and the effective extinction coefficient of Fe(II)-DPKBH at 660 nm is 1.1×10^4 L mol^{-1} cm^{-1} in the range of 0.1 μM to 30 μM (Figure 4a, b). The values of extinction coefficients in Figure 4 should be multiplied by 2.45 to account for the dilution involved in the addition of buffer solution, the DPKBH solution and ethanol to the iron standards. The stability constant for the Fe(II)-DPKBH complex in 50% ethanol is 10^9 and the stability constant for the Fe(III)-DPKBH complex in 50% ethanol is 10^8 (28).

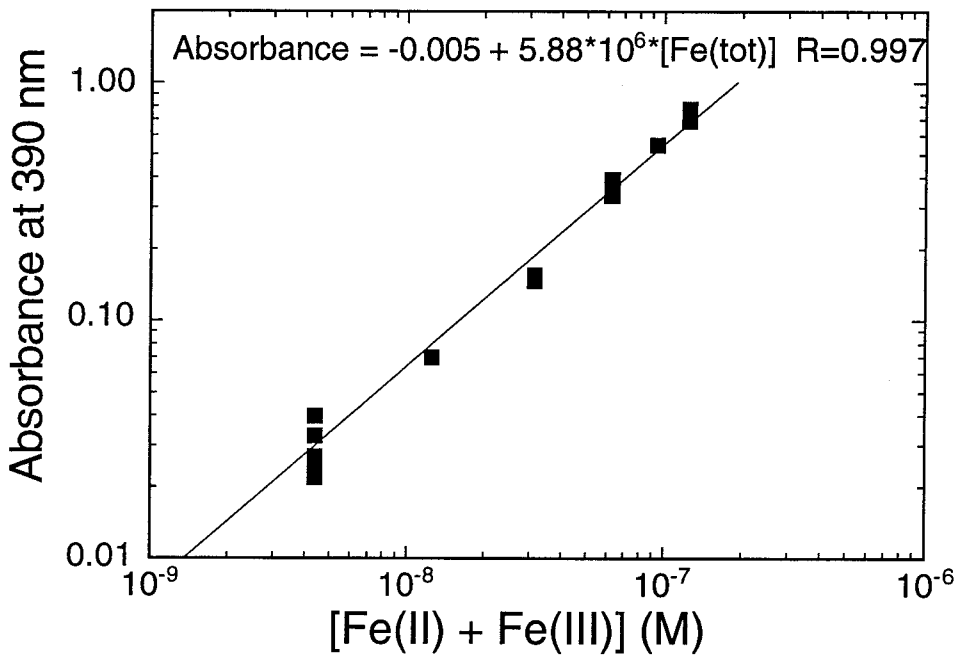

Figure 3a: Calibration curve of DPKBH-Fe complex with the $CHCl_3$-H_2O extraction using a 5-cm cell and 2.9 mM DPKBH at 390 nm, which is the wavelength of maximum absorbance for both Fe(II)-DPKBH and Fe(III)-DPKBH complexes.

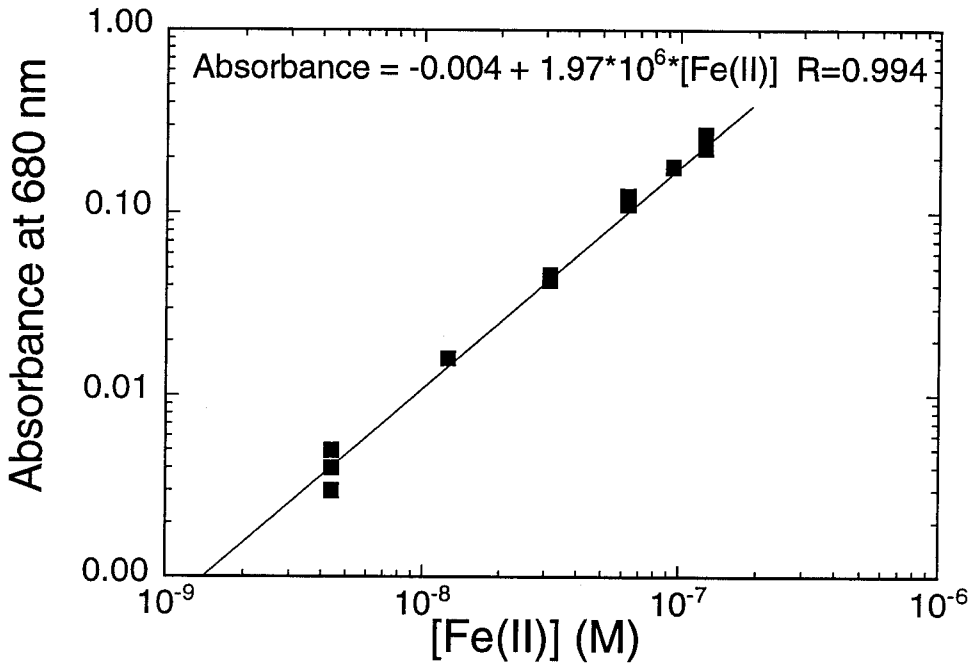

Figure 3b: Calibration curve of DPKBH-Fe complex with the $CHCl_3$-H_2O extraction using a 5-cm cell and 2.9 mM DPKBH at 680 nm, which is the wavelength of maximum absorbance for Fe(II)-DPKBH only (see Figure 2a).

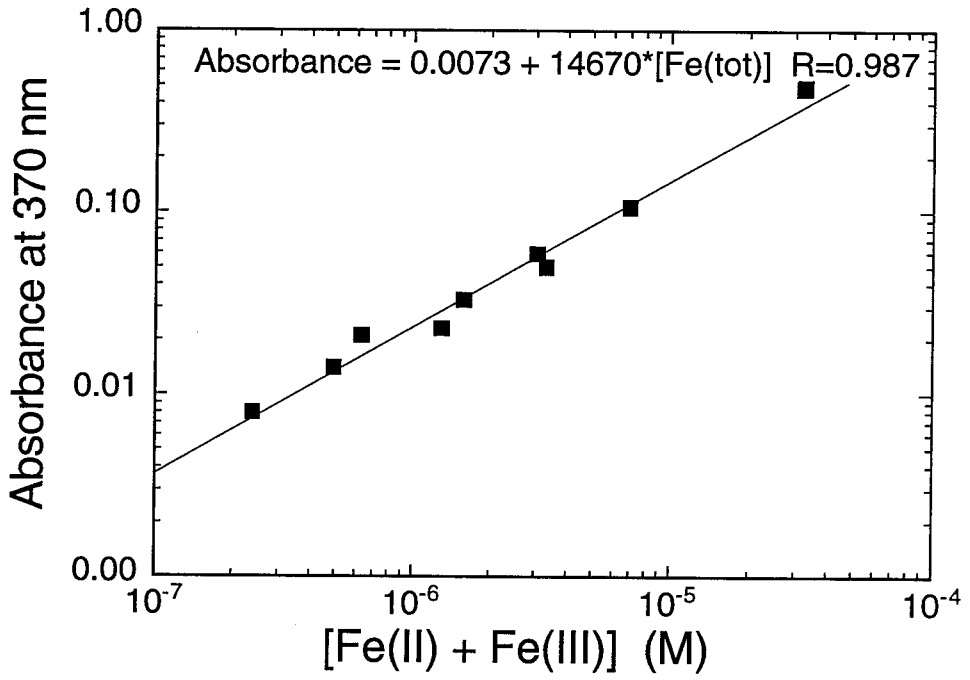

Figure 4a: Calibration curve of DPKBH-Fe complex in ethanol-water using a 1-cm cell and 1.4 mM DPKBH at 370 nm, which is the wavelength of maximum absorbance for both Fe(II)-DPKBH and Fe(III)-DPKBH complexes.

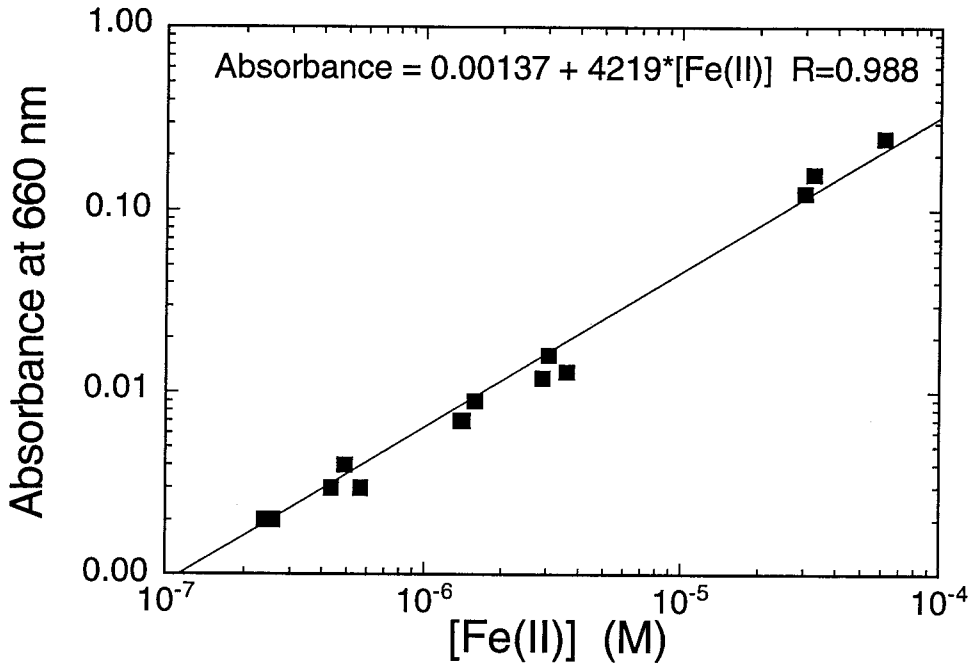

Figure 4b: Calibration curve of DPKBH-Fe complex in ethanol-water using a 1-cm cell and 1.4 mM DPKBH at 660 nm, which is the wavelength of maximum absorbance for Fe(II)-DPKBH only.

Iron(II) and iron(III) concentrations in three field samples were measured using both the liquid-liquid extraction method and the ethanol-water method in order to test the agreement between the two methods (Table 1a). The two methods were in agreement within 10-15%; the agreement in [Fe(II)] was better than in [Fe(III)] values most likely due to the interfering absorbance of the reagent itself in the determination of labile Fe_{total} at 370 nm or at 390 nm, and thus in the determination of iron(III). The concentration of iron(II) and iron(III) by DPKBH in filtered (0.025 μm Millipore® filter) cloudwater samples were also compared with total iron concentration obtained by DCP (direct current plasma spectrometer) (Table 1b) and the difference between the two methods was always less than 10 %. The reproducibility of the extraction technique was investigated and it was found that at 4 nM the standard deviation is ~ 25% and at 0.1 μM the standard deviation is ~ 10% (Table 2).

Sample Description	**[Iron(II)]**	**[Iron(III)]**
Chloroform		
Cloud sample *1* 7-25-91	2.3 μM	0.98 μM
Cloud sample *2* 7-25-91	1.7 μM	0.70 μM
Cloud sample *1* 7-23-91	4.8 μM	1.2 μM
Ethanol-Water		
Cloud sample *1* 7-25-91	2.1 μM	0.89 μM
Cloud sample *2* 7-25-91	1.5 μM	0.63 μM
Cloud sample *1* 7-23-91	4.9 μM	1.4 μM
Ratio ($CHCl_3$/EtOH)		
Cloud sample *1* 7-25-91	1.1	1.1
Cloud sample *2* 7-25-91	1.1	1.1
Cloud sample *1* 7-23-91	0.98	0.86

Table 1a: Comparison between chloroform extraction and ethanol-water method of cloudwater samples.

Sample Description	[Fe(II)+Fe(III)] by DPKBH	[Fe(II)+Fe(III)] by DCP
Cloudwater 1 (5-31-91)	4.5 μM	4.2 μM
Cloudwater 2 (6-11-91)	2.4 μM	2.7 μM
Cloudwater 3 (6-27-91)	3.6 μM	3.3 μM
Cloudwater 4 (7-23-91)	6.3 μM	6.6 μM
Cloudwater 5 (7-25-91)	2.1 μM	2.3 μM

Table 1b: Comparison between DPKBH analysis and DCP of filtered cloudwater samples.

Final Conc.(M)	Abs.(680)	Abs.(390)	Corr.Abs.(680)	Corr.Abs.(390)
blank	0.001	0.195		
6.25E-08	0.113	0.565	0.112	0.370
6.25E-08	0.124	0.544	0.123	0.349
6.25E-08	0.121	0.531	0.120	0.336
6.25E-08	0.115	0.548	0.114	0.353
6.25E-08	0.126	0.586	0.125	0.389
average	**0.120**	**0.555**	**0.119**	**0.359**
std. dev.	**0.006**	**0.021**	**0.006**	**0.021**
RSD	**4.7**	**3.8**	**4.7**	**5.7**
blank	0.001	0.195		
1.25E-07	0.229	0.888	0.228	0.693
1.25E-07	0.231	0.913	0.230	0.718
1.25E-07	0.251	0.962	0.250	0.767
1.25E-07	0.270	0.970	0.269	0.775
1.25E-07	0.240	0.922	0.239	0.727
average	**0.244**	**0.931**	**0.243**	**0.736**
std. dev.	**0.017**	**0.034**	**0.017**	**0.034**
RSD	**6.9**	**3.7**	**6.9**	**4.7**
blank	0.002	0.220		
4.38E-09	0.006	0.242	0.004	0.022
4.38E-09	0.006	0.245	0.004	0.025
4.38E-09	0.007	0.247	0.005	0.027
4.38E-09	0.005	0.260	0.003	0.040
4.38E-09	0.005	0.253	0.003	0.033
average	**0.006**	**0.249**	**0.004**	**0.029**
std. dev.	**0.0008**	**0.007**	**0.0008**	**0.007**
RSD	**14.4**	**2.87**	**22.0**	**24.4**

Corr. Abs. means absorbance adjusted for the reagent blank.

Table 2: Reproducibility of chloroform-water extraction method with three standards.

Interferences

Experiments were carried out with amorphous iron hydroxide particles prepared according to Schwertmann and Cornell (34) to see if DPKBH will form complexes with particulate iron as well as with dissolved iron. Amorphous iron hydroxide was added to a buffered (pH=6.2 by NH_4OAc) 50% ethanol solution containing 1.4 mM DPKBH. The amount of iron hydroxide that was added was equivalent to 300 μM. The solution was continuously shaken and aliquots were withdrawn at various times to see if any iron-DPKBH complexes are present. No iron-DPKBH complexes were observed after six hours of shaking. The experiment was repeated twice more and again no iron-DPKBH complexes were found. The slow kinetics of breaking the bond between Fe and O in am-$Fe(OH)_3$ and thus dissolving Fe(III) is most likely responsible for the absence of the Fe-DPKBH complexes.

The molar extinction coefficients for other important metal-DPKBH complexes are: Zn(II)-DPKBH, 4.4×10^4 L mol^{-1} cm^{-1} (375 nm); Cu(II)-DPKBH, 3.5×10^4 L mol^{-1} cm^{-1} (375 nm) and Ni(II)-DPKBH, 3.7×10^4 L mol^{-1} cm^{-1} (375 nm). These metals can therefore interfere with iron determination at 375 nm if they are present at equivalent concentrations to iron in the system of interest, which is not the case in Los Angeles atmosphere, where Zn concentration is found to be 3% of iron concentration and Cu and Ni concentrations are found to be 2% of iron concentration (30).

Storage Effect

The effect of different chemical species (i. e., possible analytical interferences) on the oxidation state of complexed iron between sampling and analysis was investigated in ethanol-water solutions. The species that were studied are S(IV), oxalate, formaldehyde,

acetaldehyde, formate, acetate (as NH_4OAc buffer), NO_2^- and chloride. All the reagents were A.C.S. grade and contained low concentration of iron (less than 0.0005 % by mass resulting in iron concentration of less than 10^{-8} M in final solution). The solution consisted of 50 ml of 50% EtOH, 0.75 ml of DPKBH reagent (0.15 g DPKBH in 25 ml of EtOH) and appropriate amounts of ligand and Fe(III) {as acidified pH=0.75 solution of 1000 ppm $FeCl_3$}. Immediately before absorbance was measured, 0.2 ml of a 10% NH_4OAc solution was added to increase the pH to ~ 6 in order to reach a maximum absorbance of the iron-DPKBH complex. The initial concentration of Fe(III) in the experiments was 36 μM or 70 μM and the concentration of the added ligands (including the buffer) was 0.1 mM. Among the various possible reductants, S(IV) appeared to reduce iron(III) the fastest. It was found that S(IV) rapidly reduced Fe(III)-DPKBH to Fe(II)-DPKBH at both pH 6.2 and pH 3.5 (Figure 5a) in the presence of light and at a similar rate in the dark (Figure 5a). The rate of reduction was quite different at the two different pH values (Figure 5a) suggesting different mechanisms of reduction in the presence and absence of light. The difference was not necessarily due to the change in pH, but could also be due to the presence of acetate, which was used to increase the pH to 6.2. It is very difficult to separate these two factors (9), since most buffers are also good ligands for metal ions and can therefore affect the rate of redox reactions of the metal. For analytical purposes, it is not crucial to know which process is controlling the rate of the reduction of iron(III), as long as we know that the reduction takes place at both pH values. When the experiments with S(IV) were repeated at pH=3.5 with the addition of HCHO 20-30 minutes prior to the addition of Fe(III), no change in the rate of iron(III) reduction was observed indicating that the S(IV)-HCHO complex does not prevent the reduction of dissolved iron(III) by S(IV) under these experimental conditions (35, 36). Oxalate reduced Fe(III)-DPKBH to Fe(II)-DPKBH in the presence of light, but not in the dark (Figure 5b). Formaldehyde and acetaldehyde reduced only 6% of Fe-DPKBH during a period of a few hours (Figure 5c). Chloride, NO_2^-, formate and acetate (as an NH_4OAc buffer) were added to Fe(III)-

DPKBH solution, but no appreciable change in the iron oxidation state was found (Figure 5d). The ratio of the final iron(II) concentration to the initial iron(III) concentration (i.e., extent of reduction) ranged from approximately zero in the case of Cl^-, NO_2^-, HCO_2^- and $CH_3CO_2^-$ to 0.5 in the case of S(IV) (Figure 5). The rapid reduction of Fe(III) by S(IV) and oxalate indicates that the absorbance readings should be taken immediately after collection and complexation of the samples, if one wants to measure the true oxidation state of iron in the sample at the time of collection. The above reactions are expected to be slower in the case of chloroform extraction, because ionic species as well as carboxylic acids are not very soluble in chloroform and would therefore stay in the aqueous phase. Significant differences in the concentration of iron(II) were observed between "short cuts" as described earlier and longer sampling, up to 80 % more iron(II) were found in the samples that were collected longer.

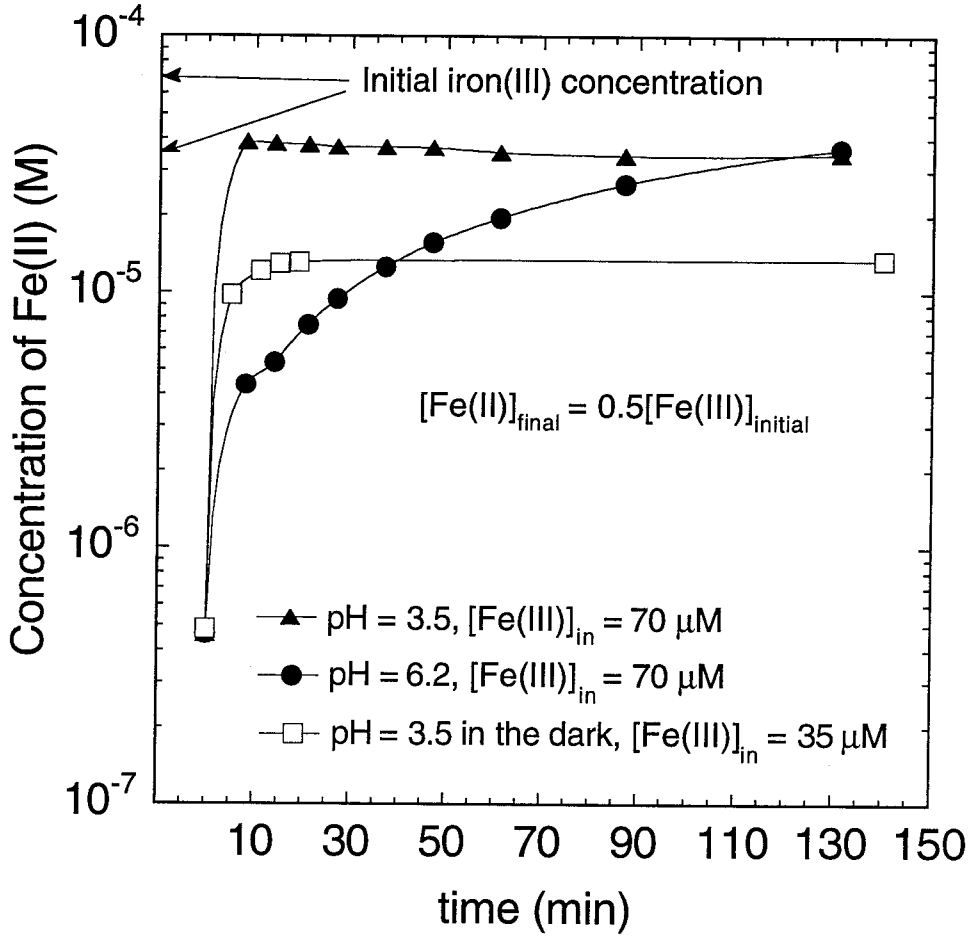

Figure 5a: Spectrophotometric measurements of Fe(II) formed due to the reduction of Fe(III)-DPKBH complex in the presence of 0.1 mM S(IV) at pH=3.5 and pH=6.2 in roomlight and in the dark. Time zero represents the moment of mixing of ligands with Fe(III)-DPKBH solution. Initial Fe(III) concentration is either 35 or 70 μM and is noted in the graphs. Initially, no Fe(II) is present.

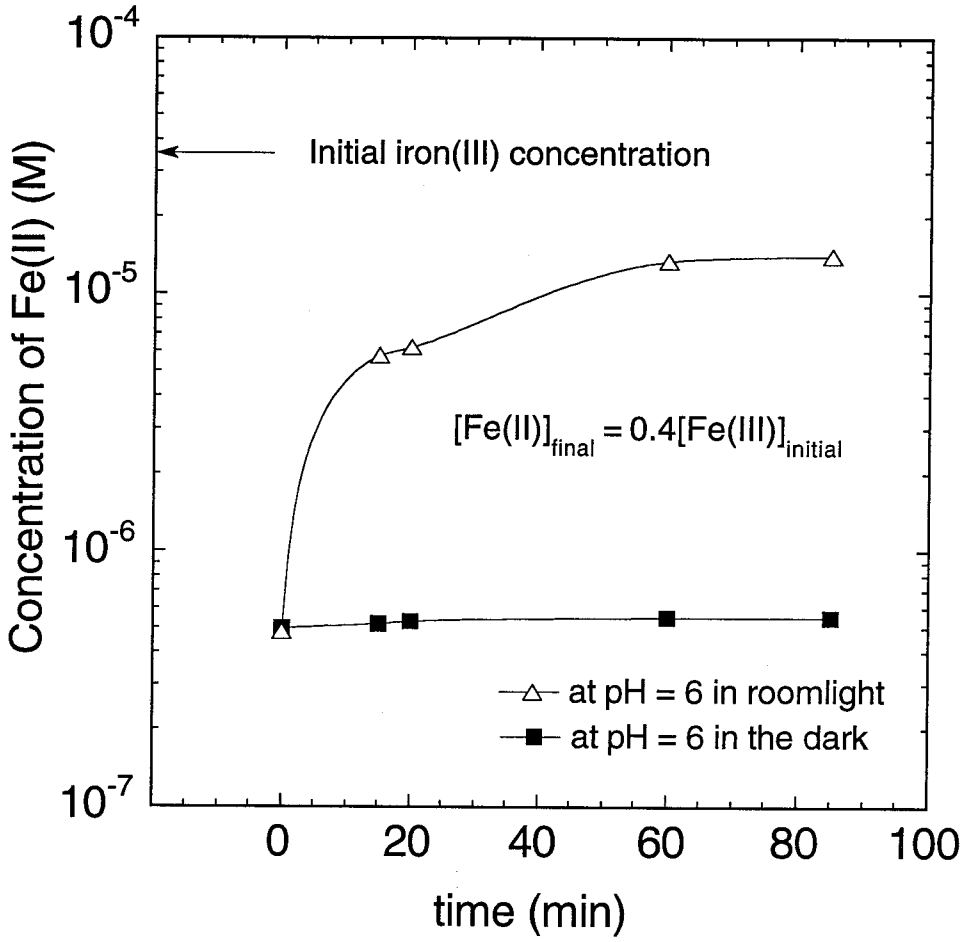

Figure 5b: Spectrophotometric measurements of Fe(II) formed due to the reduction of Fe(III)-DPKBH complex in the presence of 0.1 mM oxalate at pH=6 in roomlight and in the dark. Time zero represents the moment of mixing of ligands with Fe(III)-DPKBH solution. Initial Fe(III) concentration is either 35 or 70 μM and is noted in the graphs. Initially, no Fe(II) is present.

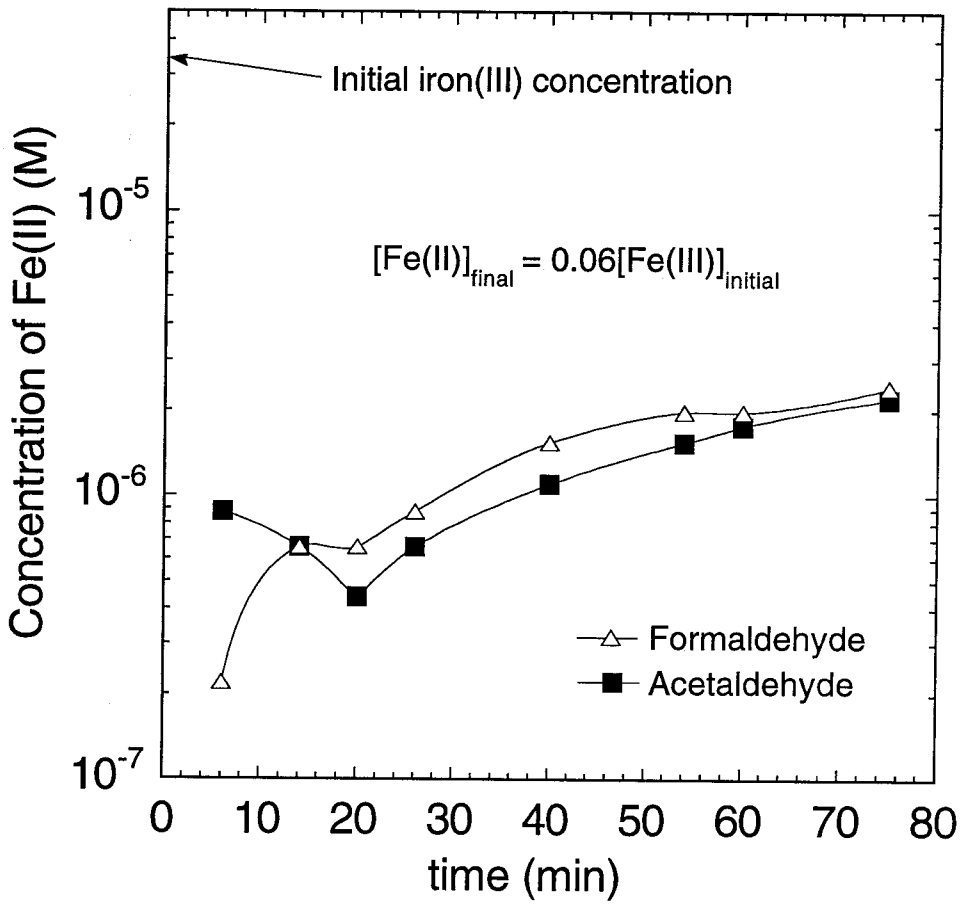

Figure 5c: Spectrophotometric measurements of Fe(II) formed due to the reduction of Fe(III)-DPKBH complex in the presence of 0.1 mM HCHO and acetaldehyde at pH=3.5 in roomlight. Time zero represents the moment of mixing of ligands with Fe(III)-DPKBH solution. Initial Fe(III) concentration is either 35 or 70 μM and is noted in the graphs. Initially, no Fe(II) is present.

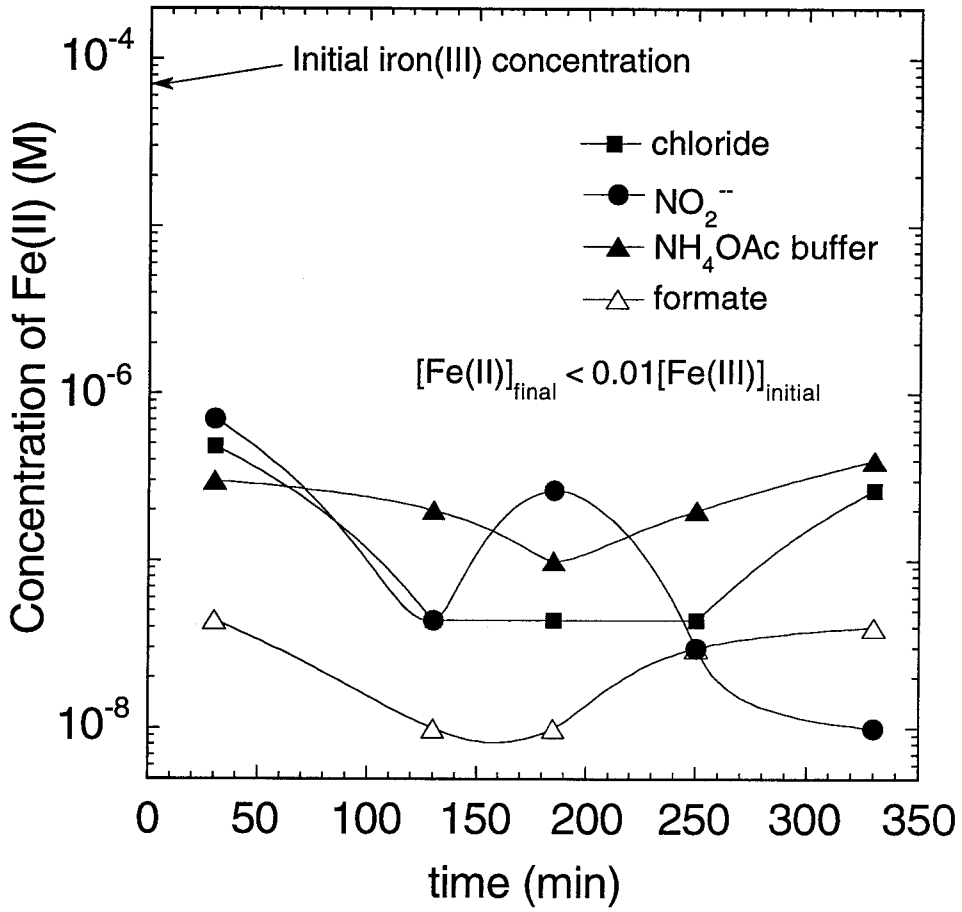

Figure 5d: Spectrophotometric measurements of Fe(II) formed due to the reduction of Fe(III)-DPKBH complex in the presence of 0.1 mM chloride, NO_2^-, formate and NH_4OAc buffer alone at pH=6. Time zero represents the moment of mixing of ligands with Fe(III)-DPKBH solution. Initial Fe(III) concentration is either 35 or 70 μM and is noted in the graphs. Initially, no Fe(II) is present.

Ferrozine, a commonly used chelating agent for iron(II) determination, was also tested with S(IV) and oxalate with no complexing agent for Fe(III) present. The ratio of the final iron(II) concentration to the initial iron(III) concentration was 0.9 in the case of S(IV) and 0.1 in the case of oxalate. The rate of reduction of Fe(III) to Fe(II) by oxalate was similar with Ferrozine and DPKBH. However, since Ferrozine does not chelate iron(III), addition of S(IV) to a solution of Fe(III) and Ferrozine resulted in an instantaneous reduction of Fe(III) to Fe(II). The reduction of Fe(III) in this case was faster than with DPKBH since it took around four minutes for the reduction of 50% of Fe(III) to Fe(II) by S(IV) in the presence of DPKBH (Figure 5a). This indicates that DPKBH is better suited for the determination of oxidation state of iron in systems with high S(IV) concentration and it can also explain the high iron(II) concentrations found by Hong and Kester (24), because Ferrozine was used in this study with significant oxidizable sulfur concentrations present in the samples. When the experiments of Ferrozine and S(IV) were repeated with EDTA present in solution, no reduction of iron(III) was observed during a period of a few hours.

Conclusions

The DPKBH technique can be very helpful in determining the role of iron in the complicated redox chemistry of many natural water systems. A spectrophotometric detection limit of 4 nM for both Fe(III) and Fe(II) with a linear response from 4 nM up to 0.1 μM was established for samples extracted with $CHCl_3$-H_2O. The DPKBH method is the only available method to measure simultaneously both iron(II) and iron(III) in a variety of natural water samples such as river water, groundwater and lake water in addition to atmospheric water. This method might be especially useful in high pH systems where reoxidation of Fe(II) to Fe(III) occurs on a short time scale. Our interference studies with S(IV), oxalate, formaldehyde, acetaldehyde, chloride, nitrite, formate and acetate suggest,

that possible fast redox reactions involving iron should always be taken into consideration when measuring iron oxidation state in natural water systems.

Acknowledgments

This work was supported by a grant ATM-9015775 from the National Science Foundation, Division of Atmospheric Sciences, Atmospheric Chemistry Section and the authors wish to thank R. L. Siefert for participation in the fog sampling and Prof. J. Morgan for helpful discussions.

References

1. Taylor, S. R.; McLennan, S. M. "The Continental Crust: its Composition and Evolution," Blackwell Scientific Publications: Palo Alto, **1985**, 46.

2. Cotton, F. A.; Wilkinson, G."Advanced Inorganic Chemistry," Wiley Interscience: New York, **1988**, 868.

3. Martin, J. H.; Gordon, R. M.; Fitzwater, S. E. *Nature* , **1990**, *344*, 156.

4. Munger, J. W.; Waldman, J. M.; Jacob, D. J.; Hoffmann, M. R. *J. Geophys. Res.*, **1983**, *88*, 5109.

5. Martin, J. H.; Fitzwater, S. E. *Nature,* **1988**, *321*, 341.

6. Martin, J. H.; Gordon, R. M.; Fitzwater, S. E.; Broenkow, W. W. *Deep-Sea Res. Part A- Ocean. Res. Pap.*, **1989**, *36*, 649.

7. Hudson, R. J. M.; Morel, F. M. M. *ABS-PAP-ACS* **1989**, *198*, 99.

8. Conklin, M. H.; Hoffmann, M. R. *Environ. Sci. Technol.*, **1988**, *22*, 899.

9. Martin, L. R.; Hill, M. W.; Tai, A. F.; Good, T. W. *J. Geophys. Res.*, **1991**, *96*, 3085.

10. Faust, B. C.; Hoffmann, M. R. *Environ. Sci. Technol.*, **1986**, *20*, 943.

11. Littler, J. S.; Sayce, I. G. *J. Chem. Soc.*, **1964**, *96*, 2445.

12. Behra, P.; Sigg, L. *Nature* , **1990**, *344*, 419.

13. Zhuang, G.; Zhen, Y.; Duce, R. A. *Nature* , **1992**, *355*, 537.

14. Landing, W. M.; Westerlund, S. *Mar. Chem.*, **1988**, *23*, 329.

15. McKnight, D. M.; Kimball, B. A.; Bencala, K. E. *Science* , **1988**, *240*, 637.

16. Tsuchiya, M.; Iwanami, Y. *Anal. Sci.*, **1990**, *6*, 701.

17. Zhang, G.; Yang, H.; Wu, H. *Lihua Jianyan, Huaxue Fence,* **1990**, *26*, 3.

18. Wang, Z.; Yao, C.; Cheng, K. L. *Mikrochim. Acta,* **1990**, *3*, 311.

19. Sun, T.; Han, Y.; Wang, J.; Ma, Y.; Zhang, Y. *Shanxi Daxue Xuebao, Ziran Kexueban,* **1990**, *13*, 292.

20. Stookey, L. L. *Anal. Chem.*, **1970**, *42*, 119.

21. Carter, P. *Anal. Biochem.*, **1971**, *40*, 450.

22. Xu, M.; Pan, Z.; Zhou, D.; Li, J. *Fenxi Huaxue,* **1990**, *18*, 863.

23. Vijayakumar, D.; Hussain, R. C.; Raju, N. A. *J. Indian Chem. Soc.,* **1990**, *67*, 786.

24. Hong, H.; Kester, D. R. *Limnol. Oceanogr.,* **1986**, *31*, 512.

25. Crumbliss, A. L.; Garrison, J. M.; Bock, C. R.; Schaaf, A.; Bonaventura, C. J.; Bonaventura, J. *Inorg. Chim. A.,* **1987**, *133*, 281.

26. Elrod, V. A.; Johnson, K. S.; Coale, K. H. *Anal. Chem.,* **1991**, *63*, 893.

27. Garcia-Vargas, M.; Belizon, M.; Hernandez-Artiga, M. P.; Martinez, C.; Perez-Bustamante, J. A. *A. Spectroscopy,* **1986**, *40*, 1058.

28. Zatar, N. A.; Abu-Zuhri, A. Z.; Al-Nuri, M. A.; Mahmoud, F. M.; Abu-Obaid, A. A. *Spec. Letters,* **1989**, *22*, 1203.

29. Church, T. M.; Veron, A.; Patterson, C. C.; Settle, D.; Erel, Y.; Maring, H. R.; Flegal, A. R. *Global Biogeochemical Cycles,* **1990**, *4*, 431.

30. Cass, G. R.; McRae, G. J. *Environ. Sci. Technol.,* **1983**, *17*, 129.

31. Munger, J. M.; Collett, J.; Daube, B. C.; Hoffmann, M. R. *Atmos. Environ.,* **1989**, *23*, 2305.

32. Daube, B. C.; Flagan, R. C.; Hoffmann, M. R. *United States Patent No. 4697462,* 1987.

33. Patterson, C. C.; Settle, D. M. *National Bureau of Standards, Special Publication,* **1976**, *422*, 321.

34. Schwertmann, U.; Cornell, R. M. "Iron Oxides in the Laboratory: Preparation and Characterization," VCH: Weinheim, Germany, **1991**, 91.

35. Boyce, S. D.; Hoffmann, M. R. *J. Phys. Chem.,* **1984**, *88*, 4740.

36. Olson, T. M.; Hoffmann, M. R. *Atmos. Environ.*, **1989**, *23*, 985.

Chapter 4

Stability, Stoichiometry And Structure Of Fe(II) And Fe(III) Complexes With Di-2-Pyridyl Ketone Benzoylhydrazone: Environmental Applications

[M. E. V. Suarez Iha, S. O. Pehkonen, M. R. Hoffmann, accepted in Environmental Science and Technology, 1994]

Abstract

The stoichiometry, structure and thermodynamics of Fe(II) and Fe(III) complexes of di-2-pyridyl ketone benzoylhydrazone (DPKBH) were studied at pH 5.3 and 25.0 °C in water-ethanol solutions. The spectrophotometric method of corresponding solutions was used to obtain overall formation constants for the 1:1 ($\beta_1 = 4.693 \times 10^6\ M^{-1}$) and 1:2 ($\beta_2 = 2.195 \times 10^{10}\ M^{-2}$) $Fe(III)(H_2O)_6^{3+}$-DPKBH complexes and 1:1 ($\beta_1 = 1.217 \times 10^5\ M^{-1}$) and 1:2 ($\beta_2 = 7.814 \times 10^9\ M^{-2}$) $Fe(II)(H_2O)_6^{2+}$-DPKBH complexes. Conductance and pH titrations indicate that DPKBH coordinates preferentially as an anion, while FTIR analysis shows that DPKBH exists in the enol form and exhibits tridentate ligand behavior. DPKBH has been shown to be a useful analytical reagent for the simultaneous spectrophotometric determination of Fe(II) and Fe(III) in natural waters.

$$Fe(H_2O)_6^{3+} + DPKBH \overset{\beta_1}{\rightleftharpoons} Fe(H_2O)_3(DPKBH)^{3+} + 3\ H_2O$$

$$Fe(H_2O)_6^{3+} + 2\ DPKBH \overset{\beta_2}{\rightleftharpoons} Fe(DPKBH)_2^{3+} + 6\ H_2O$$

Introduction

Iron (i.e., as an iron-sulfur electron transfer protein, ferredoxin) plays an essential role in photosynthesis (1-4), and is a limiting growth nutrient for phytoplankton growth in some regions of the open ocean (5-8) and plays a central role in the biosphere serving as an active center of a wide range of proteins such as oxidases, reductases and dehydrases (9). Microbial processes that result in the reduction of Fe(III), such as the dissimilative iron reduction by the marine eubacterium Alteromonas-Putrefaciens strain-200 (10), are also important pathways for the fate of Fe(III). Siderophores and some humic and fulvic acids may be important ligands for Fe(III) in surface and groundwaters (11). Fe(III) complexes have been shown to be effective catalysts for the heterogeneous autoxidation of SO_2 in cloudwater (12-14). In some cases, Fe(III) complexes act as terminal electron acceptors for reduced sulfur compounds and carbonyl compounds in haze aerosols, fogs and clouds (13-16).

Most often the analysis of iron in natural water samples has been limited to the determination of total dissolved and suspended concentrations. In several studies, the distribution of Fe between the Fe(II) and Fe(III) states has been determined (17-20). The determination of the oxidation state of iron in a variety of samples is often achieved by complexation with specific chelating agents followed by spectrophotometric measurement. Several chelating agents have been developed specifically for iron(II) determination in metal alloys (21, 22), water (23) and graphite (24). Ferrozine {3-(2-pyridyl)-5,6-diphenyl-1,2,4-triazine-p,p'-disulfonic acid, monosodium salt monohydrate} as used originally by Stookey (25) and Carter (26) is the most common chelating agent used for Fe(II) determination in natural water and blood serum samples. However, Ferrozine has been found to reduce Fe(III) to Fe(II) in a variety of environmental samples unless care is taken to protectively complex iron(III) (e.g., fluoride (17)). In a previous study (27), we

successfully determined the simultaneous concentrations of Fe(II) and Fe(III) in cloudwater samples using di-2-pyridyl ketone benzoylhydrazone (DPKBH) as a dual chelating agent. Our spectrophotometric technique with chloroform-water extraction and a wavelength of maximum absorbance of 390 nm for the Fe(II)-DPKBH and Fe(III)-DPKBH complexes and a wavelength of maximum absorbance of 680 nm for the Fe(II)-DPKBH complex resulted in detection limits as low as 4 nM. Application of this spectrophotometric procedure depends on a knowledge of the fundamental thermodynamic properties of the Fe(III)- and Fe(II)-DPKBH complexes (28-30). In a previous study, Zatar et al. (30) determined the stability constants of Fe(III)-DPKBH and Fe(II)-DPKBH complexes. Unfortunately, the determination was carried out in high concentrations of a competing ligand, acetate, which has resulted in erroneous values. A direct knowledge of the formation constants of a chelating agent such as DPKBH is important, since most natural waters contain a variety of organic acids that can also form weak to moderately strong complexes with Fe. For example, in atmospheric water oxalate, acetate and formate exist at appreciable concentrations in a range that may result in the complexation of greater than 90% of the total Fe(III) (31). In light of the potential application of DPKBH complexation for the determination of redox state of iron in natural waters, we report on the determination of the formation constants for Fe(III) / DPKBH and Fe(II) / DPKBH complexes, and on the determination of the stoichiometry of the Fe(III)/DPKBH complex.

Experimental

The synthesis of DPKBH (I) was performed according to the procedure outlined by Garcia-Vargas et al. (28). Equimolar amounts of di-2-pyridyl ketone and benzoylhydrazide were mixed in ethanol, and few drops of concentrated hydrochloric acid were added. The mixture was refluxed for 1 hour, and after cooling, distilled water was added to a 1:3 volume ratio (organic to water volume). Sodium hydroxide solution was added to the

refluxed solution to increase the pH up to ≈ 5. The resulting precipitate was collected on a Büchner funnel and recrystallized twice from an ethanol-water solution. The melting point of the product (I) (130 - 132°C) and the absorption spectrum of its complex with iron(II) were checked and compared with previously reported values (27). The complexes of Fe(II) with DPKBH are characterized by two absorption maxima at 380 and 660 nm in 50% ethanol. Solutions of DPKBH (≈ 10 mM) were prepared by dissolving the reagent in ethanol.

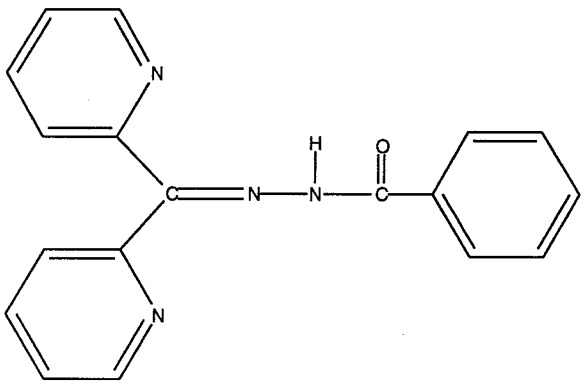

I

Solid samples of the Fe(III)-DPKBH complexes were obtained by adding DPKBH to a small volume of $Fe(H_2O)_6^{3+}$ solution in 50% ethanol followed by slow evaporation of the solvent to yield yellow-brown crystals. The FTIR spectra (4000 - 500 cm-1 ; KBr disks) were recorded on a Perkin-Elmer 1600 Series FTIR instrument.

All spectrophotometric measurements were carried out on a Hewlett-Packard (HP) Diode Array Spectrophotometer 8450 A using a HP temperature controller (Peltier system)-98100A to maintain T = (25.0 ± 0.1) °C. The precision of the absorbance measurements in 1.0 cm cells was ± 0.002 units; the photometric scale was tested according to the method recommended by Haupt (32). The mean relative error did not exceed one per cent for the absorbance scales used in this study. A wavelength of 410 nm was selected for Fe(III)-

DPKBH in order to minimize the contribution of the ligand to the total absorbance and a wavelength of 660 nm was selected for the determination of Fe(II)-DPKBH formation constants. The absorbance of three series of solutions with 30.5, 61.2 and 91.6 μM iron(III) and 21.0, 42.0 and 66.0 μM iron(II) was measured at several different ligand (DPKBH) concentrations in 50% ethanol-water. In an initial set of experiments, the ionic strength was adjusted to 0.1 M with sodium perchlorate but interference due to ClO_4^- was observed. Thus, no perchlorate was added. The resulting ionic strength of the solutions in the absence of added salts was 1.0 mM. The pH of the reaction mixtures was maintained at 5.3 ± 0.1 with NaOH. Buffers were not used in order to avoid competitive complexation with Fe(III).

The potentiometric measurements were performed on a Beckman 71 digital potentiometer with a Beckman 39534 combination glass electrode with Ag-AgCl reference electrode. The electrode was calibrated with pH 4 and pH 7 buffers at 25 °C. Conductance measurements were made on a YSI Scientific model 35 conductance meter with a cell constant K of 1.0 cm^{-1}.

A standard solution of iron(III) perchlorate (≈ 10 mM) was prepared by dissolving reagent-grade iron(III) perchlorate in water and perchloric acid. The final pH was adjusted to 1.9. The iron(III) concentration was determined by titration (33) with a standard EDTA solution in the presence of variamin. Blue indicator. Iron(II) solutions were prepared by dissolving ferrous ammonium sulfate and standardized by oxidizing the iron(II) to iron(III) (addition of H_2O_2) and measuring the iron(III) concentration with the above method.

The order of addition of the reagents was found to be critical in the case of Fe(III) complexation. Best results and higher absorbance values were obtained by addition of reagents in the following order: $Fe^{III}aq$, DPKBH, ethanol and H_2O to bring the solution

up to the desired volume. After thorough mixing, NaOH was added to adjust the pH. With this procedure, hydrolysis of Fe(III) to form am-$Fe(OH)_3$ was avoided.

Results and Discussion

Determination of Stability Constants

The complexes of Fe(III) with excess of DPKBH show a maximum absorbance at $\lambda = 360$ nm (Figure 1), while the corresponding Fe(II) complexes show a maximum at $\lambda =$ 660 nm. However, absorbance at $\lambda = 410$ nm was used for subsequent data analysis of the Fe(III)-DPKBH complexes, since DPKBH contributes to the total absorbance at $\lambda =$ 360 nm but not at $\lambda = 410$ nm.

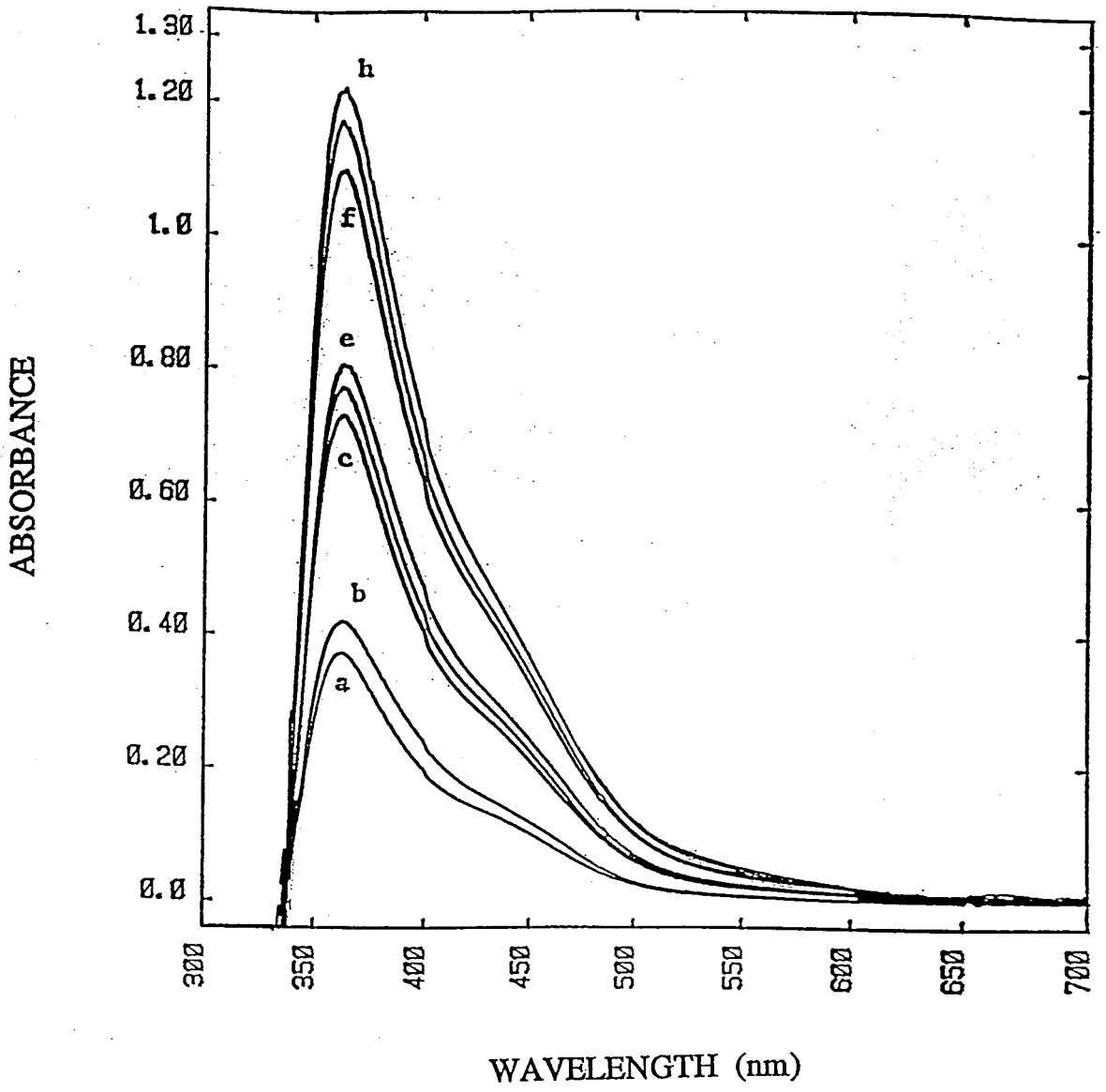

Figure 1: Absorption spectra of Fe(III) / DPKBH solutions in ethanol (50 %) at pH = 5.3 ± 0.1 with a pathlength of 1 cm.

Fe(III) / μM	DPKBH / μM
30.54	a - 41.45 ; b - 165.6
61.24	c - 82.97 ; d - 124.3 ; e - 207.3
91.61	f - 124.3 ; g - 165.6 ; h - 207.3

In order to obtain the stability constants of the complexes formed by Fe(III) and DPKBH, A was measured at $\lambda = 410$ nm for different total metal concentrations with variable ligand-to-metal ratios. Median molar absorptivities were obtained as follows:

$$\bar{\varepsilon} = \frac{A}{C_{Fe}.b} \quad (1)$$

where A is the measured absorbance, C_{Fe} is the analytical molar concentration of Fe(III) and b is the pathlength (cm) of the spectrophotometric cell.

Figure 2 shows the data obtained for three representative Fe(III) concentrations: 30.5; 61.2 and 91.6 μM. As illustrated in Fig. 2, the median molar absorptivities increased up to a 1:2 metal/ligand molar ratio. Given these favorable changes in the absorbance with variable metal and ligand concentrations, we employed the spectrophotometric method of corresponding solutions (34-36) to determine overall stability constants.

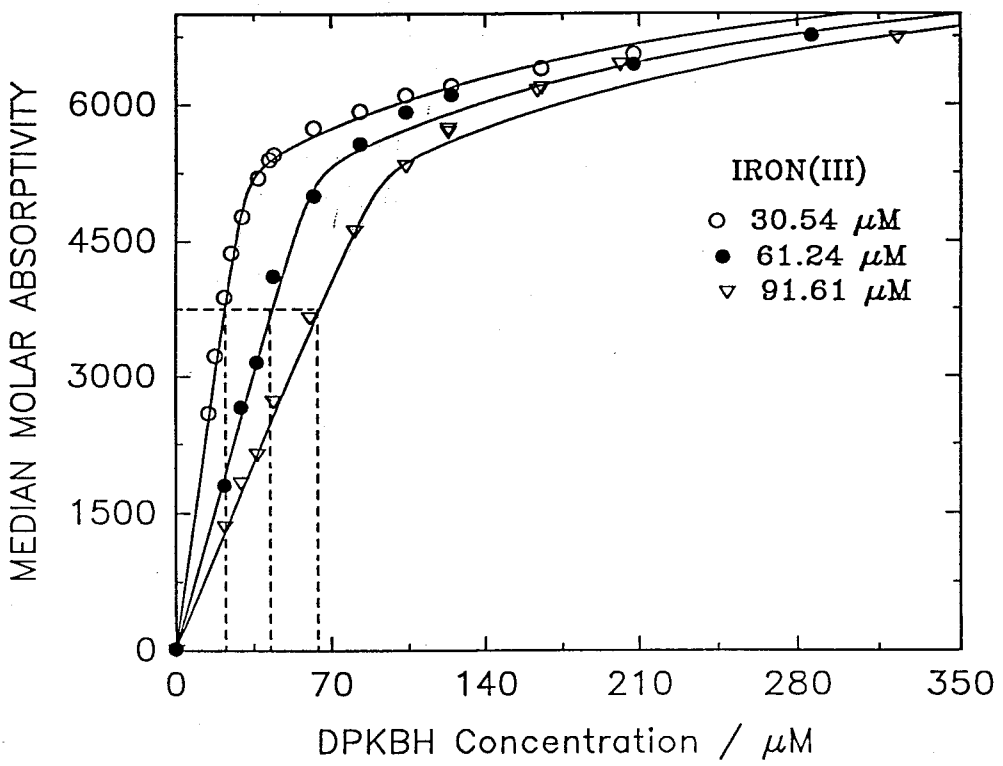

Figure 2: Experimental data of median molar absorptivities vs. analytical concentrations of DPKBH for Fe(III) at three different concentrations. Calculated curves from stability constants and individual molar absorptivities. An example of three corresponding solutions is showed by the dashed lines.

With the available experimental data ($\bar{\varepsilon}$, C_M and C_L), the average ligand number, $\bar{n}$, and the free-ligand concentrations, [DPKBH], were determined according to eq. 2 in which a plot of C_{DPKBH} *vs.* C_{Fe} should yield a straight line with an intercept that corresponds to the free ligand concentration and a slope that corresponds to the $\bar{n}$ value.

$$C_{DPKBH} = [DPKBH] + \bar{n}\ C_{Fe} \qquad (2)$$

We then plot $\bar{n}$/[L] *vs.* [L] ([DPKBH]) as shown in Fig. 3. Integration by the trapezoidal rule of $\bar{n}$/[L] *vs.* [DPKBH] gives the following functional relationship (37):

$$\ln \frac{F_o(L)}{F_o(L)_o} = \int_0^{[L]} \frac{\bar{n}}{[L]}\, d[L] \qquad (3)$$

where the limit as [L] $\rightarrow$ 0 of the function in eq. 3 yields a value of $F_o(L)_o = 0.175$. With this value, the Fronaeus (38) function values, F_o, can be obtained and related to the intrinsic stability constants by the following equation as follows:

$$F_o(DPKBH) = 1 + \sum_{i=1}^{N} \beta_i\, [DPKBH]^i \qquad (4)$$

where N corresponds to the coordination number of the Fe(III)/DPKBH complexes.

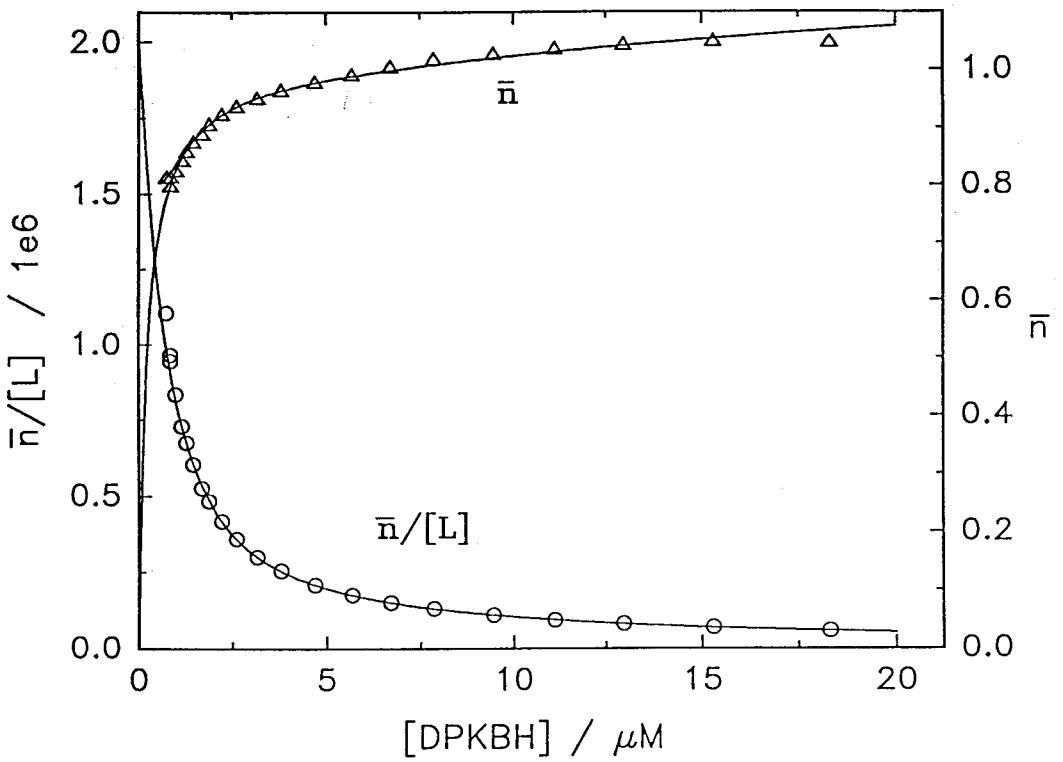

Figure 3: Values of $\bar{n}$ vs. free concentration of DPKBH. Calculated curve from the determined stability constants. Values of $\bar{n}$/[L] vs. free concentration of DPKBH, calculated curve from double decay exponential equation.

Fronaeus function values are equal to a concentrations variable, ϕ, which is defined as $\phi = [M]_T/[M]$, where [M] is the concentration of free, unbound metal ion and $[M]_T$ is the concentration of both bound and unbound metal ion in the system.

Figure 4 shows a non-linear variation of F_o(DPKBH) *vs.* [DPKBH] which shows the existence of more than one species at equilibrium. A weighted least-squares analysis of the data, (eq. 4), yields overall stability constants for the 1:1 (β_1) and 1:2 (β_2) complexes of $\beta_1 = (4.693 \pm 0.003) \times 10^6\ M^{-1}$ and $\beta_2 = (2.195 \pm 0.022) \times 10^{10}\ M^{-2}$.

With these stability constants and with the following definition (eq. 5) of $\bar{n}$ for a system with only β_1 and β_2 (39), the solid curve in Figure 3 was obtained for $\bar{n}$ *vs.* [DPKBH].

$$\bar{n} = \frac{\beta_1[L] + 2\beta_2[L]^2}{1 + \beta_1[L] + \beta_2[L]^2} \qquad (5)$$

One of the linear graphical methods based on $\bar{n}$ when N (number of metal-ligand complexes present) = 2 is the following (39):

$$\frac{(1-\bar{n})}{(2-\bar{n})[DPKBH]} = \left\{\frac{\bar{n}}{(2-\bar{n})[DPKBH]^2}\right\}\frac{1}{K_1} - K_2 \qquad (6)$$

From the graphical form of the above equation, we obtain the individual formation constants of $K_1 = 4.693 \times 10^6\ M^{-1}$ and $K_2 = 4.677 \times 10^3\ M^{-1}$. In a similar fashion, we obtain iron(II)-DPKBH formation constants of $K_1 = (1.217 \pm 0.004) \times 10^5\ M^{-1}$ and $K_2 = (6.421 \pm 0.03) \times 10^4\ M^{-1}$.

These results are consistent with the behavior of the $\bar{\varepsilon}$ *vs.* C_{DPKBH} curves which show a convergence of the data above 1:2 metal-to-ligand mole ratios. Thus, solutions of Fe(III) and DPKBH yield only two metal-ligand species.

In order to verify our results, the function F_1(DPKBH) was calculated using the intermediate term of the following equation:

$$F_1(DPKBH) = \frac{F_o(DPKBH)-1}{[DPKBH]} = \beta_1 + \beta_2[DPKBH] + \quad (7)$$

The function F_1(DPKBH)*vs.*. [DPKBH] is linear (Figure 4) and thus confirms the existence of only two metal-ligand species in solution. The constants obtained by this analysis are self-consistent with those obtained above. They are $\beta_1 = 4.64 \times 10^6\ M^{-1}$ and $\beta_2 = 2.82 \times 10^{10}\ M^{-2}$.

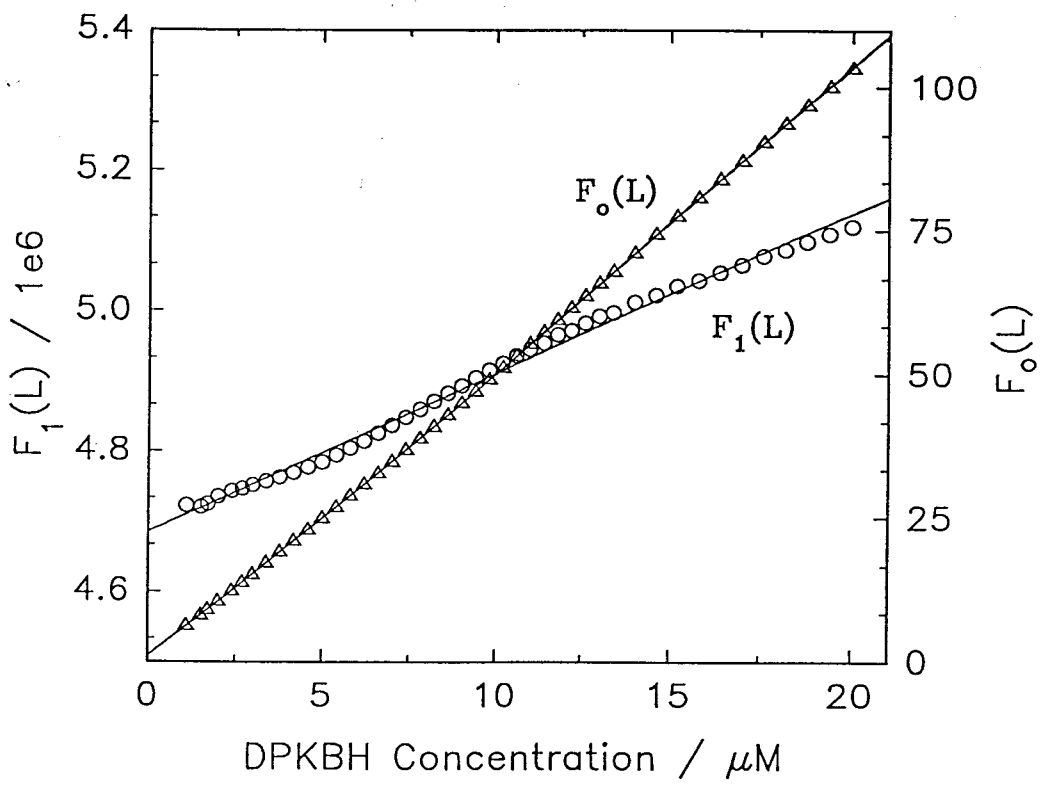

Figure 4: Curves of $F_0(L)$ and $F_1(L)$ to obtain the stability constants β_1 and β_2.

In 3 % ethanolic solutions, DPKBH has a $pK_1 = 2.75$ (protonation of the pyridine nitrogen atom) and a $pK_2 = 10.61$ (deprotonation of the hydrogen atom of the CONH group) (28). In 10% ethanol, $pK_1 = 3.18$ and $pK_2 = 10.87$ (29). We shall consider the protonated form of the ligand (pyridine nitrogen) as H_2L^+, the neutral ligand as HL and the anionic deprotonated form as L^-. The second acid dissociation can be written as:

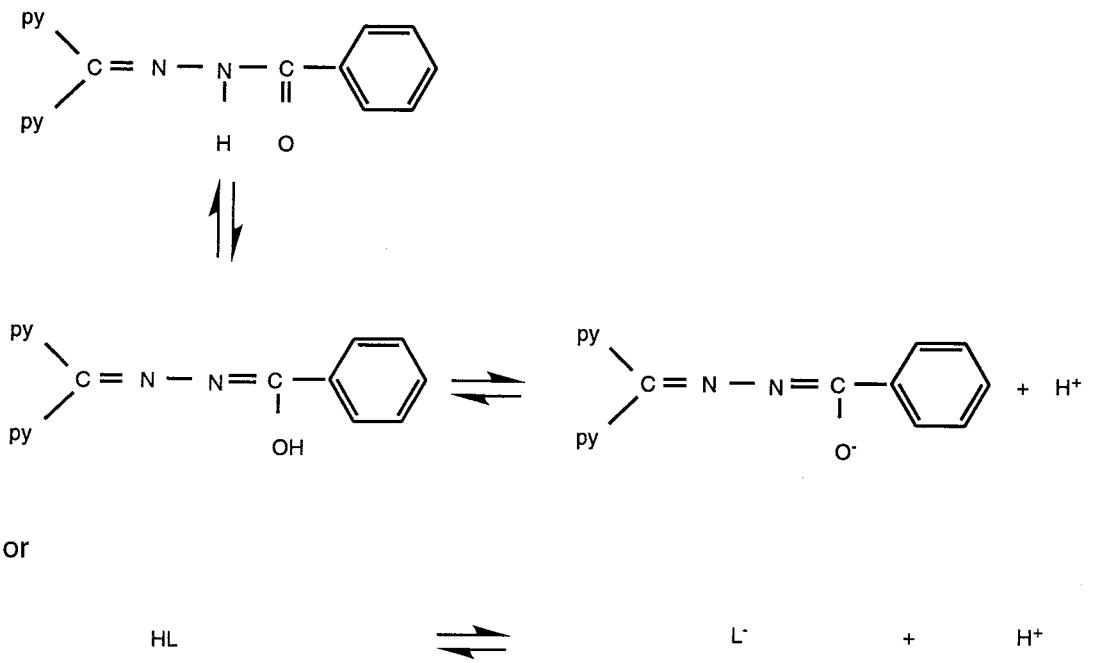

Although the dissociation of a proton from the neutral DPKBH molecule is not favorable under the conditions of our experiments, enhancement of its acidity after metal complex formation may promote its dissociation. In order to explore this possibility, we investigated the conductivity changes during complexation. A simple solution of DPKBH in a water-ethanol solvent has a very low conductance. However, the conductance varies significantly when a solution of Fe(III) is added (Figure 5). The second linear segment in the curve shown in Fig. 5 corresponds to a Fe(III)/DPKBH ratio higher than 1 and shows a lower variation than in the first linear segment. In the first region, the conductance was found to vary as a function of the $[H^+]$ present initially, plus that added in order to

suppress hydrolysis of the Fe(III), and the H^+ released from the ligand due to complexation. In the presence of excess of iron(III), the increase in $[H^+]$ is due exclusively to the hydrolysis of Fe(III).

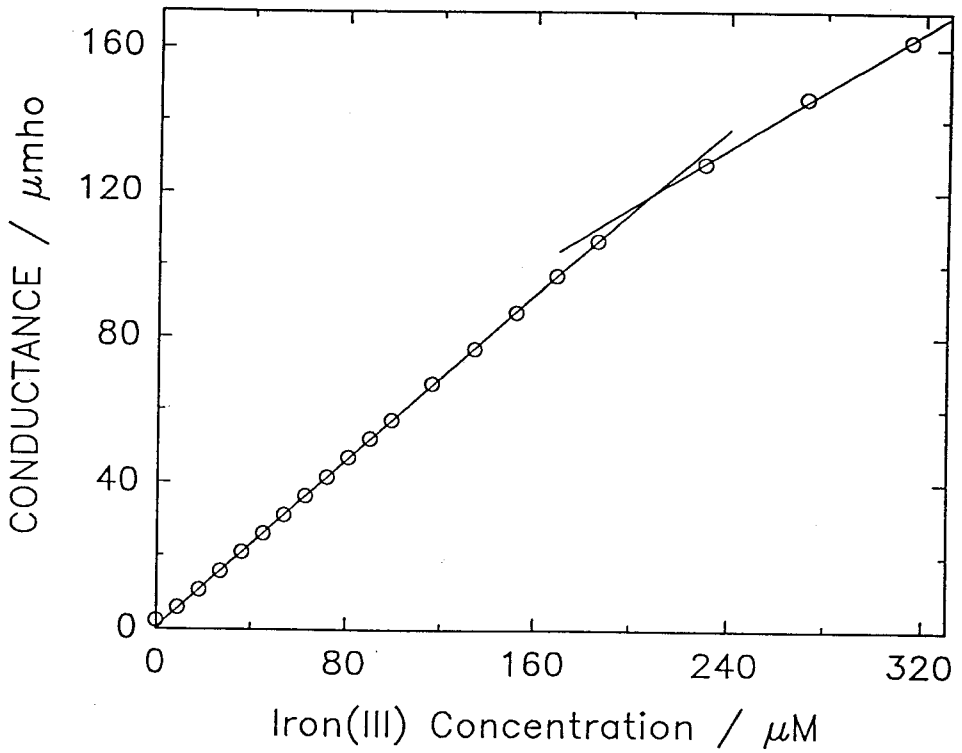

Figure 5: Variation in the conductance of a 232.6 μM solution of DPKBH with addition of Fe(III) solution in 50% ethanol. The conductance was corrected for the successive dilutions (T = 25.0 °C).

A potentiometric titration of a solution containing 92 μM Fe(III), 281 μM DPKBH in 50 % ethanol at pH 5.4 shows a change in slope at 140 μM of added $HClO_4$. A similar titration was performed on a 281 μM DPKBH solution alone and similar behavior was observed. Thus, we conclude that hydrolysis of the Fe(III) ions is a relatively minor contributor to overall conductivity changes.

Since the pK_2 value in 50% ethanol is 10.8 (29), we can estimate the stability constant for the complex formation involving Fe(III) and the L^- species. With this pK_2 value, the conditional stability constant is obtained as follows (the water molecules coordinated to iron(III) are omitted for simplification):

$$HL \Leftrightarrow L^- + H^+ \qquad K_2 = 1.58 \times 10^{-11}\ M$$

$$Fe^{3+} + L^- \Leftrightarrow FeL^{2+} \qquad \beta_1'$$

$$Fe^{3+} + HL \Leftrightarrow FeL^{2+} + H^+ \qquad \beta_1 = 4.693 \times 10^6$$

The β_1' ($= \beta_1/K_2$) value of 2.97×10^{17} represents a very stable complex that is obtained at high pH.

Molar Absorptivities

Calculation of the individual molar absorptivities for the respective complexes was simplified due to the low number of species present at equilibrium. Equation (1) can be rewritten as

$$\bar{\varepsilon} = \frac{\varepsilon_o + \varepsilon_1\beta_1[L] + \varepsilon_2\beta_2[L]^2}{1 + \beta_1[L] + \beta_2[L]^2} \qquad (8)$$

and then combined with the average ligand-number equation (eq. 5) to yield

$$y_o = \frac{\bar{\varepsilon}(\beta_1[L]+2\beta_2[L]^2)}{\bar{n}} = \varepsilon_o + \varepsilon_1\beta_1[L] + \varepsilon_2\beta_2[L]^2 \quad (9)$$

where y_o is the summation of all the absorbing species including Fe(III), Fe(III)-DPKBH and Fe(III)-$(DPKBH)_2$.

ε_o (18.56 M^{-1} cm^{-1}) was determined experimentally and corresponds to the Fe(III) molar absorptivity in the absence of DPKBH. Equation 9 can be rewritten as:

$$y = \frac{y_o - \varepsilon_o}{[L]} = \varepsilon_1\beta_1 + \varepsilon_2\beta_2[L] \quad (10)$$

where y represents a variable (defined in eq. 10) when plotted against [L] yields the molar absorptivities ε_1 and ε_2.

Analysis of the data (plot of y vs. [L]) yields the molar absorptivities (M^{-1} cm^{-1}) of the Fe(III)/DPKBH 1:1 and 1:2 complexes of $\varepsilon_1 = (5.334 \pm 0.004) \times 10^3$ and $\varepsilon_2 = (8.389 \pm 0.160) \times 10^3$, respectively. In a similar fashion, we obtain molar absorptivities (M^{-1} cm^{-1}) of the Fe(II)/DPKBH 1:1 and 1:2 complexes of $\varepsilon_1 = (3.418 \pm 0.009) \times 10^3$ and $\varepsilon_2 = (1.290 \pm 0.090) \times 10^4$, respectively.

A linear relationship exists for data at = 410 nm between $\bar{\varepsilon}$ and $\bar{n}$. Thus, we can use a linear regression to obtain the following equation:

$$\varepsilon_n = A_o + A_1 \bar{n} \quad (11)$$

A linear regression of ε_n *vs.* $\bar{n}$ yields a linear coefficient $A_o = 670.8 \pm 76.2$ and an angular coefficient $A_1 = 4567 \pm 81$ which in turn gives $\varepsilon_1 = 5238$ and $\varepsilon_2 = 9805$

(M^{-1} cm^{-1}). The best fit of the calculated $\bar{\varepsilon}$'s to the experimental data (Figure 2) was obtained from the first set of molar absorptivities. Stability constants and molar absorptivities for Fe(II)-DPKBH and Fe(III)-DPKBH are summarized in Table 1 with a comparison to previously obtained apparent stability constants by continuous variation and mole ratio methods (30). Our values differ significantly from the previous values most likely due to the presence of sodium acetate in the experiments carried out by Zatar et al. (30). They used sodium acetate as a buffer and since acetate can form complexes with iron (40), their apparent stability constants are not only reflecting complexation between iron and DPKBH but also between iron and acetate. Even if the previously measured values were the average of β_1 and β_2, the differences between the current values and the previous values are still large (e.g., the current average value of 3.08×10^7 and the previous value of 8.91×10^7 for Fe(II)-DPKBH).

With the stability constants a distribution diagram can be constructed as shown in Figure 6. It shows that in the range of concentrations employed for analytical determination, the Fe(III) and Fe(III)/DPKBH 1:1 species predominate. Even though the ML_2 concentration is low, the determination of the respective stability constants is possible because the K_1 / K_2 ratio is favorable.

	Stability Constant β_1	Stability Constant β_2	*Apparent Stability Constant*	Molar Absorptivity ε_1	Molar Absorptivity ε_2
Fe(II)-DPKBH	1.217×10^5	7.814×10^9		3.418×10^3	1.290×10^4
Fe(III)-DPKBH	4.693×10^6	2.195×10^{10}		5.334×10^3	8.389×10^3
Fe(II)-DPKBH			*8.91×10^7*		
Fe(III)-DPKBH			*9.33×10^7*		

Table 1: Stability constants and molar absorptivities of Fe(II)-DPKBH and Fe(III)-DPKBH complexes and a comparison to *previously obtained values* (28).

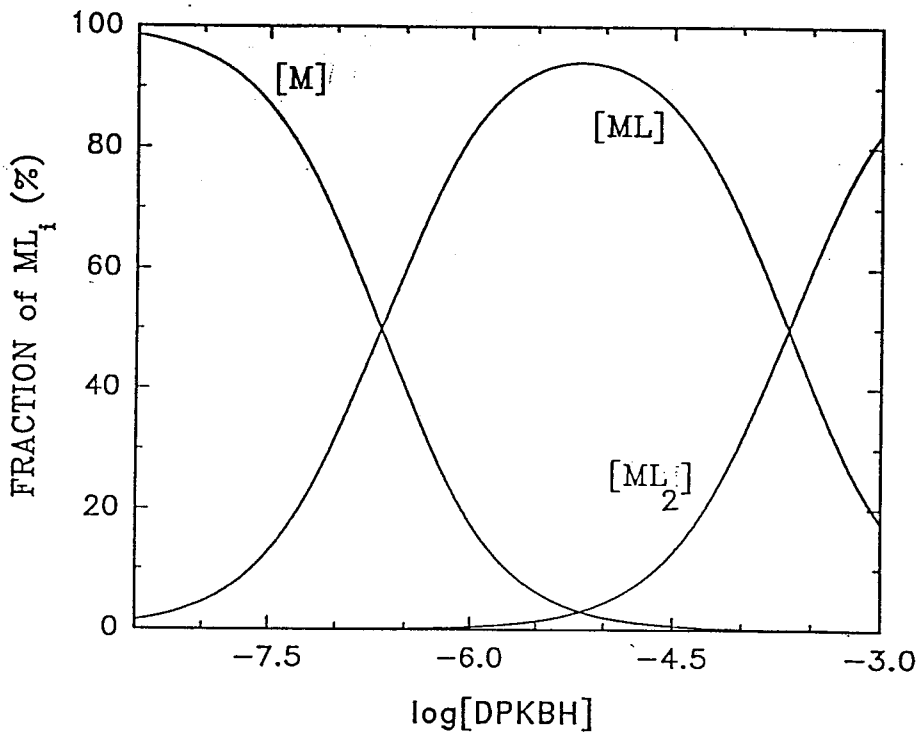

Figure 6: Distribution diagram for the species present in the system Fe(III) / DPKBH. T = (25.0 ± 0.1) ° C, pH = (5.3 ± 0.1) and 50% ethanol.

Structural Characterization of Fe(III)-DPKBH Complexes

Since DPKBH exhibits a keto-enol tautomerism (28), we must determine which form predominates in the iron complexes. The observed IR frequencies (Fig. 7) for DPKBH and $Fe(III)(DPKBH)_2$ are summarized in Table 2. From this data we clearly see that the IR spectrum of the complex differs significantly from that of the free ligand. In particular, the v (N-H) band (41) disappears in the 3000 cm^{-1} region, as a consequence of deprotonation of the CONH system. The high intensity band due to the C=O stretch (41-43) in 1684 cm^{-1} observed for the ligand is also suppressed in the spectrum of the complex. The shift of the carbonyl stretching mode to lower frequencies is in agreement with coordination through oxygen (42). The broad weak band due to the intramolecular (44, 45) H-bonded OH (2930 cm^{-1}) has also disappeared in the complex. The bands due to phenolic C-O, in 1325 and 1267 cm^{-1}, are shifted to a higher frequency in the complex with a totally new band appearing at 1378 cm^{-1}.

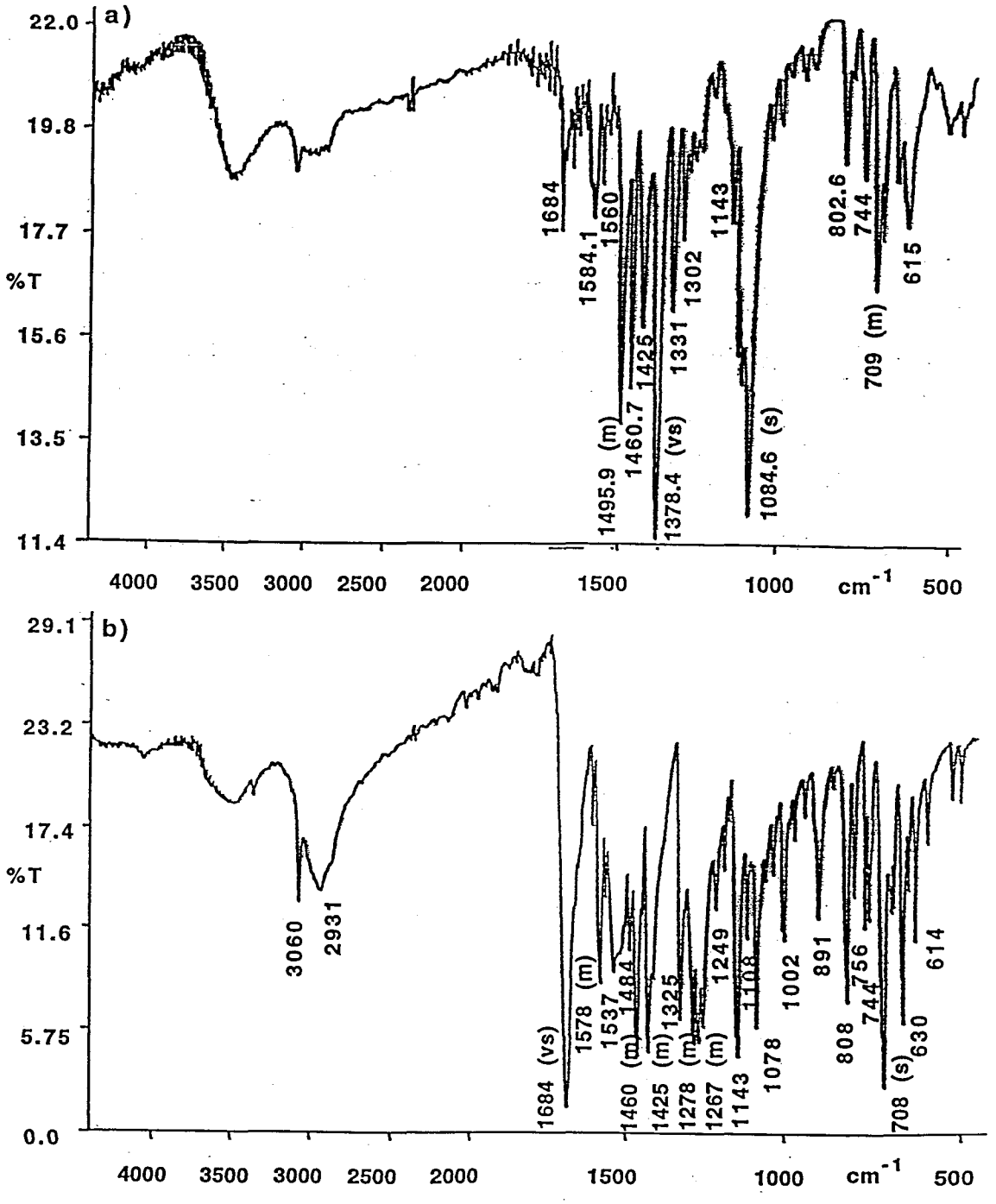

Figure 7: FTIR spectra of a) Fe(III)-DPKBH and b) DPKBH.

DPKBH	$Fe(DPKBH)_2^+$	Assignment
3060 w		ν=CH, ν N-H
2930 w	2930 sh	
1684 s	1684 w	Amide I
1578 m	1584 w	Ring
1537 m	1561 w	Amide II (CN + NH)
1485 m	1496 s	ν (CN) + Ring
1460 s	1460 s	Ring
1325 m	1378 vs.	Phenolic
1267 m		Amide III (δ NH)
708 s	709 m	δ (OH) out-of-plane

(*) w = weak; m = medium; s = strong; vs. = very strong; sh = shoulder

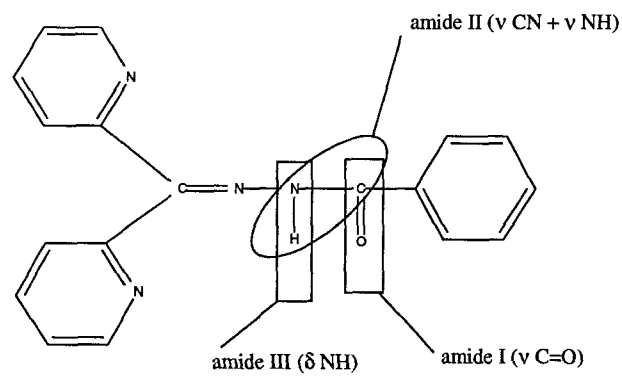

Table 2: Important infrared frequencies (in cm^{-1}) of DPKBH and Fe(III)-DPKBH complex and their assignments (*).

All of these observations suggest that in the complexes of Fe(III) and DPKBH, DPKBH exists in the enol form and exhibits tridentate behavior. This result confirms our conductance titrations which indicated that Fe(III) coordination of DPKBH is via the anionic form. With these results we propose the following structure for the 1:2 complex of Fe(III)/DPKBH:

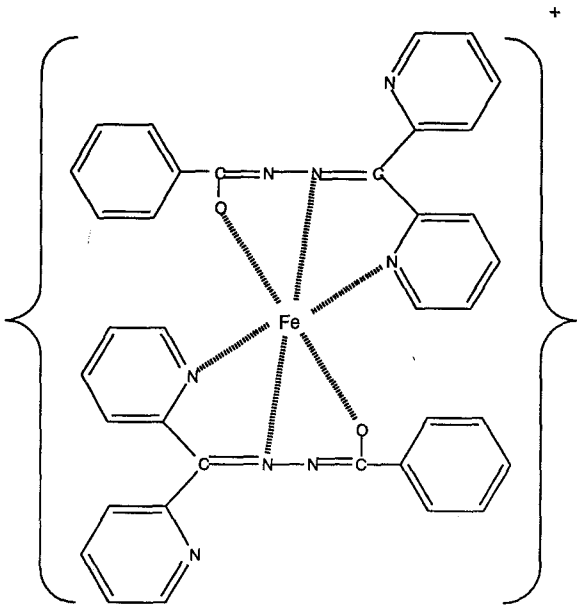

Competitive equilibria have been extensively used to determine stability constants of metals with pure organic compounds (46). Frequently, the concentration of metal complexed with the competing (auxiliary) ligand is obtained spectrophotometrically by measuring the charge-transfer absorption band of the resulting complex. Competing equilibrium methods with EDTA as the competing ligand have been used to determine conditional stability constants for iron(III) with microbially produced siderophores (47-49). However, for most systems, EDTA complexes iron much more strongly (log $K \approx 24$) than naturally occurring organic matter (NOM); thus only a small amount of metal would remain complexed with the NOM. However, a useful competing ligand should allow a nearly

equal distribution of metal ion between the ligand and the organic compound of interest. DPKBH is such a ligand with moderate affinity for Fe(III) and Fe(II).

In order to estimate the speciation of Fe(III) when a naturally-occurring ligand, L, is present in the samples, equilibrium calculations using MICROQL were carried out for two different values of stability constants of the Fe(III)-L complex. A hypothetical system with a ligand, L, that has a Fe(III)-L stability constant of 10^9 and a concentration of 10 μM with a concentration of DPKBH of 2 mM and a concentration of Fe(III) of 10 μM results in 80 % of Fe(III) as Fe(III)-$DPKBH_2$, 10 % as Fe(III)-DPKBH and 9.3 % as Fe(III)-L. Another example similar to the above but with a Fe(III)-L stability constant of 10^{11} results in 74 % of Fe(III) as Fe(III)-L, 23 % as Fe(III)-$DPKBH_2$ and 2.9 % as Fe(III)-DPKBH. For simplicity it was assumed that all Fe(III) was dissolved. These calculations illustrate how the speciation of Fe(III) may affect the application of DPKBH in natural water systems.

If an organic chromophore exists in the environmental samples and the chromophore absorbs at 370-390 nm, one can still use the wavelength 660 nm to determine Fe(II). An appropriate blank correction at 370-390 nm can solve the problem of interference as long as the absorbance due to the interfering chromophore is not excessive.

Conclusions

The speciation of trace metals in natural waters is controlled by their interactions with inorganic anions, organic ligands, reducible or oxidizable dissolved species, surfaces and organisms. Both metal speciation and biological availability or toxicity are functions of the tendency of the metal to react and to participate in competitive reactions by different pathways.

DPKBH in large excess has been used to determine both iron(II) and iron(III) in atmospheric water (27), where the concentration of DPKBH employed was ~ 1.4 mM and the concentration of iron from about 0.1 μM up to 50 μM. It has also been used to study the photoreduction of iron(III) hydroxides (electron acceptors) in the presence of important organic compounds, such as formaldehyde, formate, oxalate, acetate and butyrate, which act as electron donors (50).

The stability constant of the first complex (1:1) of Fe(III) and DPKBH (4.7×10^6) and the first complex of Fe(II) and DPKBH (1.2×10^5), which were determined in the present study, are favorable to study the competitive reactions involving organic natural ligands such as formate, acetate, oxalate, citrate and humic substances. The Fe(III)/DPKBH reagent system presents clearly distinguishable predominance regions for each species. This feature permits one to prepare solutions with predominance of the 1:1 species (≈ 95 %) in order to have good conditions to study competitive reactions between DPKBH and other ligands (11).

Acknowledgments

M. E. V. Suárez Iha is grateful to the Fundação de Amparo à Pesquisa do Estado de São Paulo (FAPESP) for the financial support. We are also grateful to the NSF (ATM 9015775) for providing the financial resources for this project.

References

1. Riley, J. P.; Chester, R. "Introduction to Marine Chemistry," Academic Press: New York, **1971**, 228.

2. Martin, J. H.; Broenkow, W. W.; Fitzwater, S. E.; Gordon, R. M. *Limnol. Oceanogr.*, **1990**, *35*, 775.

3. Martin, J. H.; Gordon, R. M.; Fitzwater, S. E. *Limnol. Oceanogr.*, **1991**, *36*, 1793.

4. Hulburt, E. M.; Rodman, I. *Limnol. Oceanogr.*, **1963**, *8*, 263.

5. Martin, J. H.; Fitzwater, S. E. *Nature*, **1988**, *331*, 341.

6. Martin, J. H.; Gordon, R. M.; Fitzwater, S. E.; Broenkow, W. W. *Deep-Sea Res. Part A - Ocean. Res. Pap.*, **1989**, *36*, 99.

7. Strickland, J. D. H. in "Chemical Oceanography," eds. Riley, J. P.; Skirrow, G.; Academic Press: London, **1965**, 477.

8. Hudson, R. J. M.; Morel, F. M. M. *Abstracts of Papers,* 198th National Meeting of the American Chemical Society; American Chemical Society: Washington, DC, 1989; ENVR 99.

9. Cotton, F. A.; Wilkinson, G. "Advanced Inorganic Chemistry," Wiley Interscience: New York, **1988**, 868.

10. DiChristina, T. J.; Arnold, R. G.; Lidstrom, M. E.; Hoffmann, M. R. *Water Science And Technology,* **1988**, *20*, 69.

11. Morel, F. M. M.; Hering, J. G. "Principles and Applications of Aquatic Chemistry," John Wiley & Sons Inc.: New York, **1993**, 358.

12. Charlson, R. J.; Lovelock, J. E.; Andreae, M. O.; Warren, S. G. *Nature,* **1987**, *326*, 655.

13. Conklin, M. H.; Hoffmann, M. R. *Environ. Sci. Technol.*, **1988**, *22*, 899.

14. Martin, L. R.; Hill, M. W.; Tai, A. F.; Good, T. W. *J. Geophys. Res.*, **1991**, *96*, 3085.

15. Faust, B. C.; Hoffmann, M. R. *Environ. Sci. Technol.*, **1986**, *20*, 943.

16. Littler, J. S.; Sayce, I. G. *J. Chem. Soc.*, **1964**, *96*, 2445.

17. Behra, P.; Sigg, L. *Nature,* **1990**, *344*, 419.

18. Zhuang, G.; Zhen, Y.; Duce, R. A. *Nature,* **1992**, *355*, 537.

19. Landing, W. M.; Westerlund, S. *Mar. Chem.*, **1988**, *23*, 329.

20. McKnight, D. M.; Kimball, B. A.; Bencala, K. E. *Science*, **1988**, *240*, 637.

21. Tsuchiya, M.; Iwanami, Y. *Anal. Sci.*, **1990**, *6*, 701.

22. Zhang, G.; Yang, H.; Wu, H. *Lihua Jianyan, Huaxue Fence*, **1990**, *26*, 3.

23. Wang, Z.; Yao, C.; Cheng, K. L. *Mikrochim. Acta*, **1990**, *3*, 311.

24. Sun, T.; Han, Y.; Wang, J.; Ma, Y.; Zhang, Y. *Shanxi Daxue Xuebao, Ziran Kexueban*, **1990**, *13*, 292.

25. Stookey, L. L. *Anal. Chem.*, **1970**, *42*, 119.

26. Carter, P. *Anal. Biochem.*, **1971**, *40*, 450.

27. Pehkonen, S. O.; Erel, Y.; Hoffmann, M. R. *Env. Sci. Technol.*, **1992**, *26*, 1731.

28. Garcia-Vargas, M.; Belizón, M.; Hernández-Artiga, M. P.; Martinez, C.; Pérez-Bustamante, J. A. *Applied Spectroscopy*, **1986**, *40*, 1058.

29. Nakanishi, T.; Otomo, M. *Microchem. J.*, **1986**, *33*, 172.

30. Zatar, N. A.; Abu-Zuhri, A. Z.; Al-Nuri, M. A.; Mahmoud, F. M.; Abu-Obaid, A. A. *Spectroscopy Letters*, **1989**, *22*, 1203.

31. Erel, Y.; Pehkonen, S. O.; Hoffmann, M. R. *J. Geophys. Res.*, **1993**, *98D*, 18423.

32. Haupt, G. W. *J. Research Nat. Bur. of Stand.*, **1952**, *48*, 414.

33. Vogel, A. I. "Vogel's - Textbook of Quantitative Inorganic Analysis," Longman Inc.: New York, **1978**, 56.

34. Bjerrum, J. *Kgl. Dan. Vidensk. Selsk. Mat-Fys. Medd.*, **1944**, *21*, 5.

35. Grabaric, B.; Piljac, I.; Filipovic, I. *Anal. Chem.*, **1973**, *45*, 1932.

36. Sommer, L.; Langová, M. *CRC Critical Rev. in Anal. Chem.*, **1988**, *19*, 225.

37. Ahrland, S. *Acta Chem. Scand.*, **1949**, *3*, 783.

38. Fronaeus, S. *Acta Chem. Scand.*, **1950**, *4*, 72.

39. Hartley, F. R.; Burgess, C.; Alcock, R. "Solution Equilibria," Ellis Horwood: Chichester, **1980**, 64.

40. Smith, R. M.; Martell, A. E. "Critical Stability Constants," Plenum: New York, **1976**, 20.

41. Conley, R. T. "Infrared Spectroscopy," Allyn and Bacon Inc.: Boston, **1972**, 60.

42. Bellamy, L. J. "The infrared Spectra of Complex Molecules," John Wiley & Sons Inc.: New York, **1954**, 1.

43. Biradar, N. S.; Havinale, B. R. *Inorganica Chimica Acta,* **1976**, *17*, 157.

44. Domiano, P.; Musatti, A.; Nardelli, M.; Pelizzi, C. *J. Chem. Soc. Dalton,* **1975**, *89*, 295.

45. Freedman, H. H. *J. Am. Chem. Soc.,* **1961**, *83*, 2900.

46. Rossotti, F. J. C.; Rossotti, H. "The Determination of Stability Constants," McGraw-Hill Inc.: New York, **1961**, 425.

47. Anderegg, G.; L'Eplattenier, F.; Schwarzenbach, G. *Helv. Chim. Acta,* **1963**, *46*, 1409.

48. Harris, W. R.; Carrano, C. J.; Cooper, S. R.; Sofen, S. R.; Avdeef, A. E.; McArdle, J. F.; Raymond, K. N. *J. Amer. Chem. Soc.,* **1979**, *101*, 6097.

49. Anderson, M. A.; Morel, F. M. M. *Limnol. Oceanogr.,* **1982**, *27*, 789.

50. Pehkonen, S. O.; Siefert, R.; Erel, Y.; Webb, S.; Hoffmann, M. R. *Env. Sci. Technol.,* **1993**, *27,* 2056.

Chapter 5

Redox Chemistry of Fe in Fog and Stratus Clouds

[The text of this chapter appeared in Y. Erel, S.O. Pehkonen, and M. R. Hoffmann, Journal of Geophysical Research, 1993, 98, 18423.]

Abstract

The redox chemistry of Fe in fog and cloudwater has been investigated at coastal and inland locations in the Los Angeles basin, in Bakersfield California, and in Delaware Bay. Samples were collected and analyzed for Fe (Fe(II), Fe(III), total Fe), sulfur (S(IV), S(VI)), organic ligands (formate, acetate, oxalate), TOC (total organic carbon), pH, major cations (Na^+, Ca^{2+}, Mg^{2+}, K^+, NH_4^+), chloride, sulfate, nitrate, peroxides (RO_2H) and aldehydes (HCHO); the amount of sunlight was also measured. The ratio $Fe(II)/Fe_{total}$ varied between 0.02 and 0.55. The concentration of Fe(II) varied between 0.1 and 5 μM, and the concentration of total Fe varied between 2 and 27 μM. The atmospheric redox cycle of Fe involves both dissolved and aerosol surface species and appears to be related to the presence of organic compounds which act as electron donors for the reduction of Fe(III). Fe(III) reduction is enhanced by light but significant Fe(II) levels were observed in the dark. We suggest that reduction of Fe(III) species by organic electron donors may be an important pathway that affects the speciation of Fe in both urban and rural atmospheres. It is possible that reactions involving Fe and organic compounds might be an important source of carboxylic acids in the troposphere.

Introduction

A knowledge of the exact speciation of all oxidation states of transition metals in atmospheric water droplets as a function of variables such as pH, organic ligand content and ionic strength is critical to the computational assessment of *in situ* reaction pathways involving S(IV), O_2, RHCO, NO_x, ROOH, and H_2O_2 (1-4). Likewise, a knowledge of the speciation of metals such as Fe and Mn in wet and dry atmospheric deposition and the subsequent speciation changes upon introduction to marine waters is important to the assessment of the ability of marine biota to utilize these atmospherically derived elements for nutritional needs (5-9).

Iron is emitted to the troposphere from both natural (e.g., windblown dust) and anthropogenic (e.g., coal combustion) sources (10, 11). It has been proposed that atmospheric Fe participates in a variety of reactions such as the oxidation of S(IV) and organic compounds by Fe(III) via direct electron transfer, and the catalytic auto-oxidation of SO_2 to SO_4^{2-} in the droplet phase (3, 12, 13). In addition, laboratory experiments have shown that Fe(III) is an important oxidant of S(IV) and organic compounds (e.g., aldehydes to carboxylic acids) (14-16). In spite of the known redox chemistry of Fe, most previous investigations of Fe in atmospheric water have been limited to the determination of the total dissolved Fe concentration. Moreover, current models of atmospheric cloud chemistry have assumed that Fe in cloudwater and aerosols is present as mostly Fe(III) in a variety of solid and aqueous-phase species (12).

Previous measurements of Fe(II) in sea water and in stream water have shown that it is also present at significant levels in oxic surface water (17-19). In addition, there are a few recent reports of the presence of Fe(II) in atmospheric water and aerosols (20-24). A study of the speciation of Fe in fog collected with the Caltech Active Strand Collector in

Zürich (20) has shown that a significant fraction of the total Fe (20 to 90 %) is present as soluble Fe(II) (up to 200 μM) over a pH range of 3-7 and that in many samples Fe(II) was the predominant oxidation state in solution (dissolved Fe is operationally defined by filtration with either a 0.45 or 0.05 μm membrane filter).

According to Zhuang et al. (22, 23) approximately 50 % of the Fe in aerosols collected from the marine environment is Fe(II), while only a few percent of the Fe in aerosols collected over China is Fe(II). Zhuang et al. attributed the large fraction of Fe(II) in marine aerosol to multiple cycles of reductive dissolution of ferric oxides followed by oxidation and precipitation taking place during the long journey of these particles in the atmosphere. They also postulated that the redox cycle of Fe is related to that of S. Zhu et al. (24), on the other hand, reported that Fe(II) makes up only 1% of the total Fe and 7.5% of the soluble Fe in marine aerosols. Zhu et al. conducted photolysis experiments with aerosol extracts and with dissolved Fe(III) in aerated acidic sodium chloride solutions both in the presence and in the absence of oxalate (as an electron donor). Zhu et al. observed that within a short time, Fe(II) concentration rose from 0.1 μM to 1.3 μM (almost 30 % of the total Fe) in aerosol extracts exposed to sunlight. The final concentration was attained within less than an hour, and was maintained as long as the samples were irradiated. Once the irradiation ceased, the concentrations of Fe(II) in solution dropped. Based on the experiments with oxalate and dissolved Fe(III), Zhu et al. concluded that oxalate participates in the formation of Fe(II) in irradiated samples via electron transfer within the dissolved Fe-oxalato complexes; however, oxalate oxidation also produces H_2O_2 which oxidizes Fe(II) back to Fe(III). The oxidation of Fe(II) by H_2O_2 takes over in the dark, leading to the observed decrease in Fe(II) concentrations. Zhu et al. did not observe substantial Fe(II) formation in irradiated goethite suspension in the presence of oxalate.

In light of these considerations, we now report on the occurrence of Fe(II) in stratus clouds collected in coastal and inland environments. In addition, we highlight important processes, chemical species, and critical environmental parameters that affect the dynamic redox cycle of Fe in the atmosphere.

Experimental

In order to reliably analyze the oxidation states of Fe and the partitioning of Fe between particulate matter and solution we carried out as many measurements as possible in the field. In addition, the low concentrations of Fe expected in some of the samples required that great care be exercised to minimize and monitor blanks during sample collection and handling.

Fog and cloudwater samples were collected with acid-cleaned Caltech Active Strand Cloudwater Collectors (CASCC; 25). Concentrations of Fe and other constituents in blanks were determined before each collection. Of all constituents analyzed, Fe blanks were always the highest relative to Fe concentrations in the samples. Nevertheless, Fe blanks never exceeded 10% of the lowest Fe value measured in a sample. The collectors were placed in two elevated locations within the Los Angeles basin. These sites were (1) a coastal station on the Palos Verdes Peninsula, and (2) an inland station at Henniger Flats near Mt. Wilson (26). In addition, we collected samples in Bakersfield California, and on board the "R.V. Cape Henlopen" (College of Marine Studies, University of Delaware) in Delaware Bay.

Fog and cloudwater samples were collected over 15-45 minute intervals (except for one sample which was collected for 120 minutes). The samples were weighed immediately after collection to determine their volume in order to calculate liquid water content (LWC;

26). Light intensity was measured with a Digital Irradiance Meter (spectral response from 380 to 750 nm; Biospherical Instruments QSP170B). An aliquot of each sample was removed to determine sample pH. A Radiometer PHM80 Standard pH meter with a GK2320C semi-micro combination electrode calibrated with pH 4 and 7 buffers was used to measure the pH in the field. Aliquots of the collected water samples were processed in real time in the field (including filtration through 0.025 μm pore-size Millipore® filters). Fe(II), Fe(III), and other reactive species were determined by spectrophotometric techniques (see below). The complete determination of reactive species in atmospheric waters other than Fe(II) and Fe(III) is beyond the scope of this study. We focused instead on some of the most abundant inorganic and organic compounds in atmospheric water which are likely to exchange electrons with Fe (26, 27). In addition, we determined the total organic carbon (TOC) content as a measure of all the other numerous natural and anthropogenic organic compounds present in atmospheric water. The species that were studied include: NH_4^+/NO_3^-, S(IV)/S(VI), monocarboxylic acids (formate, acetate), dicarboxylic acids (oxalate), and aldehydes (formaldehyde). In addition, we monitored changes in the concentration of Fe(II), Fe(III) and pH as a function of time, in samples stored both in darkness and exposed to daylight.

The aliquots of each sample removed for analysis of reactive species were stabilized in the field. Carboxylic acids (oxalate, acetate, formate), and NH_4^+ were preserved by addition of chloroform (26, 28). Aliquots for TOC analysis were preserved by addition of $HgCl_2$ solution. HCHO (formaldehyde) was reacted with NH_4^+-acetylacetone to form 3,5-dihydro-1,4-dihydrolutidine (DDL), which is stable for several weeks (29). A buffered solution of p-hydroxyphenylacetic acid (POPA) and peroxidase was used to preserve peroxides by formation of a fluorescent dimer (30). Samples for analyses of total concentrations of Fe and major cations (Na^+, K^+, Mg^{2+}, Ca^{2+}) with a direct current plasma spectrometer (DCP) were acidified (0.1 M HCl) and stored at 4 °C until analysis.

The particulate matter collected on filters was brought back to the laboratory for analysis, and was digested with concentrated HF and HNO_3. For several samples, Fe_{dgs}, the concentration of Fe in filtrate + filter digest, was compared with Fe concentration in acidified (pH = 1) filtered (Fe_{flt}) and unfiltered (Fe_{ac}) aliquots (all analyzed by a DCP) and with Fe(II) + Fe(III) concentration (determined spectrophotometrically) in unfiltered (Fe_{reac}) and filtered aliquots.

Spectrophotometric analyses were performed with: 1) Shimadzu UV-1201 Portable Spectrophotometer with a 5-cm cell, 2) Shimadzu RF-540 Recording Spectrofluorophotometer, and 3) Shimadzu 500 DOC/TOC Analyzer (100 ppb detection limit). For Fe(II) determination we applied two methods: 1) the Ferrozine {3-(2-pyridyl)-5,6-diphenyl-1,2,4-triazine-p,p'-disulfonic acid, monosodium salt monohydrate} method used originally by Stookey (31) and Carter (32), and which is the most common method for Fe(II) determination in water and blood serum samples; 2) Di-2-pyridyl ketone benzoylhydrazone (DPKBH) was selected as a second chelating agent for Fe (33), because it is known to complex both Fe(II) and Fe(III), and because of its low solubility in water which enables a preconcentration step (34, 35).

Fe chelation by DPKBH both with and without a preconcentration procedure was carried out in order to cover a wide range of Fe concentrations. A spectrophotometric detection limit of 4 nM for both Fe(III) and Fe(II) with a linear response from 4 nM up to 0.1 μM was established for samples extracted with $CHCl_3$-H_2O. DPKBH chelation without $CHCl_3$ extraction showed a linear response from 0.1 μM to 30 μM. The molar extinction coefficients of the bis-Fe(II)-DPKBH (ε_2) and bis-Fe(III)-DPKBH (ε_1) complexes are ε_1 & $\varepsilon_2 = 3.6 \times 10^4$ L mol^{-1} cm^{-1} at 370 nm and $\varepsilon_2 = 1.1 \times 10^4$ L mol^{-1} cm^{-1} at 660 nm. Analytical interference studies on the possible changes in the oxidation state of Fe with S(IV), oxalate, and other potential electron donors have also been carried out (33).

HCHO was measured after addition of I_2 (29; light absorption at λ = 415 nm). S(IV) was analyzed by the "Bunte salt" method (light absorption at λ = 412 nm; 36). Peroxide was measured by the fluorescence of the POPA dimer (peroxide excitation at λ = 320 nm and emission at 406 nm; 30). This method is sensitive to both H_2O_2 and some organic peroxides.

Cl^-, NO_3^-, SO_4^{2-}, $CH_3CO_2^-$, HCO_2^- and $C_2O_4^{2-}$were measured in the laboratory using a Dionex BIOLC ion chromatograph with PAX-500 anion column and a NaOH eluent. Gradient elution was employed to enhance the separation of the weakly retained acids and shortening the retention of the unwanted CO_3^{2-} peaks. One mM NaOH solution was mixed with 200 mM NaOH solution at different proportions to gradually increase concentration of NaOH and therefore to improve the elution of ions such as sulfate and oxalate.

Na, K, Ca, Mg, and Fe were analyzed with an ARL SpectroSpan VB direct current plasma (DCP) spectrometer. The lower linearity ranges of the instrument used were: 2.6, 4.1, 1.3, 0.4, 0.9 μM, respectively. The coefficients of variance (CV) of cation analysis by the DCP were, at most, 10%. Samples with low concentrations of Fe were analyzed with a 3030 Perkin Elmer Graphite Furnace atomic absorption spectrometer (detection limit: 0.02 μM, and a coefficient of variance (CV) of 20%).

With the aid of SURFEQL (37, 38, 1) we used the equilibrium constant approach to solve a complex chemical equilibrium problem, which is defined by a system of mass action equations (39). The thermodynamic data base consists of equilibrium constants for more than 1500 equilibria. This data base was verified and supplemented for the present calculation.

Results and Discussion

A wide range of concentrations of measured constituents were observed in the collected fog and cloudwater samples (Table 1). Inorganic anions (Cl^-, NO_3^- and SO_4^{2-}) and cations (NH_4^+ Na^+, and H^+) were the dominant species in cloudwater with their concentrations approaching mM values. The pH varied between 2.2 and 7.1. The concentration of soluble Fe(II) in cloudwater ranged from 0.1 to 5.3 μM, while the concentration of Fe_{ac} varied between 1.8 and 27 μM (Table 1). The concentrations of H_2O_2+ROOH, S(IV), $CH_3CO_2^-$, HCO_2^-, $C_2O_4^{2-}$, and HCHO were found to be on the same order of magnitude as the Fe_{ac} (Table 1).

No.	Site	Date	Sample Description	Time	Duration (min.)	Weight
1	Henniger	4/25/91	unfiltered	0215	120	NA
2	Henniger	5/30/91	filtered collector 3	0130	45	100
3	Henniger	5/30/91	unfiltered collector 3	0130	45	100
4	Henniger	5/30/91	filter digest collector 3	0130	45	100
5	Henniger	5/30/91	filtered collector 1	0215	45	100
6	Henniger	5/30/91	filtered collector 3	0215	45	100
7	Henniger	5/30/91	unfiltered collector 1	0215	45	100
8	Henniger	5/30/91	unfiltered collector 3	0215	45	100
9	Henniger	5/30/91	filter digest collector 3	0215	45	100
10	Henniger	5/30/91	filter digest collector 3	0215	45	100
11	Henniger	5/30/91	filtered collector 1	0300	45	100
12	Henniger	5/30/91	filtered collector 3	0300	45	100
13	Henniger	5/30/91	unfiltered collector 1	0300	45	100
14	Henniger	5/30/91	unfiltered collector 3	0300	45	100
15	Henniger	5/30/91	filtered collector 1	0345	75	220
16	Henniger	5/30/91	filtered collector 3	0345	75	220
17	Henniger	5/30/91	unfiltered collector 1	0345	75	220
18	Henniger	5/30/91	unfiltered collector 3	0345	75	220
19	Henniger	5/30/91	filter digest collector 3	0345	75	220
20	San Pedro	6/11/91	unfiltered	0750	20	30
21	San Pedro	6/11/91	unfiltered	0825	25	28
22	San Pedro	6/11/91	unfiltered	0900	25	61
23	San Pedro	6/11/91	unfiltered	0930	25	57
24	San Pedro	6/11/91	unfiltered	1000	30	48
25	San Pedro	6/11/91	unfiltered	1035	15	21
26	Henniger	6/27/91	unfiltered	0845	35	65
27	Henniger	6/27/91	filtered	0845	35	65
28	Henniger	6/27/91	filter digest	0845	35	65
29	Henniger	6/27/91	filter digest	0845	35	65
30	Henniger	6/27/91	unfiltered	0920	30	25
31	San Pedro	7/10/91	unfiltered	1000	35	30
32	San Pedro	7/23/91	unfiltered	0855	25	95
33	San Pedro	7/23/91	unfiltered	0920	20	90
34	San Pedro	7/23/91	unfiltered	0950	15	54
35	San Pedro	7/23/91	unfiltered	1020	25	60
36	San Pedro	7/23/91	unfiltered	1050	25	30
37	San Pedro	7/23/91	unfiltered	1125	45	23
38	San Pedro	7/25/91	unfiltered	0830	35	60
39	San Pedro	7/25/91	filtered	0830	35	60
40	San Pedro	7/25/91	filter digest	0830	35	60
41	San Pedro	7/25/91	filter digest	0830	35	60
42	San Pedro	7/25/91	unfiltered	0905	50	65
43	San Pedro	7/25/91	filtered	0905	50	65
44	San Pedro	7/25/91	filter digest	0905	50	65
45	San Pedro	7/25/91	unfiltered	0955	40	33
46	Delaware	3/5/92	unfiltered	0515	30	15
47	Delaware	3/5/92	unfiltered	0545	15	31
48	Delaware	3/5/92	unfiltered	0605	15	6
49	Delaware	3/5/92	unfiltered	0705	115	91
50	San Pedro	6/5/92	unfiltered	1047	18	48
51	San Pedro	6/5/92	unfiltered	1105	30	30
52	San Pedro	6/5/92	unfiltered	1135	25	8
53	Bakersfield	1/27/93	unfiltered	1125	55	68
54	Bakersfield	1/28/93	unfiltered	1225	42	131
55	Bakersfield	1/28/93	unfiltered	0107	46	123
56	Bakersfield	1/28/93	unfiltered	0153	53	127
57	Bakersfield	1/28/93	unfiltered	0246	60	129

Table 1: The concentrations (μM) of various components measured in fog and cloudwater samples. BDL = below detection limit. NA = not measured or not applicable.

No.	pH	LWC (g/m3)	Light ($qs^{-1}cm^{-2}$)	Temp (°c)	Fe(II)* (DPKBH)	Fe(III)* (DPKBH)	Fe(II) * (Ferrozine)	Fe (DCP)	H_2O_2	Oxalate	HCHO
1	3.1	NA	dark	NA	13.1	5.0	NA	NA	12.0	BDL	3.6
2	NA	0.11	dark	NA	NA	NA	NA	9.1	4.2	BDL	41
3	NA	0.11	dark	NA	NA	NA	NA	25.5	4.2	BDL	41
4	NA	0.11	dark	11.0	NA	NA	NA	25.9	NA	NA	NA
5	2.5	0.11	dark	11.0	NA	NA	NA	NA	4.6	BDL	35
6	2.5	0.11	dark	11.0	NA	NA	NA	4.0	4.6	BDL	35
7	2.5	0.11	dark	11.0	4.9	6.7	NA	26.5	4.6	BDL	35
8	2.5	0.11	dark	11.0	2.9	6.1	NA	20.7	4.6	BDL	35
9	2.5	0.11	dark	11.0	NA	NA	NA	19.0	NA	NA	NA
10	2.5	0.11	dark	11.0	NA	NA	NA	17.6	NA	NA	NA
11	2.8	0.11	dark	10.5	NA	NA	NA	NA	5.2	BDL	48
12	2.8	0.11	dark	10.5	NA	NA	NA	NA	5.2	BDL	48
13	2.8	0.11	dark	10.5	4.1	3.3	NA	13.2	5.2	BDL	48
14	2.8	0.11	dark	10.5	3.8	4.1	NA	10.9	5.2	BDL	48
15	2.8	0.14	dark	10.5	NA	NA	NA	NA	3.5	BDL	47
16	2.8	0.14	dark	10.5	0.0	2.3	NA	2.2	3.5	BDL	47
17	2.8	0.14	dark	10.5	1.2	2.0	NA	4.3	3.5	BDL	47
18	2.8	0.14	dark	10.5	0.9	2.5	NA	6.7	3.5	BDL	47
19	2.8	0.14	dark	10.5	NA	NA	NA	23.7	NA	NA	NA
20	4.2	0.07	3.3E+16	NA	NA	NA	NA	NA	33.7	BDL	19.4
21	4.0	0.05	5.2E+16	NA	3.9	4.2	NA	4.5	48.1	BDL	16.8
22	3.8	0.11	5.4E+16	NA	1.4	1.2	NA	2.6	29.4	BDL	17.8
23	3.8	0.11	6.3E+16	NA	1.5	1.1	NA	2.3	53.4	BDL	17.9
24	3.5	0.08	7.6E+16	NA	2.0	1.5	NA	2.9	64.2	BDL	17.4
25	NA	0.07	9.0E+16	NA	4.3	3.2	NA	3.3	78.6	BDL	19.7
26	3.9	0.09	1.0E+16	16.0	7.6	3.4	4.2	8.2	2.1	BDL	23
27	3.9	0.09	1.0E+16	16.0	NA	NA	NA	7.0	2.1	BDL	23
28	3.9	0.09	1.0E+16	16.0	NA	NA	NA	1.5	NA	NA	NA
29	3.9	0.09	1.0E+16	16.0	NA	NA	NA	1.5	NA	NA	NA
30	3.7	0.04	7.5E+16	16.0	7.7	2.4	5.3	9.7	1.5	BDL	25.6
31	3.4	0.04	6.0E+16	18.0	1.1	0.0	1.1	3.9	7.0	BDL	32.1
32	3.2	0.18	3.2E+16	15.0	7.9	4.1	3.8	9.5	3.6	BDL	12
33	2.5	0.21	3.7E+16	15.0	8.0	3.3	4.7	10.2	4.8	BDL	12.2
34	2.2	0.17	4.0E+16	15.0	9.9	NA	NA	9.0	4.8	BDL	11.7
35	2.4	0.11	5.0E+16	15.5	9.3	NA	NA	8.8	8.3	BDL	11.5
36	2.8	0.06	6.4E+16	16.2	11.1	NA	NA	12.2	9.6	5.7	12.3
37	2.6	0.02	9.5E+16	19.0	18.7	NA	NA	20.6	6.2	9.1	15.7
38	3.2	0.08	1.7E+16	14.5	1.7	1.2	0.5	2.0	24.3	7.7	8.62
39	3.2	0.08	1.7E+16	14.5	0.7	0.3	NA	1.4	24.3	7.7	8.62
40	3.2	0.08	1.7E+16	14.5	NA	NA	NA	4.4	NA	NA	NA
41	3.2	0.08	1.7E+16	14.5	NA	NA	NA	4.2	NA	NA	NA
42	2.6	0.06	3.0E+16	14.5	1.1	0.8	0.3	1.8	32.6	8.3	8.35
43	2.6	0.06	3.0E+16	14.5	0.4	0.1	NA	BDL	32.6	8.3	8.35
44	2.6	0.06	3.0E+16	14.5	NA	NA	NA	4.3	NA	NA	NA
45	3.4	0.04	4.0E+16	14.5	1.8	1.2	0.7	2.7	40.5	13.2	10.1
46	NA	0.02	1.1E+15	NA	NA	NA	NA	4.2	NA	NA	NA
47	2.9	0.10	4.2E+14	NA	NA	NA	0.7	3.0	NA	16.8	NA
48	NA	0.02	7.0E+13	NA	NA	NA	NA	NA	NA	13.5	NA
49	3.8	0.04	2.0E+13	NA	NA	NA	0.4	1.0	NA	8.6	NA
50	4.4	0.13	7.4E+16	14.0	0.6	0.6	0.6	0.9	NA	13.5	1.52
51	4.3	0.05	8.5E+16	14.0	1.5	1.2	1.1	2.0	NA	1.5	NA
52	4.2	0.01	1.0E+17	14.0	2.0	1.6	NA	NA	NA	5.3	NA
53	6.4	0.06	dark	10.0	NA	NA	0.1	5.9	0.0	8.5	NA
54	6.7	0.15	dark	10.0	NA	NA	0.3	5.4	1.1	4.0	NA
55	6.8	0.13	dark	10.0	NA	NA	0.2	2.7	1.4	5.0	NA
56	7.1	0.11	dark	10.0	NA	NA	0.3	4.9	2.4	4.0	NA
57	6.8	0.10	dark	10.0	NA	NA	0.2	2.8	5.4	4.0	NA

Table 1 (cont.):

No.	S(IV)	TOC (mg/l)	Formate	Acetate	SO_4^{2-}	Cl^-	NO_3^-	NH_4^+	Na^+	K^+	Ca^{2+}	Mg^{2+}
1	NA	NA	55.4	BDL	376	2299	2563	1400	960	49	38	NA
2	NA	NA	56.3	19.3	631	947	3342	1500	481	20	65	60
3	NA	NA	56.3	19.3	631	947	3342	1500	493	25	63	64
4	NA	NA	NA	NA	NA	NA	NA	NA	19	16	5	14
5	NA	NA	56.9	26.3	320	589	1639	1300	NA	NA	NA	NA
6	NA	NA	56.9	26.3	320	589	1639	1300	552	20	58	65
7	NA	NA	56.9	26.3	320	589	1639	1300	627	32	64	78
8	NA	NA	56.9	26.3	320	589	1639	1300	567	25	54	69
9	NA	NA	NA	NA	NA	NA	NA	NA	BDL	11	6	8
10	NA	NA	NA	NA	NA	NA	NA	NA	BDL	12	5	6
11	NA	NA	46.2	BDL	382	595	1989	1400	NA	NA	NA	NA
12	NA	NA	46.2	BDL	382	595	1989	1400	NA	NA	NA	NA
13	NA	NA	46.2	BDL	382	595	1989	1400	345	16	27	42
14	NA	NA	46.2	BDL	382	595	1989	1400	307	14	26	41
15	NA	NA	54.6	11.4	313	539	1777	1100	NA	NA	NA	NA
16	NA	NA	54.6	11.4	313	539	1777	1100	213	9	16	26
17	NA	NA	54.6	11.4	313	539	1777	1100	224	10	18	28
18	NA	NA	54.6	11.4	313	539	1777	1100	222	9	17	30
19	NA	NA	NA	NA	NA	NA	NA	NA	19	16	6	15
20	17.8	19.5	29.9	BDL	397	444	757	NA	NA	NA	NA	NA
21	2.4	11.3	43.4	BDL	185	206	426	NA	16	4	5	6
22	0.0	11.4	26.2	BDL	206	636	323	NA	22	4	7	7
23	0.0	8.4	30.1	BDL	193	702	359	NA	31	4	7	7
24	1.9	11.1	47.5	BDL	239	729	461	NA	60	7	17	12
25	0.9	16.1	51.3	BDL	318	931	602	NA	106	10	30	19
26	1.9	14.0	26.5	BDL	64	2320	392	630	199	10	24	27
27	1.9	NA	26.5	BDL	64	2320	392	630	193	9	22	26
28	NA	NA	NA	NA	NA	NA	NA	NA	BDL	1	2	BDL
29	NA	NA	NA	NA	NA	NA	NA	NA	BDL	1	2	BDL
30	2.4	NA	28.6	BDL	61	2700	679	700	352	17	41	46
31	7.7	15.0	23.6	36.6	364	118	572	880	31	8	29	8
32	17.0	10.4	28.1	24.9	411	163	839	730	232	12	46	35
33	15.0	10.8	27.2	26.6	394	168	869	690	223	13	59	38
34	13.0	13.5	29.6	32.0	503	179	1040	790	250	12	69	43
35	12.7	14.8	34.3	36.9	644	238	1180	1000	337	16	85	55
36	15.3	NA	42.6	47.6	903	315	1550	1200	441	16	160	74
37	22.1	NA	75.6	88.2	1400	470	2480	NA	721	39	260	133
38	7.1	7.1	22.7	17.4	147	56	284	440	29	6	13	6
39	7.1	7.1	22.7	17.4	147	56	284	440	28	6	13	5
40	NA	NA	NA	NA	NA	NA	NA	NA	BDL	4	5	BDL
41	NA	NA	NA	NA	NA	NA	NA	NA	BDL	4	5	BDL
42	5.8	7.4	27.7	21.7	167	62	304	560	20	6	BDL	4
43	5.8	7.4	27.7	21.7	167	62	304	560	18	5	BDL	4
44	NA	NA	NA	NA	NA	NA	NA	NA	BDL	4	5	BDL
45	4.2	12.3	39.8	36.8	264	95	515	1500	26	9	22	9
46	NA	NA	NA	NA	NA	NA	NA	NA	91	25	79	70
47	NA	NA	21.2	49.0	527	299	552	NA	43	15	43	41
48	NA	NA	13.4	25.6	526	239	514	NA	NA	NA	NA	NA
49	NA	NA	16.9	19.4	319	115	310	NA	13	8	29	17
50	2.5	NA	31.7	30.5	72	106	84	NA	12	3	4	9
51	NA	NA	14.3	10.7	111	175	134	NA	31	9	14	25
52	NA	NA	19.5	18.2	236	345	299	NA	NA	NA	NA	NA
53	NA	NA	66.0	153.0	318	27	1840	NA	12	4	34	7
54	NA	NA	40.0	92.0	145	17	987	NA	6	6	19	5
55	NA	NA	45.0	109.0	131	18	793	NA	3	4	10	2
56	NA	NA	38.0	119.0	118	13	638	NA	4	4	13	4
57	NA	NA	61.0	123.0	198	18	1190	NA	4	4	10	2

Table 1 (cont.):

In order to test the role of light in controlling the reduction of Fe(III), we monitored the production of Fe(II) as function of time both in the light (approximately 5×10^{16} quanta/sec cm^2 of sun light) and in the dark immediately after the collection of cloudwater samples which contained appreciable quantities of S(IV) and organic compounds (Table 2). Fe(II) concentrations always increased faster in the presence of light than in the dark. Nevertheless, the observed coexistence of Fe(II) and H_2O_2 (which itself is a major oxidant of Fe(II) at the pH range of most of the cloudwater samples; 16) in cloudwater samples that were collected in the dark both in California and in Delaware (Table 1) suggests a thermal reduction pathway of Fe(III). In addition, [Fe(II)] values in cloudwater samples collected during the night in Los Angeles were comparable to those found in samples collected long after sun-rise (Fig. 1a). It has been shown previously that thermal reduction of Fe(III) by organic compounds that are present in cloudwater (e.g., phenols, aldehydes but not $CH_3CO_2^-$ and HCO_2^-) and by S(IV) is much slower and much less important than photoreduction (14, 15). Thus, our measurements suggest that either thermal reduction is a viable complementary pathway for the *in situ* production of Fe(II) in the atmosphere (in contrast to laboratory experiments), or that both reduction and oxidation rates decrease during nighttime to the same extent, leading to unchanged steady state levels of Fe(II).

sample	Fe(II) μM	time lapsed min.	dark/light	ΔFe(II)/Δt nM/sec*
San Pedro1	1.43	0	light	-
San Pedro1	3.04	30	light	0.90
San Pedro1	4.18	105	dark	0.25
San Pedro1	5.14	165	dark	0.27
San Pedro2	9.80	0	light	-
San Pedro2	12.05	~10	light	-
San Pedro2	12.34	~20	dark	-
San Pedro2	12.23	~30	dark	-
San Pedro3	13.05	0	light	-
San Pedro3	14.81	~10	light	-
San Pedro3	14.66	~20	dark	-

* change in [Fe(II)] and time lapsed since the last measurement

Table 2: Changes of Fe(II) concentrations in cloudwater samples stored in day light and in the dark as a function of time.

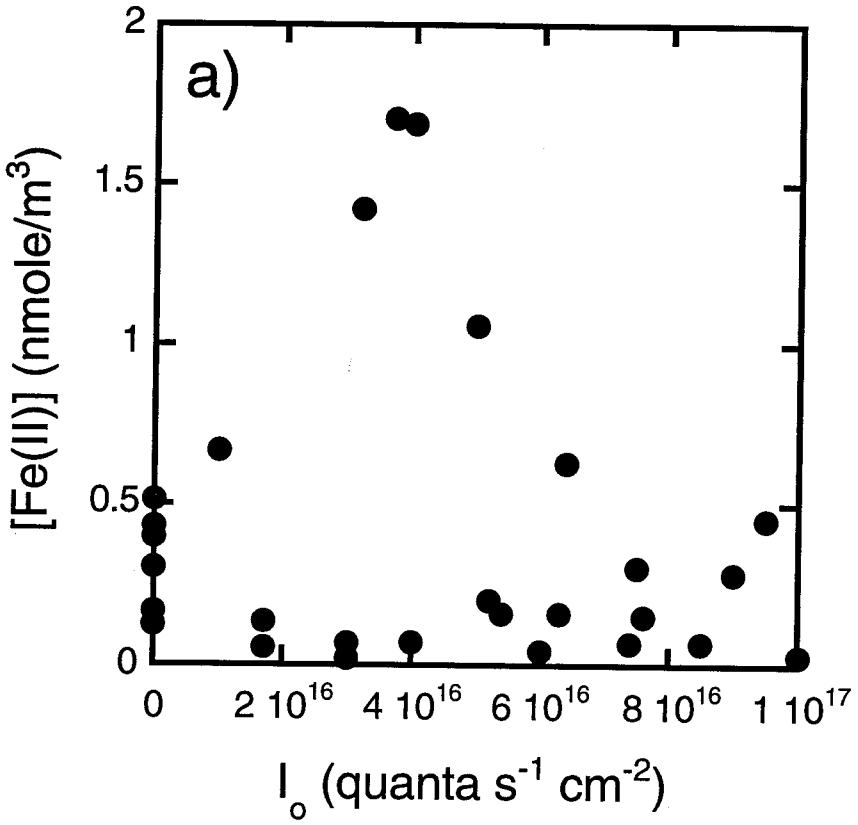

Figure 1a: Correlation between Fe(II) and light in cloudwater samples. Concentrations were obtained by multiplying the measured concentration in a sample with the liquid water content of the cloud in order to obtain concentration per unit volume of air.

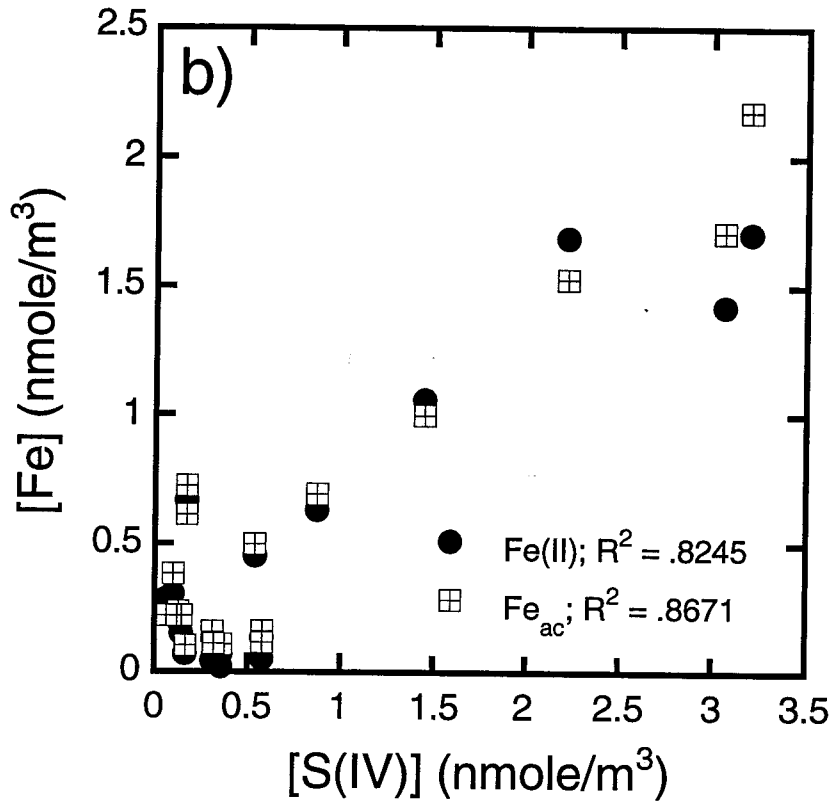

Figure 1b: Correlation between both Fe(II) and $Fe_{acidified}$ {Fe(II)+Fe(III)} and S(IV) concentration in unfiltered cloudwater samples. Concentrations were obtained by multiplying the measured concentration in a sample with the liquid water content of the cloud in order to obtain concentration per unit volume of air.

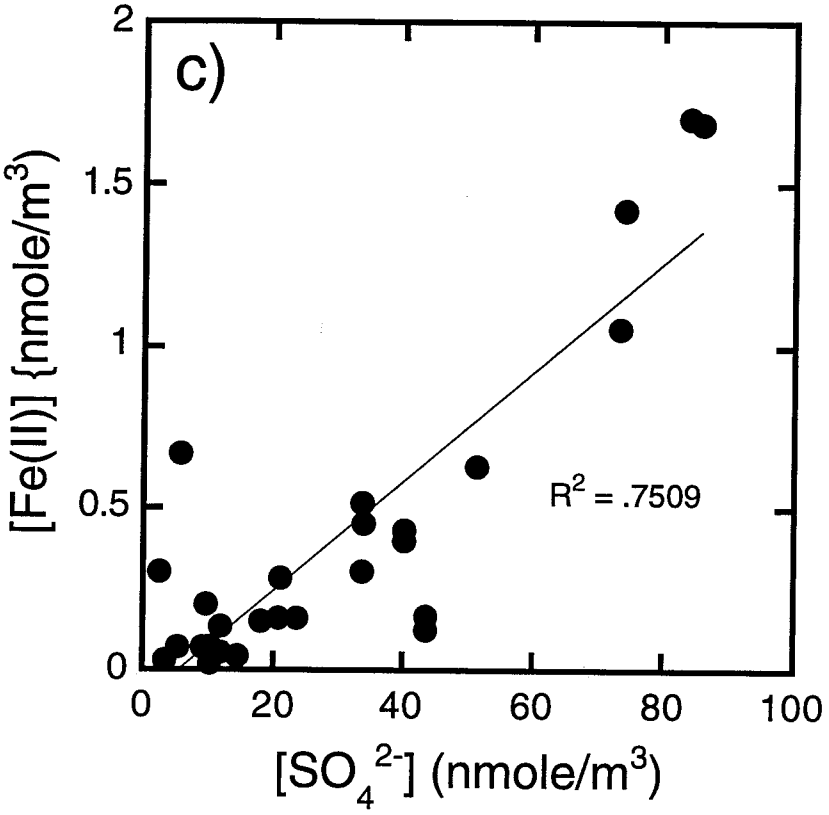

Figure 1c: Correlation between Fe(II) and SO_4^{2-} in cloudwater samples. Concentrations were obtained by multiplying the measured concentration in a sample with the liquid water content of the cloud in order to obtain concentration per unit volume of air.

We found a strong linear correlation between the concentrations of Fe of both oxidation states {Fe(III), Fe(II)} and the concentrations of both oxidation states of sulfur {S(IV), S(VI)} (Fig. 1b, c). This type of correlation indicates that the relationship between Fe(II) and S(IV) is not determined solely by *in situ* redox chemistry but that their relationship might also be controlled by a common source of S and Fe. The measured values of S/Cl ratios suggest that most of the S in the cloudwater samples comes from non marine (most likely anthropogenic) sources. More study is needed to test the importance of Fe in controlling the oxidation of S(IV) in cloud and fog samples, as well as the possibility that the reversible formation of aldehyde-bisulfite adducts prevent S(IV) from complexing Fe in cloud and fog samples (40, 41).

Among the organic compounds in cloudwater, we studied HCHO, HCO_2^-, $CH_3CO_2^-$ and $C_2O_4^{2-}$, as potential electron donors for the reduction of Fe(III) to Fe(II) (26, 27). The sum of $[HCO_2^-]$ + $[CH_3CO_2^-]$ +[HCHO] in the cloudwater samples correlates strongly with TOC ($R^2 = 0.984$), and comprises approximately 20% of the TOC ($[C_2O_4^{2-}]$ values were below detection limit in many of the samples). A plot of [Fe(II)] vs. $[HCO_2^-]$ shows two distinctive trends (Fig. 2a). The data points that are correlated along the line with a steeper slope (i.e., more Fe(II) per mole of HCO_2^-) represent cloudwater samples that have higher total Fe (Fe_{ac}) concentrations (Fig. 2b) and in general higher $[CH_3CO_2^-]/[HCO_2^-]$ ratios (~ 1:1) than the data obtained from samples falling on the line with a lower slope ($[CH_3CO_2^-]/[HCO_2^-] \sim 0.5$). Anthropogenic continental air masses appear to have higher $[CH_3CO_2^-]/[HCO_2^-]$ ratios than air masses originating in remote environments (42-44). Therefore, the relationship between Fe and HCO_2^- appears to be determined primarily by their common source region, although redox reactions cannot be ruled out. Samples correlated along the line with a steeper slope in Figure 2a are indicative of air masses of anthropogenic origin, while those correlated along the line with a lower slope appear to be cleaner air masses. In contrast, it seems that redox reactions, rather than

a common source, control the relationship between Fe and $CH_3CO_2^-$. This is suggested by the fact that the correlation between $CH_3CO_2^-$ and Fe(II) (Fig. 2c) is much better than the correlation between $CH_3CO_2^-$ and Fe_{ac} (Fig. 2d) and between Fe(II) and HCO_2^-. Acetate is formed either by the oxidation of aldehydes as catalyzed by Fe(III)/Fe(II) or it is depleted by direct electron transfer to Fe(III) species; or both processes may take place simultaneously. The Fe-catalyzed oxidation of aldehydes to produce carboxylic acids might provide an important source of these acids to the troposphere (45).

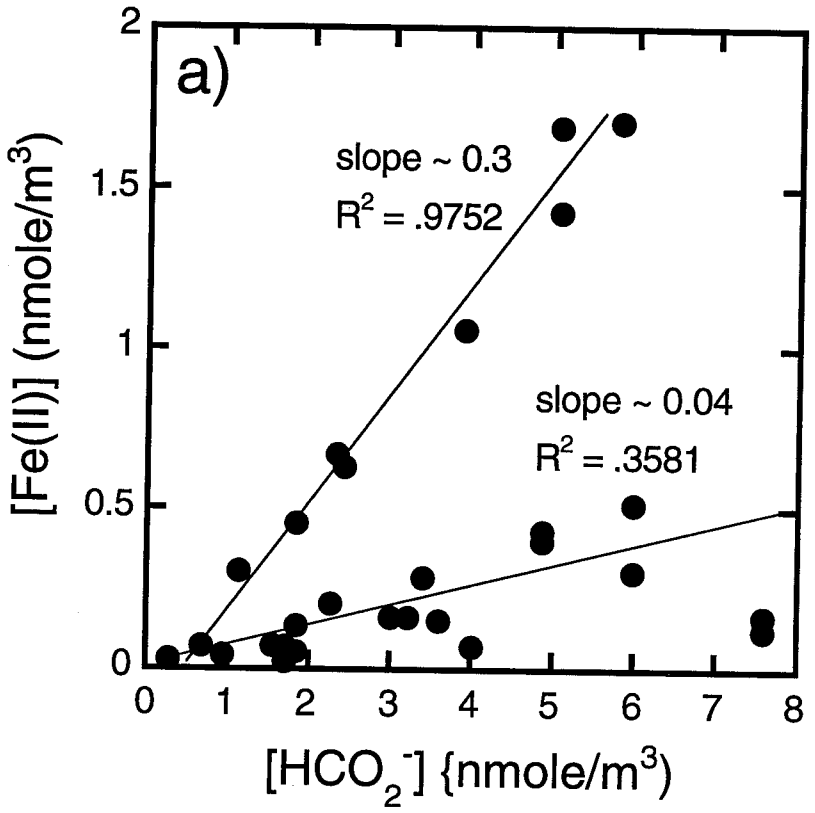

Figure 2a: The correlation between Fe(II) and formate in cloudwater samples.

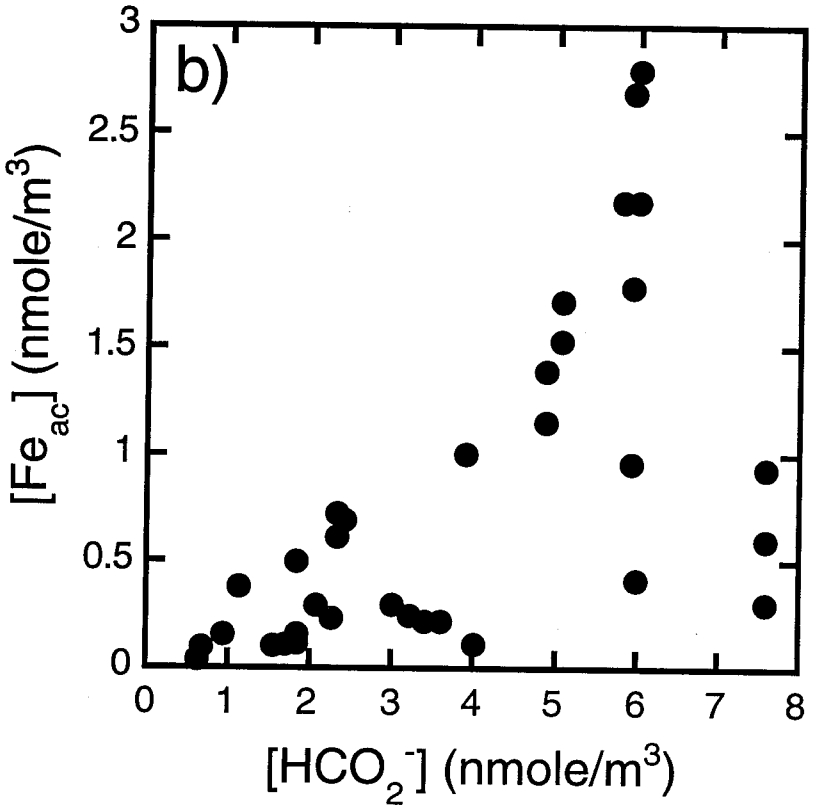

Figure 2b: The correlation between $Fe_{acidified}$ and formate in cloudwater samples.

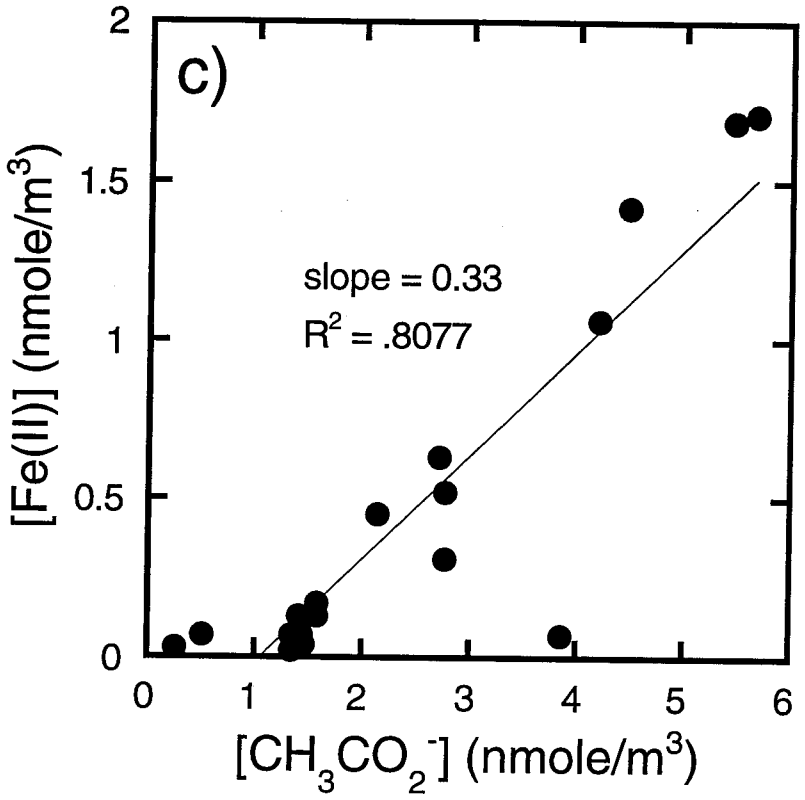

Figure 2c: The correlation between Fe(II) and acetate in cloudwater samples.

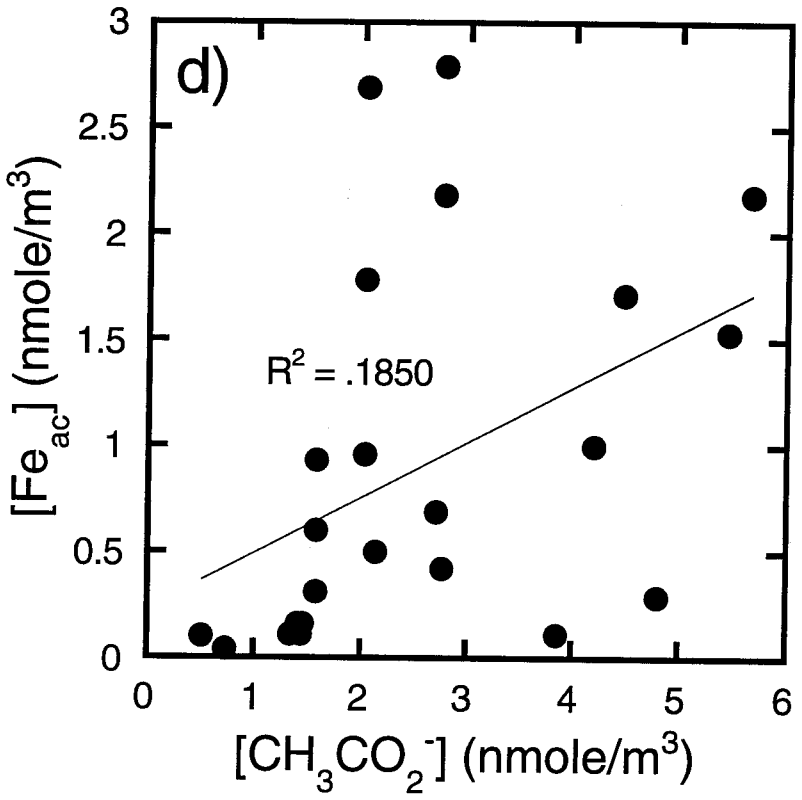

Figure 2d: The correlation between $Fe_{acidified}$ and acetate in cloudwater samples.

The relationship between Fe and $C_2O_4^{2-}$ is different from the observed linear relationships between Fe(II) and both HCO_2^- and $CH_3CO_2^-$ (Fig. 3). Although we have analyzed relatively few cloudwater samples with measurable Fe(II) and $C_2O_4^{2-}$ concentrations, it appears that there is no correlation between their concentrations (Table 1, Fig. 3). Therefore, it is suggested that Fe and $C_2O_4^{2-}$ do not have common sources, and that $C_2O_4^{2-}$ has no net effect on the formation of Fe(II). On the other hand, the $C_2O_4^{2-}$ (but neither HCO_2^- nor $CH_3CO_2^-$) concentrations in cloudwater samples show a positive correlation with H_2O_2 (Fig. 3). These observations suggests that Fe may have had a primary source of emission to the atmosphere while $C_2O_4^{2-}$ had a secondary source (i.e., photochemical production involving peroxide) in the atmosphere (46).

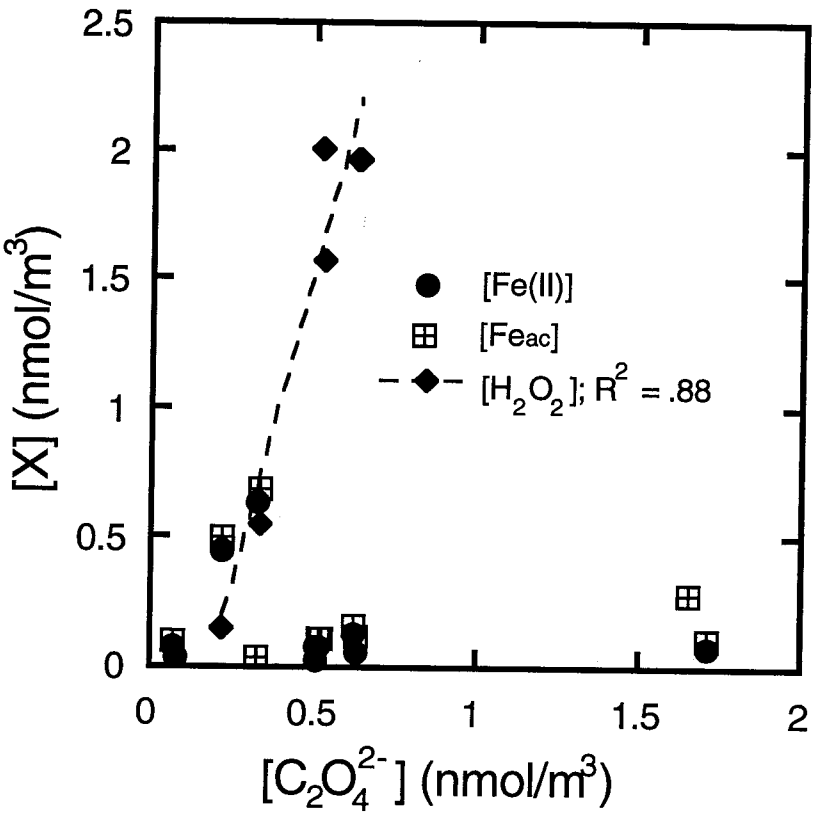

Figure 3: Fe(II), Fe_{ac}, and H_2O_2+ROOH vs. $C_2O_4^{2-}$.

Results from our ongoing laboratory investigation on the photoreduction of aerated suspensions of goethite (α-FeOOH), hematite (α-Fe_2O_3), amorphous Fe hydroxide (*am*-$Fe(OH)_3$), and ambient aerosol particles are consistent with the results obtained in the field. In these laboratory experiments, no Fe(II) was detected in irradiated particle suspensions in the presence of $C_2O_4^{2-}$, while at the same time high concentrations of H_2O_2 were produced (47). When similar experiments were performed in the presence of HCO_2^- and $CH_3CO_2^-$, a significant fraction of Fe(III) was reduced to Fe(II) without the concomitant production of H_2O_2. Our observations are consistent with those of Wehrli et al. (48) and Siffert and Sulzberger (49); they noted that Fe(II) is not produced in irradiated α-Fe_2O_3 suspensions in the presence of $C_2O_4^{2-}$ under oxic conditions. In these cases, adsorbed $C_2O_4^{2-}$ appears to be oxidized by dioxygen (O_2) adsorbed on the surface of the Fe(III) oxyhydroxides to form H_2O_2 and CO_2. The H_2O_2 in turn oxidizes Fe(II) released from the particle surface before it diffuses to the bulk solution. However, under anoxic conditions appreciable concentrations of Fe(II) were detected (48, 49). Based on these observations, there appears to be a unique photochemical behavior for $C_2O_4^{2-}$ in the presence of Fe(III) oxyhydroxide surfaces.

In order to assist in the interpretation of the aqueous-phase speciation of Fe, we have predicted, via rigorous thermodynamic calculation, the soluble Fe-containing species in the cloudwater samples. For these calculations we used the measured concentrations of components {including Fe(III) and Fe(II)} observed in an 1/2 hour period in a stratus cloud event that was 5 hours in duration (sample # 45 Table 1; similar results were obtained with all the samples which contained appreciable concentrations of $C_2O_4^{2-}$). The major Fe species were as follows: $Fe(C_2O_4)_3^{3-}$, $Fe(H_2O)_2(C_2O_4)_2^-$, $Fe(H_2O)_4(C_2O_4)^+$, and $Fe(H_2O)_6^{2+}$ (Fig. 4a, b). Under the above assumptions (not considering any other organic ligands that might be present in solution), the three Ferric iron species constitute more than 95% of the total dissolved Fe(III). This computation demonstrates the strong chemical

interaction between $C_2O_4^{2-}$ and Fe(III). However, most of the cloudwater samples contained low levels of $C_2O_4^{2-}$ (< 1-2 μM). Similar calculations done on these samples show that hydrolysis is the main reaction which controls the speciation of Fe(III). Among the Fe(III)-$C_2O_4^{2-}$ species, $Fe(H_2O)_2(C_2O_4)_2^-$ which is photochemically reactive (50) makes up 85 % of the Fe(III) concentration. Oxalate reacts with hexaquo Fe(III) to form an inner-sphere complex which then undergoes a ligand-to-metal electron transfer (i.e., to produce $Fe(II)C_2O_4^{-\cdot}$; 46). Fe(II), which is present mostly as $Fe(H_2O)_6^{2+}$, is likely to be oxidized via one of the following pathways: 1) oxidation by O_2 (reasonably fast at pH above 5; 51, 52), 2) H_2O_2, and 3) O_3 (53). Of the three pathways it seems that in cloudwater samples of pH below 4.5 (i.e., all the samples except the ones collected in Bakersfield) Fe(II) reaction with H_2O_2 to form •OH is the predominant pathway:

$$Fe^{2+} + H_2O_2 \xrightarrow{k_1} Fe^{3+} + {}^{\bullet}OH + OH^- \qquad (1)$$

$$FeOH^+ + H_2O_2 \xrightarrow{k_2} Fe(OH)_2^+ + {}^{\bullet}OH \qquad (2)$$

The species-dependent reactivity of Fe(II) toward H_2O_2 is seen clearly by comparison of k_1 (76 $M^{-1}s^{-1}$; 54) and k_2 (1.9 x 10^6 $M^{-1}s^{-1}$; 55). Fe(II) also reacts with hydroperoxyl radical to form H_2O_2,

$$Fe^{2+} + HO_2^{\bullet} + H_3O^+ \longrightarrow Fe^{3+} + H_2O_2 + H_2O \qquad (3)$$

and with peroxymonosulfate (56) to yield Fe(III) and S(V) as $SO^-_4{}^{\bullet}$:

$$Fe^{2+} + HSO_5^- \longrightarrow FeOH^{2+} + SO_4^{\bullet-} \qquad (4)$$

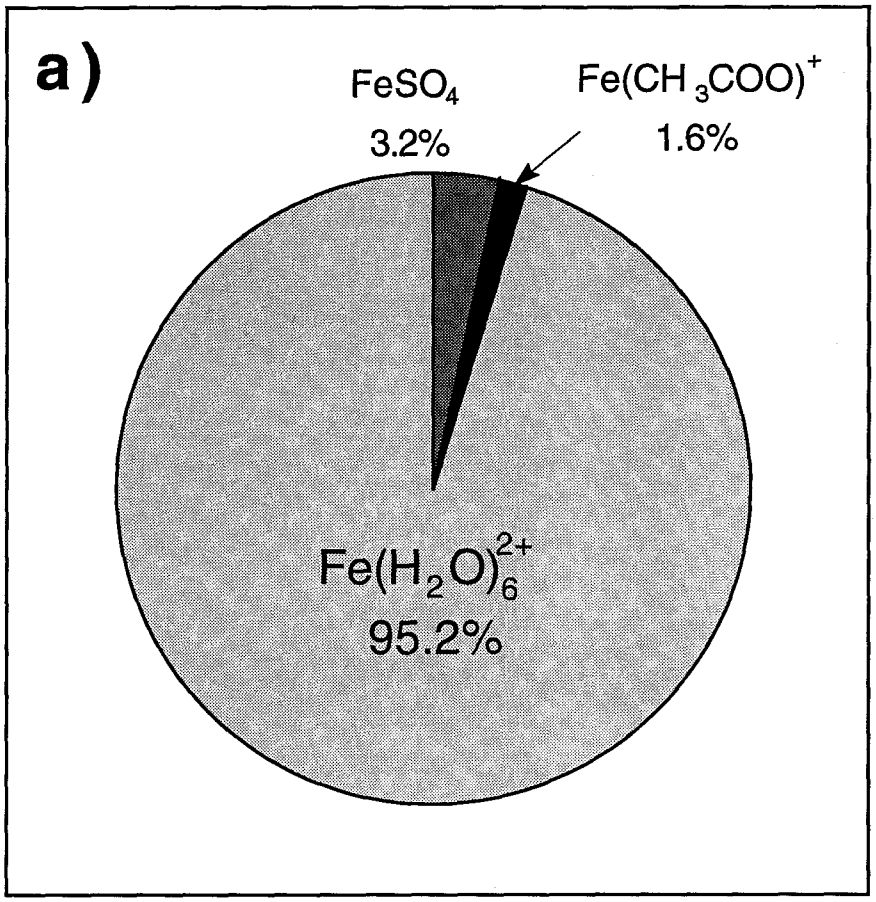

Figure 4a: Speciation calculation of Fe(II). Calculation was carried out on sample # 45, Table 1. The measured concentrations are (μM): [Fe(III)] = 1.2; [Fe(II)] = 1.8; $[SO_4^{2-}]$ = 260; $[(CH_3COO + COO)_{tot}]$ = 77; $[(C_2O_4)_{tot}]$ = 13; $[H_2O_2]$ = 41; [HCHO] = 10; pH = 3.4.

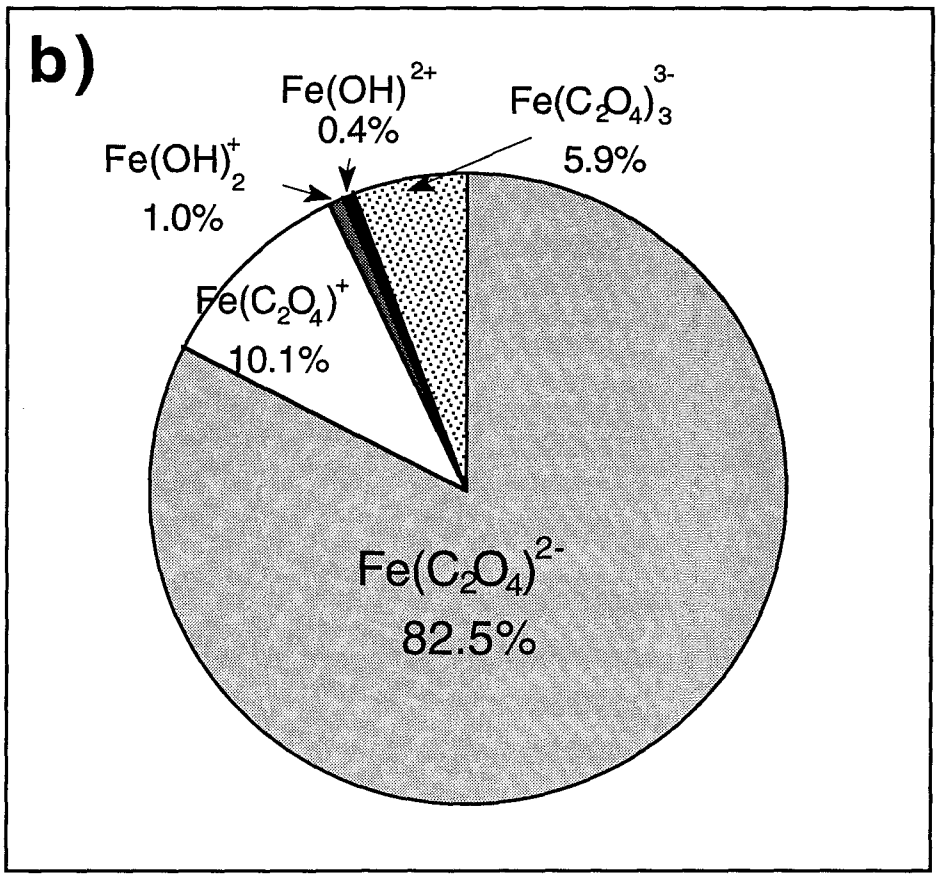

Figure 4b: Speciation calculation of Fe(III). Calculation was carried out on sample # 45, Table 1. The measured concentrations are (μM): [Fe(III)] = 1.2; [Fe(II)] = 1.8; $[SO_4^{2-}]$ = 260; $[(CH_3COO + COO)_{tot}]$ = 77; $[(C_2O_4)_{tot}]$ = 13; $[H_2O_2]$ = 41; [HCHO] = 10; pH = 3.4.

The samples collected in Bakersfield have the lowest content of Fe(II) although their Fe_{ac} content is similar to other samples (Table 1). It is interesting to note that the Bakersfield samples have pH values above 6.4. At this pH range oxidation of Fe(II) by oxygen (Haber-Weiss mechanism) is a rapid process operating in addition to the oxidation of Fe(II) by peroxides (which itself is faster at high pH) to suppress the concentration of Fe(II) in solution. Another explanation for the low Fe(II) content of the Bakersfield samples is discussed in the next paragraph.

The similarity between the field results and the laboratory experiments on particle suspensions implies that photo-assisted heterogeneous reactions are taking place within cloudwater droplets. The presence of surface-bound Fe is indicated by the results shown in Figure 5. In this case, the concentration of reactive Fe (Fe_{reac} = [Fe(II)] + [Fe(III)]) was always found to be larger than filtered Fe, Fe_{flt} (i.e., [Fe(II)+Fe(III)] < 0.025μm), and was either smaller or equal to [Fe_{ac}]. [Fe_{ac}] is the sum of [Fe(II)] and [Fe(III)] measured as total Fe in an unfiltered sample at pH = 1. This latter value includes Fe that is dissolved, Fe released to solution from particle surfaces and Fe released to solution from the dissolution of oxyhydroxides at pH 1. Fe_{ac} values in the samples were always lower than total Fe values (Fe_{dgs}, the concentration of Fe in filtrate + filter digest; i.e., digested with concentrated HF and HNO_3), suggesting that only a fraction of the total Fe in aerosols is likely to be released to cloudwater either by proton promoted or by reductive dissolution. Fe_{ac}/Fe_{dgs} ratios varied largely from one sample to another, suggesting that the fraction of reactive Fe in aerosol samples was sensitive to the nature of the Fe-containing phases, which in turn were determined by the sources of Fe to the atmosphere. Such observations might explain the discrepancies between different authors regarding the fraction of reactive Fe in atmospheric aerosols (22-24). Based on selective leaching experiments (Ron Siefert, California Institute of Technology, personal communication) it appears that approximately 5-10% of the total Fe in aerosols collected in Los Angeles was associated with natural and

anthropogenic organic compounds via surface coatings and inter-growth. These organic compounds could serve as electron donors to reduce particulate Fe(III). Furthermore, the low Fe(II) content of the high pH samples from Bakersfield is in accordance with the well documented observations that both organic ligands and bisulfite are not likely to be adsorbed to Fe-rich phases at high pH, and therefore heterogeneous electron transfer reactions are less likely to take place (57, 58).

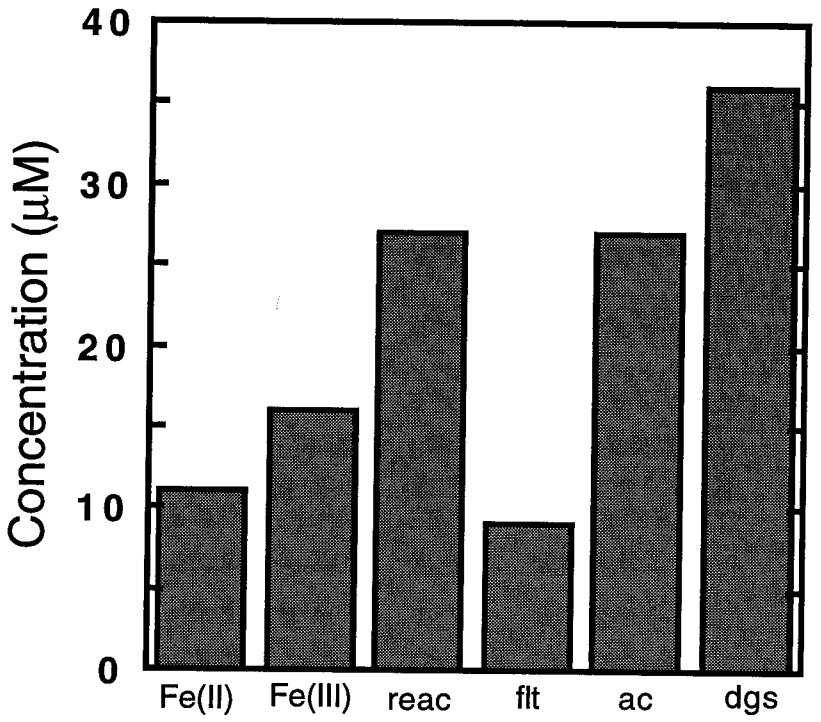

Figure 5: Distribution of Fe between small colloidal (< 0.025 μm) and particulate phases in a cloudwater sample. Fe(II), Fe(III) were measured spectrophotometrically in an unfiltered sample aliquot, reac = Fe_{reac} the sum of the previous columns, flt = Fe_{flt}, (both oxidation states) measured by DCP in a filtered aliquot of the sample (0.025 μm Millipore® filter) ; ac = Fe_{ac}, (both oxidation states) measured by DCP in an aliquot of the sample that was acidified to pH = 1 and then filtered; dgs = Fe_{dgs}, sum of Fe_{flt} and Fe (both oxidation states) measured by DCP in particles collected on the filter after they were digested with concentrated HF and HNO_3.

Conclusions

We suggest that the redox cycle of Fe in the near-shore continental troposphere involves both dissolved and aerosol surface species. Only a fraction of the total Fe measured in atmospheric aerosols is likely to participate in these redox reactions, and this fraction varies greatly from one sample to another. Photoreduction of Fe(III) in fog and cloudwater samples appears to be more significant than thermal reduction, although Fe(II) was also detected in the dark. Fe(III) reduction is determined primarily by oxidizable organic compounds, which undergo thermal and photo-assisted oxidation by Fe(III) to yield carboxylic acids. The strong correlation observed between Fe(II) and organic matter, in the face of much weaker correlation between total Fe and organic matter, suggests chemical interdependency between Fe and some organic compounds (e.g., $CH_3CO_2^-$) in fog and cloudwater samples. In addition, Fe(III)-organic compounds reactions may provide an important source of carboxylic acids in the troposphere.

Acknowledgments

The authors wish to thank Drs. George Luther, Tom Church, Alan Veron, and the crew of R.V. Cape Henlopen, the College of Marine studies at the University of Delaware, Cliff Weinman and his staff at the FAA radar facility in San Pedro, Drs. Ted Murphy and Mel Dutton of the California State University Bakersfield, and the staff of LA county fire department at Henniger Flats for their help in sample collection. The authors also wish to thank J. J. Morgan, B. Faust and J. Winchester for their helpful comments. Support for this work was provided by a grant from the National Science Foundation (ATM 9015775), additional support for the work in Delaware Bay was provided by NSF grant OCE 8916804.

References

1. Jacob, D. J.; Hoffmann, M. R. *J. Geophys. Res.*, **1983**, *88*, 6611.

2. Hoffmann, M. R.; Jacob, D. J. "Kinetics and Mechanism of the Catalytic Oxidation of Dissolved SO_2 in Atmospheric Droplets: Free Radical, Polar and Photoassisted Pathways" in "SO_2, NO, NO_2 Oxidation Mechanisms: Atmospheric Considerations," Butterworth Publishers: Boston, **1984**, 101.

3. Weschler, C. J.; Mandich, M. L.; Graedel, T. E. *J. Geophys. Res. A.*, **1986**, *91*, 5189.

4. Faust, B. C.; Hoigne, J. *Atmos. Environ. A.*, **1990**, *24*, 79.

5. Jackson, G. A.; Morgan, J. J. *Limnol. Oceanog.*, **1978**, *230*, 268.

6. Anderson, M. A.; Morel, F. M. M. *Limnol. Oceanogr.*, **1982**, *27*, 789.

7. Duce, R. A. "The Impact of Atmospheric Nitrogen, Phosphorous and Iron Species on Marine Biological Productivity" in "The Role of Air-Sea Exchange in Geochemical Cycling," D. Reudel Publishing: Dordrecht, **1986**, 497.

8. Martin, J. H.; Fitzwater, S. E. *Nature,* **1988**, *331*, 341.

9. Martin, J. H.; Gordon, R. M.; Fitzwater, S. E.; Broenkow, W. W. *Deep-Sea Research Part A- Oceanographic Research Papers,* **1989**, *36*, 649.

10. Morales, C. "Saharan Dust - Mobilization, Transport, Deposition," Wiley: New York, **1979**, 320.

11. Hansen, L. D.; Silberman, D.; Fisher, G. L.; Eatough, D. J. *Environ. Sci. Technol.*, **1984**, *18*, 181.

12. Pandis, S. N.; Seinfeld, J. H. *J. Geophys. Res.*, **1989**, *94*, 2911.

13. Pandis, S. N.; Seinfeld, J. H.; Pilinis, C. *Atmos. Env. A,* **1992**, *26*, 2509.

14. Cunningham, K. M.; Goldberg, M. C.; Weiner, E. R. *Photochem. Photobiol.*, **1985**, *41*, 409.

15. Faust, B. C.; Hoffmann, M. R. *Environ. Sci. Technol.*, **1986**, *20*, 943.

16. Martin, L. R.; Hill, M. W.; Tai, A. F.; Good, T. W. *J. Geophys. Res.*, **1991**, *96*, 3085.

17. Hong, H.; Kester, D. R. *Limnol. Oceanogr.*, **1986**, *31*, 512.

18. Landing, W. M.; Westerlund, S. *Mar. Chem.*, **1988**, *23*, 329.

19. McKnight, D. M.; Kimball, B. A.; Bencala, K. E. *Science,* **1988**, *240*, 637.

20. Behra, P.; Sigg, L. *Nature,* **1990**, *344*, 419.

21. Dedik, A. N.; Hoffmann, P.; Ensling, J. *Atmos. Env. A.*, **1992**, *26*, 2545.

22. Zhuang, G.; Yi, Z.; Duce, R. A.; Brown, P. R. *Global Biogeochemical Cycles,* **1992**, *6*, 161.

23. Zhuang, G.; Yi, Z.; Duce, R. A.; Brown, P. R. *Nature,* **1992**, *355*, 537.

24. Zhu, X. R.; Prospero, J. M.; Savoie, D. L.; Millero, F. J.; Zika, R. G.; Saltzman, E. S. *J. Geophys. Res. A.*, **1993**, *98*, 9039.

25. Daube, B. C. J.; Flagan, R. C.; Hoffmann, M. R. *United States Patent No. 4,697,462,* **1987**.

26. Munger, J. W. "The Chemical Composition of Fogs and Clouds in Southern California," Ph. D. thesis, California Institute of Technology, **1989**, 67.

27. Kawamura, K.; Kaplan, I. R. "Organic Compounds in Rainwater" in "Organic Chemistry of the Atmosphere," CRC Press: Boca Raton, **1991**, 233.

28. Jacob, D. J.; Munger, J. W.; Waldman, J. M.; Hoffmann, M. R. *J. Geophys. Res. A,* **1986**, *91*, 1073.

29. Smith, R. V.; Erhardt, P. W. *Anal. Chem.*, **1975**, *47*, 2462.

30. Kok, G. L.; Thompson, K.; Lazrus, A. L. *Anal. Chem.*, **1986**, *58*, 1192.

31. Stookey, L. L. *Anal. Chem.*, **1970**, *42*, 119.

32. Carter, P. *Anal. Biochem.*, **1971**, *40*, 450.

33. Pehkonen, S. O.; Erel, Y.; Hoffmann, M. R. *Environ. Sci. Technol.*, **1992**, *26*, 1731.

34. Garcia-Vargas, M.; Belizon, M.; Hernandez-Artiga, M. P.; Martinez, C.; Perez-Bustamante, J. A. *A. Spectroscopy,* **1986**, *40*, 1058.

35. Zatar, N. A.; Abu-Zuhri, A. Z.; Al-Nuri, M. A.; Mahmoud, F. M.; Abu-Obaid, A. A. *Spec. Letters,* **1989**, *22*, 1203.

36. Humphrey, R. E.; Ward, M. H.; Hinze, W. *Anal. Chem.*, **1970**, *42*, 698.

37. Morel, F. M. M.; Morgan, J. J. *Environ. Sci. Technol.*, **1972**, *6*, 58.

38. Faughnan, M. "SURFEQL - An Interactive Code for Circulation of Chemical Equilibria in Aqueous Solution," California Institute of Technology, **1981.**

39. Westall, J. C. "Adsorption Mechanisms in Aquatic Surface Chemistry" in "Aquatic Surface Chemistry," John Wiley & Sons: New York, **1987**, 3.

40. Conklin, M. H.; Hoffmann, M. R. *Environ. Sci. Technol.*, **1988**, *22*, 899.

41. Olson, T. M.; Hoffmann, M. R. *Atmos. Environ.*, **1989**, *23*, 985.

42. Keene, W. C.; Galloway, J. N. *Atmos. Environ.*, **1984**, *18*, 2491.

43. Talbot, R. W.; Beecher, K. M.; Harriss, R. C.; Cofer, W. R. *J. Geophys. Res.*, **1988**, *93*, 1638.

44. Gunz, D. W.; Hoffmann, M. R. *Atmos. Environ.*, **1990**, *24A*, 1601.

45. Keene, W.; Galloway, J. N. *J. Geophys. Res.*, **1986**, *91*, 14466.

46. Zuo, Y.; Hoigné, J. *Environ. Sci. Technol.*, **1992**, *26*, 1014.

47. Pehkonen, S. O.; Siefert, R. L.; Erel, Y.; Webb, S.; Hoffmann, M. R. *Env. Sci. Technol.*, **1993**, *27*, 2056.

48. Wehrli, B.; Sulzberger, B.; Stumm, W. *Chem. Geol.*, **1989**, *78*, 167.

49. Siffert, C.; Sulzberger, B. *Langmuir*, **1991**, *7*, 1627.

50. Vincze, L.; Papp, S. *J. Photochem.*, **1987**, *36*, 289.

51. Stumm, W.; Morgan, J. J. "Aquatic Chemistry," Wiley: New York, **1981**, 345.

52. Millero, F. J.; Sotolongo, S.; Izaguirre, M. *Geochim. Cosmochim Acta*, **1987**, *51*, 793.

53. Hoigne, J.; Bader, H.; Haag, W. R.; Staehelin, F. *Water Res.*, **1985**, *19*, 993.

54. Walling, C. *Acct. Chem. Res.*, **1975**, *8*, 125.

55. Moffett, J. W.; Zika, R. G. *Environ. Sci. Technol.*, **1987**, *21*, 804.

56. Sato, T.; Gotto, T.; Okabe, T.; Lawson, F. *Bull. Chem. Soc. Jpn.*, **1984**, *57*, 2082.

57. Stumm, W.; Morgan, J. J. "Aquatic Chemistry," Wiley: New York, **1981**, 390.

58. Faust, B. C.; Hoffmann, M. R.; Bahnemann, D. W. *J. Phys. Chem.*, **1989**, *93*, 6371.

Chapter 6

Photoreduction of Iron Oxyhydroxides in the Presence of Important Atmospheric Organic Compounds

[The text of this chapter appeared in S. O. Pehkonen, R. Siefert, Y. Erel, S. Webb, and M. R. Hoffmann, Environmental Science and Technology, 1993, 27, 2056.]

Abstract

The photolytic reduction of amorphous iron hydroxide (am-$Fe(OH)_3$), lepidocrocite(γ-FeOOH), goethite(α-FeOOH), hematite (α-Fe_2O_3), maghemite (γ-Fe_2O_3) and natural iron-containing aerosol-particles in the presence of formaldehyde, formate, acetate, oxalate and butyrate has been investigated. Important parameters in the photoreduction experiments are pH, wavelength of the irradiating light, the nature of the electron donor and the characteristics of the iron phase. The present results show that the fastest rates of photoreduction of Fe(III) to Fe(II) are achieved with am-$Fe(OH)_3$ as the electron acceptor and formate as the electron donor. Maximum rates of photoreduction were observed at 330 nm with a continuous decrease to 405 nm. Natural iron-containing aerosol particles show similar photochemical behavior to am-$Fe(OH)_3$ and γ-FeOOH. These results suggest that a significant fraction of the reactive atmospheric iron in urban aerosol could be present as am-$Fe(OH)_3$ and γ-FeOOH. Ambient iron-containing aerosol particles with oxalate as the electron donor resulted in a significant photochemical production of H_2O_2.

Introduction

Iron is one of the most abundant elements in the earth's crust, where it is present both as Fe(II) and Fe(III) (1). Crustal iron is readily transferred into the atmosphere by wind and to a lesser extent by volcanic activity. Once in the atmosphere, iron {as Fe(II) and Fe(III)} plays an important role in the multiphase atmospheric chemistry of S(IV) (2-9). Graedel and co-workers (5, 6) have stressed the importance of iron speciation as a major factor controlling the reactivity of Fe(III) as a catalyst, as an oxidant and as a photolytic source of OH radical (10). Much of the total measured iron is predicted to be in the form of ferric oxides and oxyhydroxides based on thermodynamic considerations (11), and actual identification of α-Fe_2O_3, Fe_3O_4, α-FeOOH, and γ-FeOOH in airborne particles (12, 13). Some of the total iron in aerosols has also been found as Fe(II) (14).

When iron(III)-containing aerosols serve as cloud and fog condensation nuclei, particulate Fe is expected to participate in electron transfer reactions within the cloud droplet The Fe(II)/Fe(III) redox system also has a chemical and catalytic effect on other chemical species of interest in cloud, fog, haze aerosol and rain and other natural water systems (e.g., iron is an important component in the redox chemistry of chromium in estuarine water (15). Moreover, Fe(III) and Fe(II) have been found to co-exist in oxic surface waters (16-19).

Laboratory research in recent years has been focused on the photoreduction of a variety of iron phases in the presence of a variety of electron donors e.g., S(IV), benzoate, EDTA and oxalate (20-28). However, experiments that utilize as reductants important atmospheric organics (e.g., formate, acetate, formaldehyde) have not received much attention, although these organics, in addition to oxalate, may be controlling the redox chemistry of iron in atmospheric water (29-31). In addition, most of the previous

photoreduction studies, including a study of the photoreductive dissolution of hematite with oxalate (21), have been carried under anoxic conditions (e.g., under N_2 atmosphere) to minimize the reaction of Fe(II) with O_2. In this paper, we present results of experiments that probe the photoreduction of iron phases (natural and synthetic) in the presence of organic reductants such as formaldehyde, formate, acetate, oxalate and butyrate in aerated suspensions and over pH range typically observed in cloudwater (3.5 to 4.5). Our principal experimental objectives were to examine the photoreduction rates {Fe(III) ----> Fe(II)} of a variety of iron oxide polymorphs as a function of pH, λ_{irrad} and e^- donor. Results of these experiments are compared to photoreduction reactivity of collected aerosol particles. Comparison of the quantitative and qualitative trends in photoreduction may provide insight into the reactive iron phases in ambient aerosol.

Experimental

Amorphous iron hydroxide(am-$Fe(OH)_3$) was prepared using the method described by Schwertmann and Cornell (32). Fresh iron hydroxide colloids were prepared every 10 days to avoid difficulties that arise from the slow transformation of am-$Fe(OH)_3$ to goethite (33). This transformation was monitored with a Scintag PAD-5 X-Ray Diffractometer with an automated $\theta/2\theta$ goniometer by following the appearance of distinct X-ray diffraction peaks of goethite. Goethite was prepared according to Scott (34), lepidocrocite was prepared using a method by Sorensen and Thorling (35), maghemite was prepared using the method described by Schwertmann and Cornell (32) and hematite was purchased from Harcros Pigments Inc.. All of the iron phases were washed several times with Milli-Q water to remove residual ionic species.

The identity of the iron phases was determined by X-ray diffraction analysis using a Scintag PAD-5 X-Ray Diffractometer with an automated $\theta/2\theta$ goniometer. The particle

size distribution of the different iron phases was determined by photon correlation spectroscopy (PCS) method with a sub-micron particle-size analyzer (Malvern 4700 M/SM). In addition, the size and the shape of the crystals were determined by TEM (Phillips 430 {300 kV} Analytical Electron Microscope).

The wavelengths of irradiation were controlled by the selective use of filters (I, 320-370 nm; II, 325-800 nm; III, 410-800 nm) having windows in those regions or by use of a monochromator with a 5 nm bandwidth. The photochemical reaction vessel (shaped like a beaker) had a capacity of 100 ml and was stirred using a magnetic stirrer. The vessel had a flat window with an area of 8.5 cm^2 on one side for the illuminating light. The vessel was open to the atmosphere in order to simulate conditions similar to those found in a cloud droplet or haze aerosol particle. The pH and ionic strength were kept constant by the presence of the electron donors at concentrations of 6 mM, with the exception of HCHO, in which case the pH was adjusted by the addition of a small amount of $HClO_4$ as pH increased slightly during the reaction due to the consumption of protons. When electron donors served as the buffers, the pH increase was limited to 0.05 to 0.1 pH units during the course of the reaction with the exception of experiments carried out with oxalate, in which case pH increased several pH units during the course of the reaction. The electron donors (formate, acetate, butyrate and oxalate) have pK_a's in the region from 3.7 to 4.7 and by adjusting the ratio of the protonated form of the electron donor to the unprotonated form, one can adjust the pH of the electron donor solution within 0.5 of the pK_a without greatly reducing the buffering capacity. The temperature of the reaction vessel was kept constant at 25 °C (room temperature) via fan-driven air cooling. Aliquots were withdrawn with a syringe at different times and filtered through a 0.2 μm cellulose acetate syringe filter before the addition of Ferrozine (36, 37) (iron(II) measurement), DPKBH (38-40) (iron(II) and iron(III)), POPA (fluorescence of a 4-hydroxyphenylacetic acid dimer formed with H_2O_2) (41) (H_2O_2 measurement) or pH measurement. Oxalate was measured by Dionex

Capillary Electrophoresis system with the buffer: 5.0 mM potassium hydrogen phthalate, 0.5 mM tetradecyltrimethyl ammonium bromide and 2.0 mM sodium borate.

In most cases a minimum of three replicate experiments were performed and the iron(II) concentrations at different times (e.g., at 50, 300 and 1000 minutes) during the replicate experiments were averaged and the relative standard deviation (100% x standard deviation / the average) was used as the magnitude of the error bars in the graphs. Initial rates of photoreduction of iron and photoproduction of H_2O_2 were determined by a linear least squares fit when the data points formed a straight line from the beginning of the experiment to the end and by a linear least squares fit of the first three data points in cases where linearity did not persist. Apparent quantum efficiencies were calculated using the standard equation described elsewhere (20) with the exception that absorbance in Table 2 refers to the am-$Fe(OH)_3$ suspension in the presence of formate with same concentrations as used in the photoreduction experiments and therefore includes light scattering by the particles in addition to absorbance.

The photon flux of the light source was measured using Aberchrome 540 {(E)-α-(2,5-dimethyl-3-furylethylidene) (isopropylidene) succinic anhydride} (42) and also by a digital irradiance meter, which has been used in related field studies (31) to measure light intensity on a cloudy day at the time of atmospheric water collection. The light intensity of our 450 W xenon lamp is similar to the light intensity measured on a cloudy, foggy summer morning between 8 am and 11 am from 380 nm to 750 nm (~15 - 40 x 10^{15} quanta sec^{-1} cm^{-2}).

The filters used in all experiments were 47 mm Gelman Zeflour Teflon ® filters with a pore size of 1 μm. The filters were cleaned in a 10% HF bath for 24 hours, and in a 10% HCl bath for 24 hours prior to aerosol collection (Seastar acids and 18 MΩ Milli-Q water were used). The filters were also rinsed 4 times with 18 MΩ Milli-Q water between

the baths, and after the final bath. Aerosol samples were collected on the roof of the Millikan Library of the California Institute of Technology on 9 filters from 11:30 am on 9/1/92 to 1:30 PM on 9/10/92 (218 hr) with the pumping rate of 10 L $min.^{-1}$. After the collection each filter had an aerosol mass of ~ 6.5 mg. One filter was used for each photoreduction experiment. Each filter was sonicated inside the reaction vessel for 90 minutes with ~ 100 g of 18 MΩ Milli-Q water in order to suspend the aerosol into solution with ~ 80 % mass removal efficiency. After the sonication the filter was removed from the reaction vessel and the photoreduction experiment was initiated.

The concentration of {>FeOH} of each iron phase was calculated using the following formula (43).

$$[\{> FeOH\}] = \frac{\frac{M_{Fe}}{d_{Fe} \cdot V} \cdot SA \cdot d_{OH} \cdot \frac{10^{18}\,\mathrm{nm}^2}{1\,\mathrm{m}^2}}{N} \quad (\mathrm{M}) \qquad (1)$$

where

SA = Surface area of a particle (m^2)

d_{OH} = Site density of OH groups (per nm^2)

N = Avogadro's number

M_{Fe} = Mass of Iron (g)

V = Volume of a particle (cm^3)

d_{Fe} = Density of a particle (g/cm^3)

In this formula the density of surficial OH groups, d_{OH}, was assigned to be 22 for hematite, 11 for amorphous iron and 16 for goethite (44) and 10 for lepidocrocite. Values of density of particles of each iron phase were obtained from Schwertmann and Cornell (45). The surface area of a particle and the volume of a particle were calculated from the shape and size obtained from TEM. Cylindrical and round were the two geometries used in this calculation.

Results and Discussion

Effects of the Electron Donor and pH

The rates of photoreduction of iron oxyhydroxide polymorphs with formate, acetate, butyrate and formaldehyde are summarized in Table 1. Figure 1 shows the trends of photochemical reduction of iron in the case of am-$Fe(OH)_3$. Other iron oxyhydroxides show similar behavior and therefore are not plotted, but rather the rates are summarized in Table 1. As can be seen in Figure 1 there are a number of important trends in the photoreduction of iron phases in the presence of the different organic electron donors. First of all, formate reduced iron(III) at the fastest rate (critical stability constant is $10^{3.1}$ for formate-iron(III) complex), acetate being the second most efficient reductant. Butyrate appears to be a less effective electron donor than acetate, indicating that the formation of a reactive surface complex (step 2) and/or the subsequent electron-transfer reaction (step 3) can be the rate-limiting steps in the case of am-$Fe(OH)_3$ as originally hypothesized by Siffert and Sulzberger (21) for iron phases less stable than hematite. This hypothesis is contrary to the generally accepted mechanism shown below in equations 2-4 (46). Furthermore, the resulting rate law from this mechanism is: $d[Fe]/dt = k_4k_3k_2[\{>Fe(III)\text{-}OH\}][R]$. This rate law does not seem to be consistent with our experimental results in Figure 2, where the rate of reductive dissolution is plotted against the concentration of {>FeOH}. The difference in rate of photoreduction of iron between acetate and butyrate can be attributed to the steric hindrance effect of butyrate complexation compared to acetate (i.e., butyrate blocks some of the adjacent surface hydroxyl sites therefore reducing the overall observed rate of photoreduction) and not to the difference in surface complex stability, since the critical stability constants of acetate and butyrate complexes of iron(III) are so similar (i.e., $10^{3.4}$ for acetate (47) and ~$10^{3.4}$ for butyrate). The value for butyrate

has been estimated from propionate constant of iron(III) and from butyrate constants of Al and Cu (47).

	Goethite	Hematite	Maghemite	Lepidocrocite	Am-$Fe(OH)_3$	$Fe_{Aerosol}$
Formate	1.1	2.0	0.6	3.0	21	5.9
Acetate	0.33	0.50	0	0.69	4.4	2.4
Butyrate	0.48	0.80	-	-	3.2	-
HCHO	-	-	-	0.76	-	-
No Donor	0.019	0.0	-	0.19	1.1	-

Table 1: Initial rates (nM/min.) of photoreduction of iron oxyhydroxides with organic electron donors.

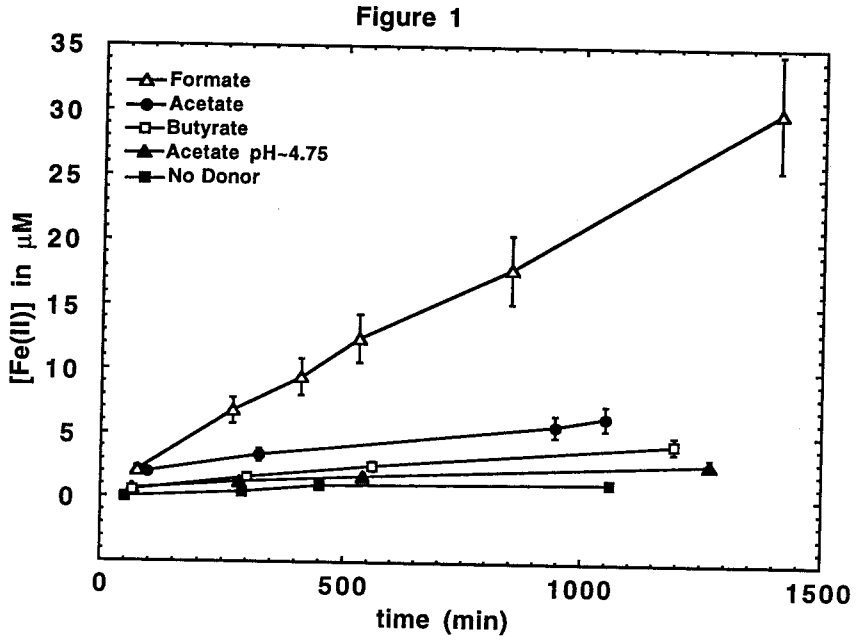

Figure 1: Photoreductive dissolution of amorphous $Fe(OH)_3$ with formate, acetate, butyrate and no organic electron donor. $[Fe(III)]_{initial}$ = 130 μM, $[Electron\ Donor]_{initial}$ = 6.0 mM, λ_{irrad} from 325 to 800 nm and pH ~ 4.25, except where noted.

Figure 2

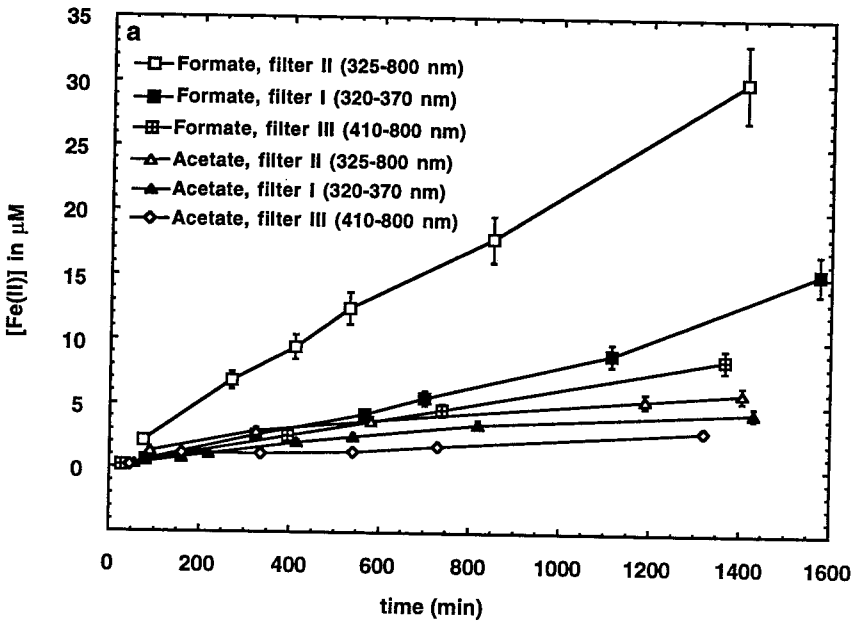

Figure 2a: The dependency of photoreduction of am-$Fe(OH)_3$ on the λ_{irrad}, $[Fe(III)]_{initial}$ = 130 µM, $[Electron\ Donor]_{initial}$ = 6.0 mM and pH ~ 4.25, in the presence of formate and acetate with three different filters having windows in the indicated regions: Filter I (320-370 nm), Filter II (325-800 nm) and Filter III (410-800 nm).

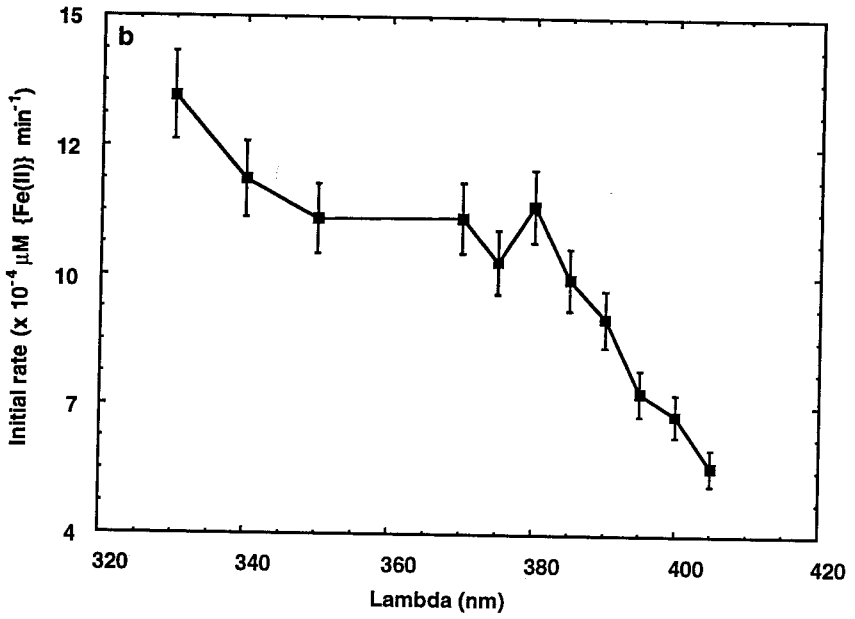

Figure 2b: The dependency of photoreduction of am-$Fe(OH)_3$ on the λ_{irrad}, $[Fe(III)]_{initial}$ = 130 µM, $[Electron\ Donor]_{initial}$ = 6.0 mM and pH ~ 4.25, in the presence of formate with monochromatic light of bandwidth of 5 nm from 330 to 405 nm.

$$\underset{\equiv \text{Fe(III)-OH}}{\text{Surface sites}} + \underset{\text{Reductant,R}}{\text{Reactants}} \underset{\text{fast}}{\overset{k_2}{\rightleftharpoons}} \underset{\equiv \text{Fe(III)-R}}{\text{Surface Species}} \qquad (2)$$

$$\underset{\equiv \text{Fe(III)-R}}{\text{Surface Species}} \underset{\text{electron transfer}}{\overset{h\nu \;\; k_3}{\rightleftharpoons}} \underset{\equiv \text{Fe(II)} \quad + \quad \text{R}^{\cdot}}{\text{Reduced surface species + oxidized reactant}} \qquad (3)$$

$$\underset{\equiv \text{Fe(II)}}{\text{Reduced surface species}} \xrightarrow[\text{slow detachment of Fe(II)}]{k_4} \text{Fe(II) (aq) + surface site} \qquad (4)$$

The similarity of pK_a's of acetic and butyric acid (4.7 & 4.8) eliminates any effect due to the acid dissociation of these two carboxylic acids, since both of them are dissociated to the same extent at any given pH. Oxalate in the presence of the iron oxide polymorphs shows completely different reactivity and does not result in net photoproduction of Fe(II) (vide infra). Based on related work in our laboratory by Carraway et al. (48) on carboxylate photooxidations, the following mechanism (i.e., with acetate as a specific example) is proposed to account for the fate of the electron donors:

$$H^+ + CH_3CO_2^- + >Fe^{III}OH \rightleftharpoons >Fe^{III}O_2CCH_3 + H_2O \quad (5)$$

$$>Fe^{III}O_2CCH_3 \xrightarrow{h\nu} >Fe^{II} + CH_3^\bullet + CO_2 \quad (6)$$

$$>Fe^{II} \rightleftharpoons > + Fe^{2+} \quad (7)$$

$$CH_3^\bullet + O_2 \longrightarrow CH_3O_2^\bullet \quad (8)$$

$$2\,CH_3O_2^\bullet \longrightarrow CH_3OOH + HCOOH \quad (9)$$

$$HCOOH + >Fe^{III}OH \rightleftharpoons >Fe^{III}CO_2H + H_2O \quad (10)$$

$$>Fe^{III}CO_2H \xrightarrow{h\nu} >Fe^{II} + HCO_2^\bullet \quad (11)$$

$$HCO_2^\bullet + CH_3OOH \longrightarrow CO_2 + CH_3O^\bullet + H_2O \quad (12)$$

$$CH_3O^\bullet + HO_2^\bullet \longrightarrow CH_3OH + O_2 \quad (13)$$

Siffert and Sulzberger (21) have proposed two mechanisms for the photochemical reductive dissolutions of an iron(III) hydr(oxide) in the presence of oxalate: the intramolecular process and the intermolecular process. We have not attempted to determine which is operative in our systems due to the difficulties described by Siffert and Sulzberger (21).

As shown in Figure 1 an increase in the rate of iron photoreduction in the am-$Fe(OH)_3$-acetate system is observed with a decrease in pH. Similar, but smaller effects were observed in the case of goethite. These trends are consistent with the known behavior of anion adsorption (i.e., surface complexation) on solid surfaces (i.e., surface

complexation increases with a decrease in pH, even though the fraction of the anionic form of the carboxylic acids decreases) (33).

The rate of photochemical reduction as a function of irradiation wavelength is illustrated in Figure 3a. In this case, the rate of photoreduction of am-$Fe(OH)_3$ with formate was found to increase as the wavelength band of irradiation was decreased from 410-800 nm to 320-370 nm, even though the overall light intensity was greater in 410-800 nm band. This result is consistent with the onset of a bulk-phase O^{2-} to Fe(III) charge transition common to all of the iron-oxide polymorphs (20, 49), although the absorption of light by the surface complex, >Fe(III)-R, cannot be ruled out. A further investigation of the wavelength dependency of the photoreduction of am-$Fe(OH)_3$ in the presence of formate was carried out using monochromatic light in the range of 330 to 405 nm. The observed initial rate of iron photoreduction had a maximum value at 330 nm and a continuous decrease from 330 nm to 405 nm (Figure 3b). The quantum efficiency of the photoreduction of am-$Fe(OH)_3$ in the presence of formate also decreases continuously from 330 nm to 405 nm (Table 2). These trends are qualitatively consistent with the results obtained by other researchers (21, 27).

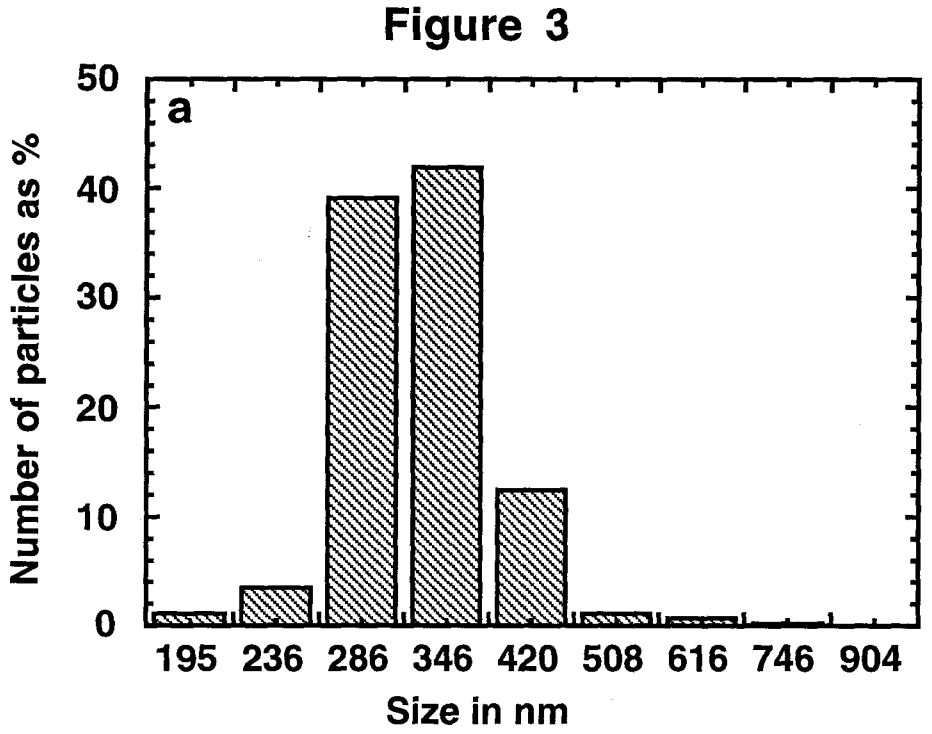

Figure 3a: Size distribution of am-$Fe(OH)_3$ by photon correlation spectroscopy.

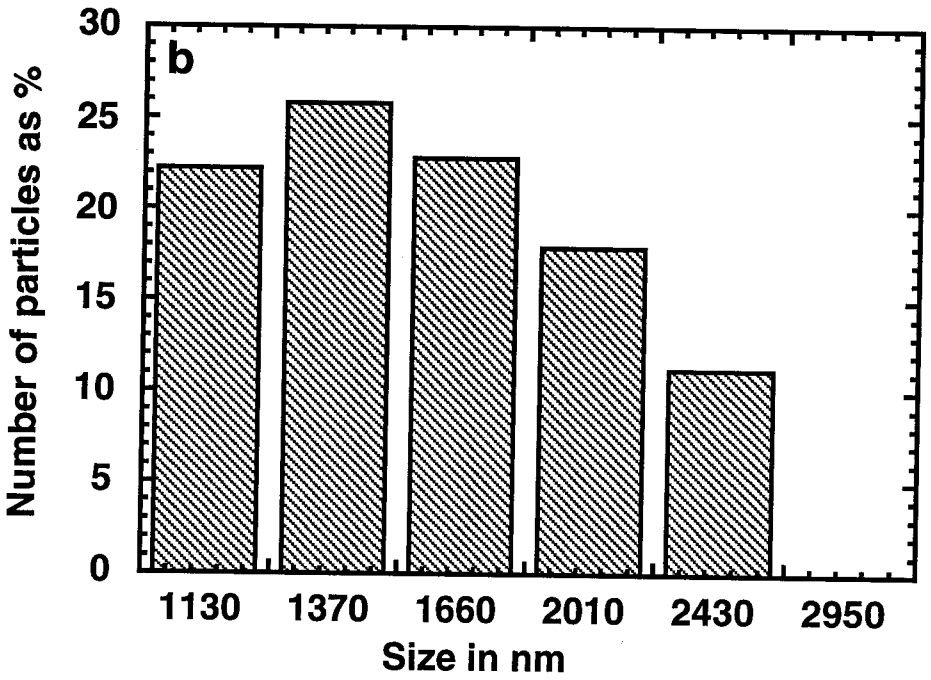

Figure 3b: Size distribution of goethite by photon correlation spectroscopy.

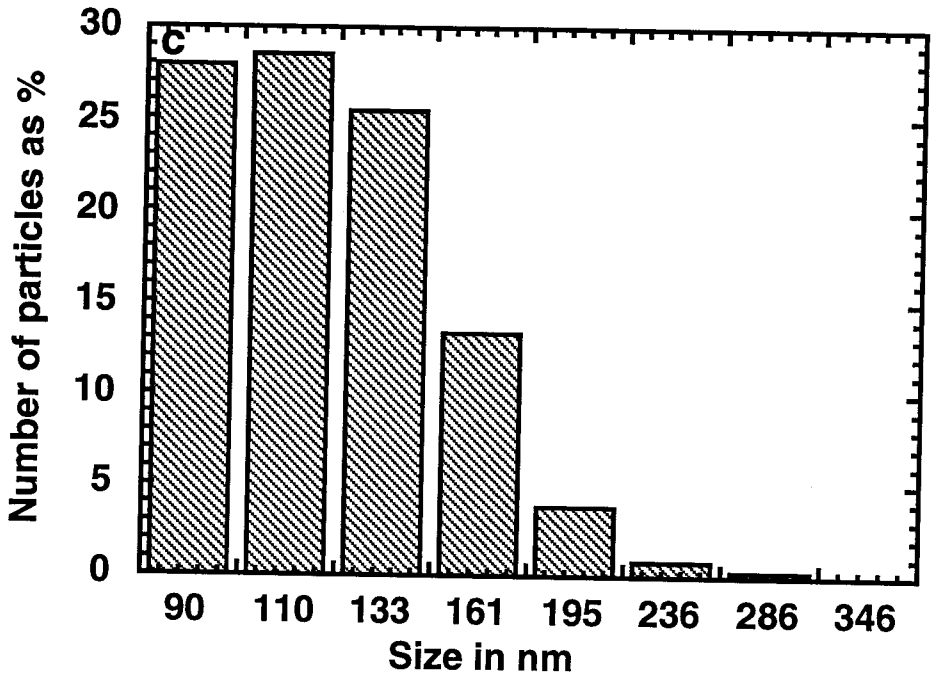

Figure 3c: Size distribution of hematite by photon correlation spectroscopy.

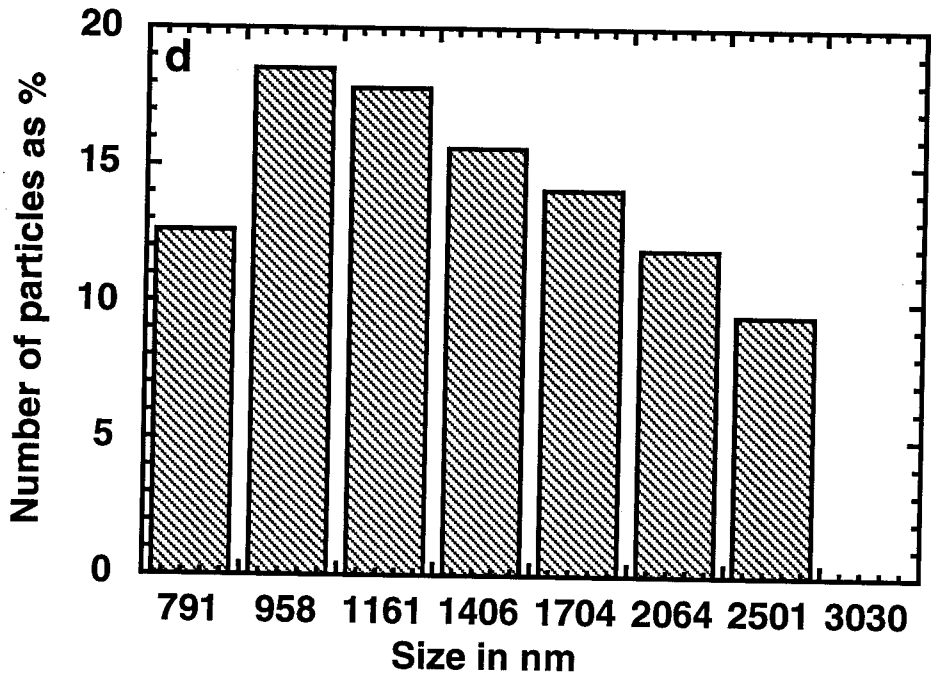

Figure 3d: Size distribution of lepidocrocite by photon correlation spectroscopy.

λ (nm)	d(Fe(II))/dt (nM/min.)	Absorbance*	Quantum Efficiency
330	9.4	0.46	1.4×10^{-3}
340	8.2	0.44	1.2×10^{-3}
350	7.6	0.41	1.1×10^{-3}
370	7.6	0.35	9.9×10^{-4}
380	7.8	0.34	9.8×10^{-4}
405	5.4	0.27	5.8×10^{-4}

*** includes absorbance and scattering**

Table 2: Quantum efficiencies of photoreduction of am-$Fe(OH)_3$ with formate.

Effect of the Iron Phase

The relative reactivities of the iron oxide polymorphs are shown on the first line in Table 1. The photoreduction rates in the presence of formate at pH = 4.25 for am-$Fe(OH)_3$, lepidocrocite, hematite, goethite are compared; the order of reactivity is am-$Fe(OH)_3$ >> γ-FeOOH ≥ α-Fe_2O_3 ≥ α-FeOOH, even though goethite particles were ten times larger than the hematite particles (Figure 4). The observed order of reactivity is an indication of the importance in the strength of Fe-O bond in the different iron phases; there appears to be no correlation between photochemical reactivity and calculated (using eq. 1) {>FeOH} concentrations (Figure 2). am-$Fe(OH)_3$ lacks a clearly-defined structure (45) and thus bonding between iron and oxygen in am-$Fe(OH)_3$ is weaker than in the other iron oxyhydroxide polymorphs. Hematite has a higher concentration of {>FeOH} compared to am-$Fe(OH)_3$. Nevertheless, the rate of photoreduction of iron is much lower in the case of hematite than in the case of am-$Fe(OH)_3$. The range of {>FeOH} of each mineral in Figure 2 is the result of the variation in size and morphology of the crystals in each of the iron phases as observed by TEM. It is obvious from Figure 2 that the concentration of surface active sites per unit volume is not controlling the rate of iron(II) photoproduction. This result is also supported by the results of Leland and Bard (Table 3) with rates of photooxidation of sulfite and oxalate in the presence of a variety of iron oxide polymorphs (49).

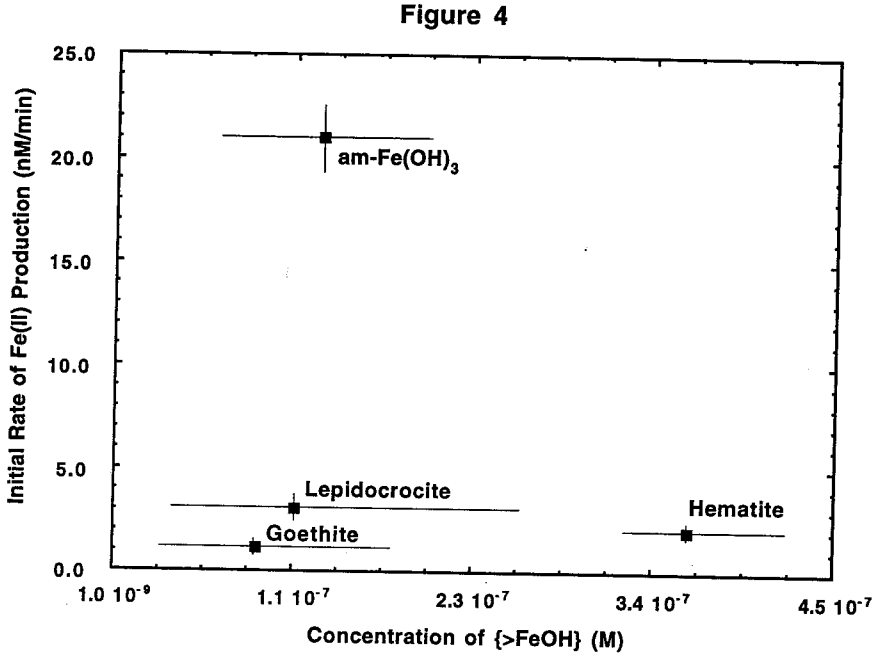

Figure 4: Initial rate of iron photoreduction with formate versus concentration of {>FeOH} of hematite, am-$Fe(OH)_3$, goethite and lepidocrocite calculated using eq. 1. Error bars based on the variation in size of crystals as observed by TEM and the error in the rate of photoreduction.

Iron Oxide	Band Gap Energy (eV)	$\lambda(O^{2-} \rightarrow Fe^{3+})$ (nm)	Hydrodynamic Diameter (μm)	$k_{oxalate}$[49] (s^{-1})	$k_{sulfite}$[49] (s^{-1})
Hematite	2.02	380	0.14	1.2×10^{-4}	42×10^{-4}
Lepidocrocite	2.06	~ 340	0.37	12.0×10^{-4}	52×10^{-4}
Goethite	2.10	~ 340	0.17	2.5×10^{-4}	2.7×10^{-4}

Table 3: Observed first-order rate constants for the photooxidation of oxalate and sulfite and comparison to particle size, band gap energy and onset of O^{2-} to Fe(III) charge transition (20, 49).

Hydrogen Peroxide Production

The production of H_2O_2 in the presence of iron oxyhydroxides and oxalate is postulated to take place according to the following mechanism (30):

$$Fe^{III} + C_2O_4^{2-} \longrightarrow Fe^{III}(C_2O_4)^+ \quad (14)$$

$$Fe^{III}(C_2O_4)^+ \xrightarrow{h\upsilon} Fe^{II}(C_2O_4)^+ \quad (15)$$

$$Fe^{II}(C_2O_4)^+ + O_2 \longrightarrow Fe^{II} + O^{\cdot}_2{}^- + 2\,CO_2 \quad (16)$$

$$O^{\cdot}_2{}^- \overset{H^+}{\rightleftharpoons} HO^{\cdot}_2 \quad (17)$$

$$HO^{\cdot}_2 / O^{\cdot}_2{}^- + Fe^{II} \longrightarrow H_2O_2 + Fe^{III} \quad (18)$$

Oxalate can induce H_2O_2 production because it can reduce O_2 to O_2 radical anion, whereas the other studied electron donors (formate, acetate, butyrate and formaldehyde) cannot. The rate of H_2O_2 production is compared with the different iron oxyhydroxides and with oxalate as the electron donor (Figure 5a). The structure of the iron oxyhydroxide is once more important as can be seen with the rapid increase and a subsequent rapid decrease in the concentration of H_2O_2 in the case of lepidocrocite, am-$Fe(OH)_3$ and maghemite compared to the slow increase in the case of goethite and hematite. The rapid rise and fall in the concentration of H_2O_2 in conjunction with the destruction of the electron donor (Figure 5b, c) can be explained by the scavenging of the holes (generated by the transfer of valence band electrons to the conduction band) by H_2O_2 (reaction 21) after the initial scavenging of the holes by oxalate. Experimental evidence for this mechanism can be found in Figures 5b, c, where the pH in the case of lepidocrocite is about 4.6 compared with 6 in the case of am-$Fe(OH)_3$ at the same extent of reaction. The extent of reaction is determined by the concentration of oxalate. The lower pH in the case of lepidocrocite is believed to be due to the reaction 21, which is only operative with semiconductors such as lepidocrocite and which results in the production of protons. Another explanation for the

rapid rise and fall in the concentration of H_2O_2 is the increasing rate of reaction 19 when complexation of Fe(II) by oxalate becomes less effective with decreasing concentration of oxalate. In the case of am-$Fe(OH)_3$, which is not a semiconductor, the rapid destruction of H_2O_2 is probably due to the reaction of H_2O_2 with surficial and dissolved iron(II) (19) and iron(III) (20) as follows:

Figure 5

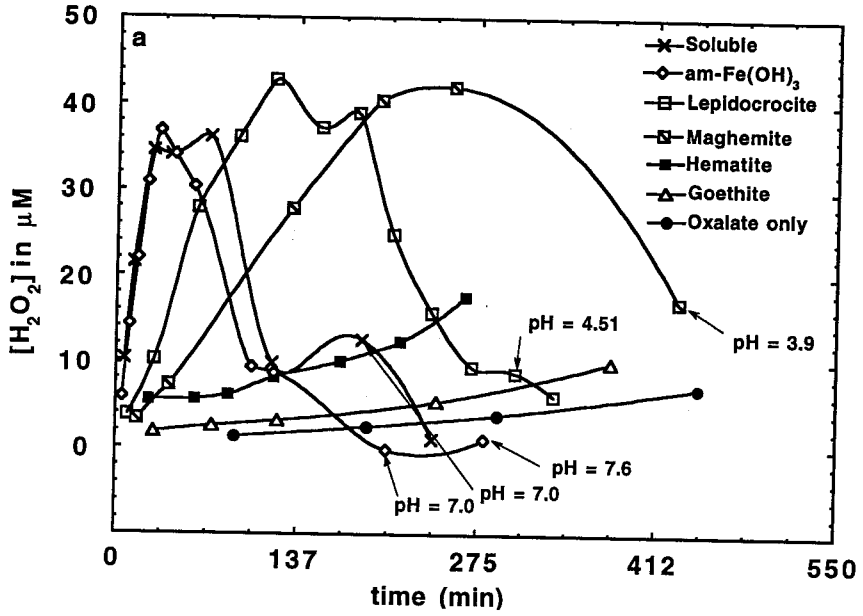

Figure 5a: Photochemical production of H_2O_2 by photoreductive dissolution of hematite, goethite, lepidocrocite, maghemite, soluble iron {from $Fe(NO_3)_3$ salt} and am-$Fe(OH)_3$ in the presence of oxalate and by photolysis of oxalate with $[Fe(III)]_{initial}$ = 130 µM, $[Oxalate]_{initial}$ = 6.0 mM, λ_{irrad} from 320 to 370 nm and pH ~ 3.2, except where noted.

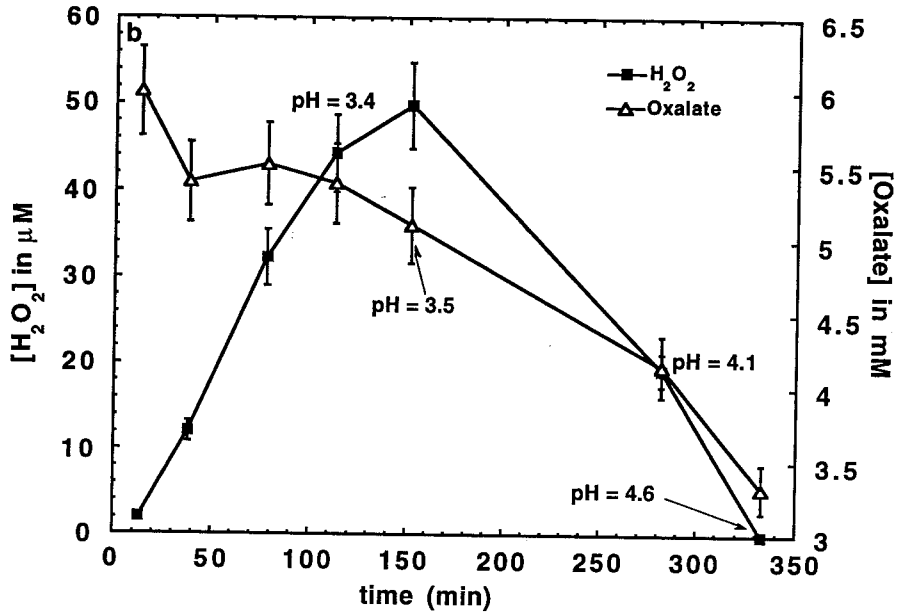

Figure 5b: Photochemical production of H_2O_2 and destruction of oxalate by photoreductive dissolution of lepidocrocite with $[Fe(III)]_{initial}$ = 130 μM, $[Oxalate]_{initial}$ = 6.0 mM, λ_{irrad} from 320 to 370 nm and pH ~ 3.2, except where noted.

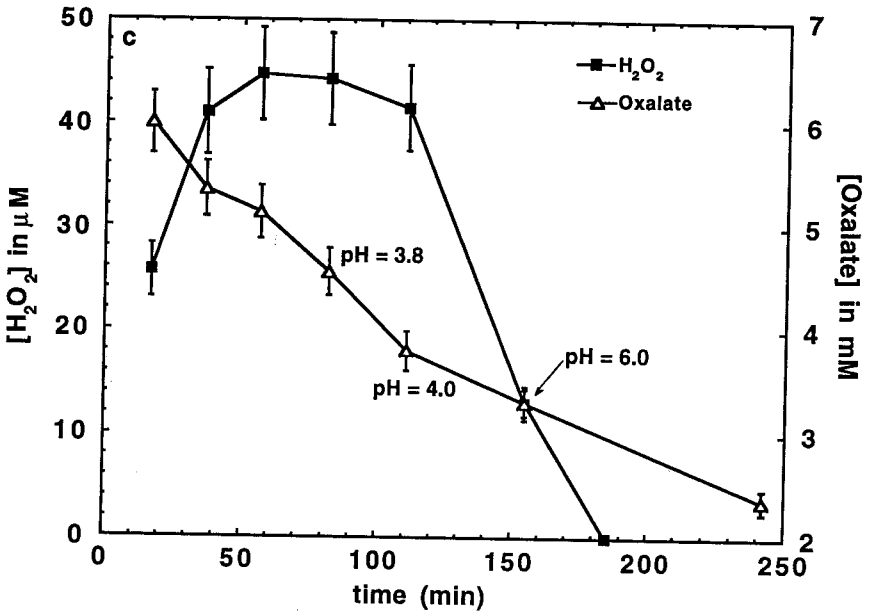

Figure 5c: Photochemical production of H_2O_2 and destruction of oxalate by photoreductive dissolution of am-$Fe(OH)_3$ with $[Fe(III)]_{initial}$ = 130 μM, $[Oxalate]_{initial}$ = 6.0 mM, λ_{irrad} from 320 to 370 nm and pH ~ 3.2, except where noted.

$$Fe(II) + H_2O_2 \longrightarrow Fe(III) + OH^{\cdot} + OH^{-} \quad (19)$$

$$>Fe(III) + H_2O_2 \longrightarrow >Fe(II) + HO_2^{\cdot} + H^{+} \quad (20)$$

$$2h^{+}_{vb} + H_2O_2 \longrightarrow O_2 + 2H^{+} \quad (21)$$

The reaction of H_2O_2 with iron(II) or iron(III) in the case of am-$Fe(OH)_3$ or the reaction of H_2O_2 with holes in the case of lepidocrocite occurs likely from the beginning of the reaction but is masked during the early stages of the reaction because of the much faster rate of H_2O_2 production during the initial stages of the reaction. Later in the reaction, when most of the oxalate has been consumed and the rate of H_2O_2 production is much lower, the rapid destruction of H_2O_2 by the above pathways becomes obvious in the observed rapid net decrease in the concentration of H_2O_2. This rapid destruction has been verified by additional experiments, where 40 μM of H_2O_2 was added to lepidocrocite and am-$Fe(OH)_3$ suspensions while being irradiated. Instantaneous destruction of H_2O_2 was observed in both cases.

In the case of goethite and hematite, the behavior is quantitatively and qualitatively different from am-$Fe(OH)_3$, maghemite and lepidocrocite, since no peak in the concentration of H_2O_2 was observed. In contrast, a smooth continuous increase in the concentration of H_2O_2 was observed. Furthermore, iron oxides with a α crystal structure (hematite, goethite) appear to behave similarly and differently from iron oxides with a γ crystal structure (lepidocrocite, maghemite). This is further evidence to the importance of bonding in the iron oxide in determining the rate of photoreduction. In Figure 5a, the production of H_2O_2 in the presence of oxalate without iron particles is also plotted. The slow increase in H_2O_2 with oxalate alone can be explained by the photolysis of oxalate. Oxalate has an absorption spectrum which has a small overlap ($\lambda \sim 320$ nm) with the

spectrum of our irradiating light and thus it is conceivable that direct photolysis of oxalate resulted in the increase in H_2O_2 concentration. An additional experiment was carried out to prove this hypothesis. In this experiment irradiating light with a wavelength range of 410 to 800 nm (oxalate has no absorbance in this range) was used and no H_2O_2 was produced. Blank water was also tested to see if trace organics, which are present in our Milli-Q water supply, were responsible for the increase in H_2O_2 concentration. When Milli-Q water was irradiated under the same experimental conditions, no H_2O_2 was detected. Soluble iron(III) (from nitrate salt and present as $Fe(III)(C_2O_4)_3^{3-}$) was also studied and it was found to behave similarly to am-$Fe(OH)_3$ and lepidocrocite with a maximum concentration of H_2O_2 achieved earlier than in the case of both am-$Fe(OH)_3$ and lepidocrocite and a subsequent rapid decrease in the concentration of H_2O_2. Our rate of H_2O_2 production with $Fe(III)(C_2O_4)_3^{3-}$, 18 nM/min., is lower by a factor of ~4 compared with the results of Zuo and Hoigne (30). This difference is most likely due to the shorter wavelengths of irradiation used by Zuo and Hoigne. The rates of H_2O_2 production are summarized in Table 4. Additional experiments were carried out with lower oxalate (100 μM) and lower iron (5 μM) concentrations, which are more representative of ambient concentrations of these species, and similar initial rates of H_2O_2 production were observed with an earlier onset of decrease in H_2O_2 concentration compared with the results with oxalate concentration of 6 mM and iron concentration of 130 μM.

Mineral Phase	H_2O_2 (nM/min.)
Hematite	38
Goethite	23
Amorphous $Fe(OH)_3$	590
Lepidocrocite	470
Maghemite	210
Soluble Fe(III)	1100
Iron in Aerosol	230

Table 4: Rates of Photoproduction of H_2O_2 with Iron Oxyhydroxides in the Presence of 6 mM of Oxalate.

Comparison between synthetic iron oxyhydroxides and natural iron-containing aerosols

Preliminary results indicate that the photochemical behavior of natural iron-containing aerosol suspensions (iron content ~ 5%) is similar to the behavior of am-$Fe(OH)_3$ and lepidocrocite. This is illustrated by the experiments of ambient iron-containing aerosols with oxalate, acetate and formate as shown in Figure 6. In the oxalate experiment (Figure 6a), the H_2O_2 increased sharply and decreased abruptly shortly after attainment of the maximum in the H_2O_2 concentration. This trend is similar to the behavior of am-$Fe(OH)_3$ and lepidocrocite with oxalate (Figure 5a). The experiments of ambient iron-containing aerosols with acetate and formate (Figure 6b) had initial rates of photoreduction similar to that of am-$Fe(OH)_3$. These three experiments provide us with preliminary support that a significant fraction of the iron in the atmospheric aerosols is in the form of am-$Fe(OH)_3$ and/or lepidocrocite as postulated (15) and measured (12) by others. Control experiments were carried out to eliminate the possibility that organic compounds originating from the aerosol filters were resulting in the H_2O_2 production instead of the added oxalate or Fe(III) reduction instead of the added formate and acetate. A small amount of peroxide (3-4 μM after several hours) was produced when no oxalate was introduced to the reaction vessel containing the ambient aerosol suspension with the known organic compounds present in L.A. aerosol (pH at 4.2 maintained by perchloric acid) and the initial rate of iron reduction was smaller, although non-zero, when no acetate or formate was introduced to the reaction vessel (pH at 4.2 maintained by perchloric acid).

Figure 6

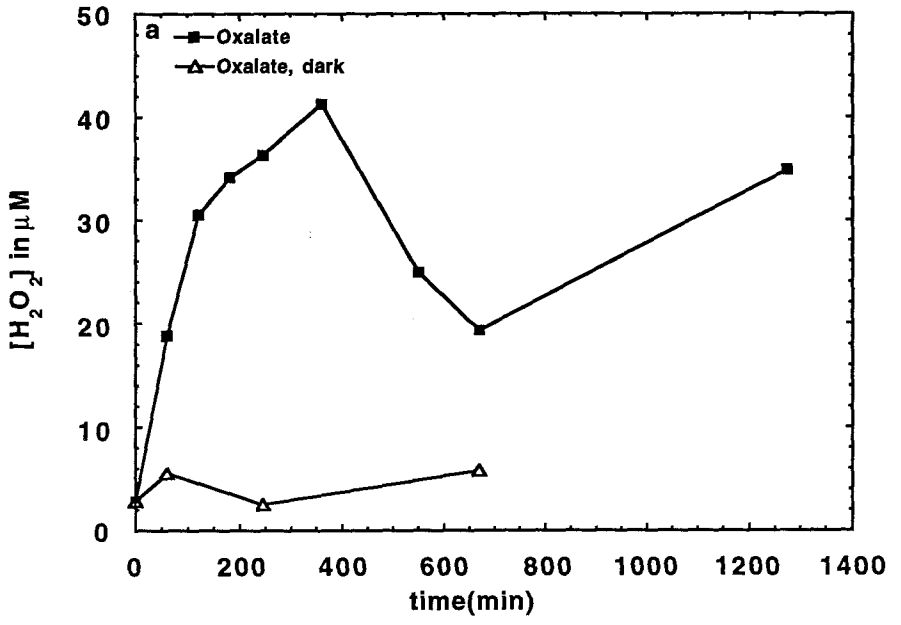

Figure 6a: Photoreductive dissolution of ambient iron-containing aerosols. $[Fe(III)]_{initial}$ ~ 13 μM, $[Electron\ Donor]_{initial}$ = 6.0 mM and λ_{irrad} from 320 to 370 nm with oxalate as the electron donor, pH ~ 3.5 to 4.0 and dark equilibrium control experiment.

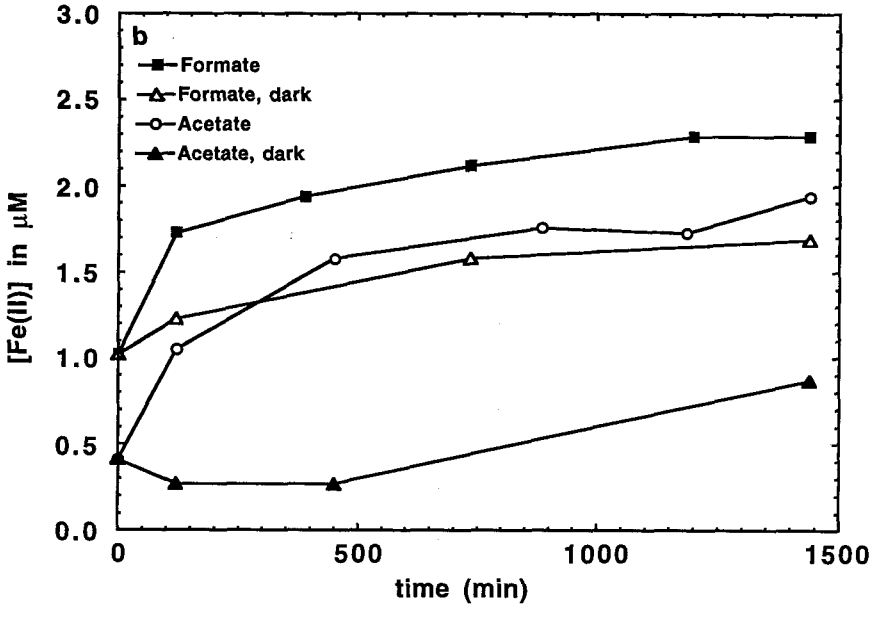

Figure 6b: Photoreductive dissolution of ambient iron-containing aerosols. $[Fe(III)]_{initial}$ ~ 13 μM, $[Electron\ Donor]_{initial}$ = 6.0 mM and λ_{irrad} from 320 to 370 nm with formate and acetate as the electron donor, pH ~ 4.25 and dark equilibria control experiment.

Conclusions

The photoreduction experiments of a variety of iron phases in the presence of important atmospheric organic compounds give us insight into the complex redox chemistry of iron in atmospheric water. The results indicate clearly that atmospheric organic compounds, such as formate and acetate, along with S(IV) (20, 27, 50) can photochemically reduce iron. Both of these photochemical redox processes are likely to be taking place simultaneously in atmospheric water. Our laboratory results are consistent with the trends that we have observed in cloudwater (31). In our on-going field work, we have shown a positive correlation between formate and acetate concentrations and the appearance of Fe(II) and a negative correlation between oxalate and Fe(II) (31). Our results also support the hypothesis of Kieber and Helz (15) that atmospheric Fe(III) is present predominantly as amorphous iron hydroxide and lepidocrocite and are consistent with the observations of Fukasawa et al. (12). In addition, we provide evidence for the destruction of H_2O_2 by valence-band holes of the iron oxide semiconductors.

Acknowledgments

Support for this research has been provided by a grant from the National Science Foundation, Division of Atmospheric Sciences, Atmospheric Chemistry Section (ATM 9015775). The authors wish to thank Mr. Michael Wong for his help in the photoreduction experiments and Prof. J. J. Morgan for helpful discussions.

References

1. Taylor, S. R.; McLennan, S. M. "The Continental Crust: its Composition and Evolution," Blackwell Scientific Publications: London, **1985**, 9.

2. Jacob, D. J.; Hoffmann, M. R. *J. Geophys. Res.*, **1983,** *88*, 6611.

3. Martin, L. R.; Hill, H. W. *Atmos. Environ.*, **1987,** *21*, 1487.

4. Hoffmann, M. R.; Jacob, D. J. In "Kinetics and Mechanism of the Catalytic Oxidation of Dissolved SO_2 in Atmospheric Droplets: Free Radical, Polar and Photoassisted Pathways," Calvert, J. G., Ed., Butterworth Publishers: Boston-London, **1984**, 101.

5. Weschler, C. J.; Mandich, M. L.; Graedel, T. E. *J. Geophys. Res.*, **1986**, *91*, 5189.

6. Graedel, T. E.; Mandich, M. L.; Weschler, C. J. *J. Geophys. Res.*, **1986**, *91*, 5205.

7. Conklin, M. H.; Hoffmann, M. R. *Environ. Sci. Technol.*, **1988,** *22*, 899.

8. Jacob, D. J.; Gottlieb, E. W.; Prather, M. J. *J. Geophys. Res.*, **1989**, *94*, 12975.

9. Martin, L. R.; Hill, M. W.; Tai, A. F.; Good, T. W. *J. Geophys. Res.*, **1991**, *96*, 3085.

10. Faust, B. C.; Hoigné, J. *Atmos. Environ.*, **1990,** *24*, 79.

11. Stumm, W.; Morgan, J. J. "Aquatic Chemistry," Wiley: New York, **1981**, 334.

12. Fukasawa, T.; Iwatsuki, M.; Kawakubo, S.; Miyazaki, K. *Anal. Chem.*, **1980**, *52*, 1784.

13. Dedik, A.N.; Hoffmann, P.; Ensling, J. *Atmos. Environ.*, **1992**, *26A*, 2545.

14. Zhuang, G.; Zhen, Y.; Duce, R. A. *Nature,* **1992**, *355*, 537.

15. Kieber, R. J.; Helz, G. R. *Environ. Sci. Technol.*, **1992**, *26*, 307.

16. Hong, H.; Kester, D. R. *Limnol. Oceanogr.*, **1986**, *31*, 512.

17. Landing, W. M.; Westerlund, S. *Marine Chem.*, **1988**, *23*, 329.

18. McKnight, D. M.; Kimball, B. A.; Bencala, K. E. *Science,* **1988**, *240*, 637.

19. Sulzberger, B.; Schnor, J. L.; Giovanoli, R.; Hering, J. G. *Aquatic Sciences,* **1990**, *52*, 56.

20. Faust, B. C.; Hoffmann, M. R. *Environ. Sci. Technol.*, **1986**, *20*, 943.

21. Siffert, C.; Sulzberger, B. *Langmuir,* **1991**, *7*, 1627.

22. Waite, T. D.; Morel, F. M. M. *Environ. Sci. Technol.*, **1984**, *18*, 860.

23. Waite, T. D.; Torikov, A.; Smith, J. D. *J. Coll. Int. Sci.*, **1986**, *112*, 412.

24. Cunningham, K. M.; Goldberg, M. C.; Weiner, E. R. *Environ. Sci. Technol.*, **1988**, *22*, 1090.

25. Litter, M. I.; Baumgartner, E. C.; Urrutia, G. A.; Blesa, M. A. *Environ. Sci. Technol.*, **1991**, *25*, 1907.

26. Littler, J. S.; Sayce, I. G. *J. Chem. Soc.*, **1964**, *96*, 2445.

27. Faust, B. C.; Hoffmann, M. R.; Bahnemann, D. W. *J. Phys. Chem.*, **1989**, *93*, 6371.

28. Sulzberger, B.; Laubscher, H. *Abstracts of Papers*, 188th National Meeting of the American Chemical Society, San Francisco, CA; American Chemical Society: Washington, DC, 1992; ENVR 32.

29. Kawamura, K.; Kaplan, I. R. In "Organic compounds in rainwater," Hansen, L. D.; Eatough, D. J., Ed., CRC Press: Boston, **1991**, 233.

30. Zuo, Y.; Hoigné, J. *Environ. Sci. Technol.*, **1992**, *26*, 1014.

31. Erel, Y.; Pehkonen, S. O.; Hoffmann, M. R. H. *J. Geophys. Res.*, **1993**, *98*, 18423.

32. Schwertmann, U.; Cornell, R. M. "Iron Oxides in the Laboratory;" VCH: Weinheim, Germany, **1991**, 91.

33. Dzombak, D. A. "Adsorption of Metals on Hydrous Ferric Oxides," Ph.D. thesis, Massachusetts Institute of Technology, **1986**, 123.

34. Scott, M. J. "Kinetics of Adsorption and Redox Processes on Iron and Manganese Oxides: Reactions of As(III) and Se(IV) at Goethite and Birnessite Surfaces," Ph. D. thesis, California Institute of Technology, **1991**, 67.

35. Sorenson, J.; Thorling, L. *Geochimica et Cosmochimica Acta*, **1991**, *55*, 1289.

36. Stookey, L. L. *Anal. Chem.*, **1970**, *42*, 119.

37. Carter, P. *Anal. Biochem.*, **1971**, *40*, 450.

38. Garcia-Vargas, M.; Belizon, M.; Hernandez-Artiga, M. P.; Martinez, C.; Perez-Bustamante, J. A. *A. Spectroscopy*, **1986**, *40*, 1058.

39. Zatar, N. A.; Abu-Zuhri, A. Z.; Al-Nuri, M. A.; Mahmoud, F. M.; Abu-Obaid, A. A. *Spec. Letters*, **1989**, *22*, 1203.

40. Pehkonen, S. O.; Erel, Y.; Hoffmann, M. R. *Environ. Sci. Technol.*, **1992**, *26*, 1731.

41. Kok, G. L.; Thompson, K.; Lazrus, A. L. *Anal. Chem.*, **1986**, *58*, 1192.

42. Heller, H. G.; Langan, J. R. *J. C. S. Perkin I*, **1981**, *1*, 341.

43. Jones, P.; Hockey, J. A. *Trans. Faraday, Soc.*, **1971**, *67*, 2679.

44. James, R. O.; Parks, G. A. In "Surface and Colloid Science: Characterization of Aqueous Colloids by Their Electrical Double-Layer and Intrinsic Surface Chemical Properties," Matijevic, E., Ed., Plenum Press: NY, **1982**, 142.

45. Schwertmann, U.; Cornell, R. M. "Iron Oxides in the Laboratory;" VCH: Weinheim, Germany, **1991**, 6.

46. Stumm, W.; Sulzberger, B. *Geochim. Cosmochim. Acta,* **1992**, *56*, 3233.

47. Smith, R. M.; Martell, A. E. "Critical Stability Constants," Plenum: New York, **1976**, 23.

48. Carraway, E. R.; Hoffman, A. J.; Hoffmann, M. R. H. *Environ. Sci. Technol.*, **1994**, *28*, 786.

49. Leland, J. K.; Bard, A. J. *J. Phys. Chem.*, **1987**, *91*, 5076.

50. Behra, P.; Sigg, L. *Nature,* **1990**, *344*, 419.

Chapter 7

Photoreduction of Iron Oxyhydroxides and Photooxidation of Halogenated Acetic Acids: Implications for Tropospheric Chemistry

[S. O. Pehkonen, R. L. Siefert, M. R. Hoffmann, submitted to Environmental Science and Technology in June 1994.]

Abstract

The photolytic reduction of ferrihydrite (am-$Fe_2O_3 \cdot 3H_2O$), lepidocrocite (γ-FeOOH), goethite (α-FeOOH), hematite (α-Fe_2O_3), maghemite (γ-Fe_2O_3) and natural iron-containing aerosol particles with the concomitant photooxidation of halogenated acetic acids (HAA's) has been studied. Halogenated acetic acids are predicted to be stable products of HCFC (hydrofluorocarbon) degradation in the troposphere. The concentrations of the HAA's are expected to increase dramatically as the production and use of HCFC's increases in the near future.

Experimental results show that the fastest rates of photoreduction of Fe(III) to Fe(II) are achieved with ferrihydrite as the electron acceptor and fluoroacetic acid as the electron donor. The observed rates of photoreduction are enhanced with fluoroacetic acid or chloroacetic acid as the electron donor compared to acetic acid. The pseudo zero-order rate constants of ferrihydrite photoreduction are 27 nM $min.^{-1}$ for bromoacetate, 35 nM $min.^{-1}$ for chloroacetate and 70 nM $min.^{-1}$ for fluoroacetate. Trihaloacetic acids and dihaloacetic acids were less effective electron donors compared to monohaloacetic acids with a pseudo zero-order rate constant of 3.1 nM $min.^{-1}$ for trichloroacetate and 4.4 nM $min.^{-1}$ for dichloroacetate. Maximum rates of photoreduction were observed at 325 nm with a continuous decrease in rate down to 400 nm in the case of ferrihydrite and trifluoroacetate. The main products of photoreduction of ferrihydrite with bromoacetic acid as the electron donor are bromide and glycolic acid.

Strong kinetic isotope effects are observed for deuterated chloroacetic acid. These results suggest that the oxidation of substrates proceeds via hydrogen-atom abstraction by photochemically-produced surficial hydroxyl radicals to produce surface-bound haloacetate radicals. Similar experiments show that iron in ambient aerosol particles is photoreduced to

release Fe(II) to solution. Results of this study indicate that halogenated acetic acids can be destroyed in the atmosphere by photooxidation in the presence of naturally-occurring iron oxide polymorphs.

Introduction

Iron is one of the most abundant elements in the earth's crust, where it is present both as Fe(II) and Fe(III) (1). Crustal iron is readily transferred into the atmosphere by wind and to a lesser extent by volcanic activity. When entrained in the atmosphere, iron {as Fe(II) and Fe(III)} plays an important role in the multiphase atmospheric chemistry of S(IV) (2-9) and a variety of organic compounds (10-14).

Iron(III)-containing aerosols, which may serve as cloud and fog condensation nuclei, are expected to participate in electron-transfer reactions within atmospheric water droplets (15). The Fe(II)/Fe(III) redox system also has a chemical and catalytic effect on other chemical species of interest in natural water systems. For example, iron is an important component in the redox chemistry of chromium in estuarine water (16) and in the redox chemistry of copper in atmospheric water (17).

Halogenated acetic acids are predicted to be one of the major degradation products of hydrochlorofluorocarbons (HCFC's) and hydrofluorocarbons (HFC's) in the troposphere. The HCFC and HFC family of compounds are being considered as substitutes for chlorofluorocarbons (CFC's) (18). One possible homogeneous gas-phase reaction mechanism that results in the production of trifluoroacetic acid is as follows:

$$F_3CCH_2Cl + OH^{\bullet} \rightarrow F_3CCHCl^{\bullet} + H_2O \quad (1)$$

$$F_3CCHCl^{\bullet} + O_2 \rightarrow F_3CCHClO_2^{\bullet} \quad (2)$$

$$F_3CCHClO_2^{\bullet} + NO \rightarrow F_3CCHClO^{\bullet} + NO_2 \quad (3)$$

$$F_3CCHClO^{\bullet} + HO_2^{\bullet} \rightarrow F_3CCHClOH + O_2 \quad (4)$$

$$F_3CCHClOH \rightarrow F_3CCHO + HCl \quad (5)$$

$$F_3CCHO + {}^{\bullet}OH \rightarrow F_3C\dot{C}O + H_2O \quad (6)$$

$$F_3C\dot{C}O + O_2 \rightarrow F_3CCO_3\cdot \quad (7)$$

$$F_3CCO_3\cdot + NO \rightarrow F_3CCO_2\cdot + NO_2 \quad (8)$$

$$F_3CCO_2\cdot + HO_2^{\bullet} \rightarrow F_3CCOOH + O_2 \quad (9)$$

Many of the halogenated acetic acids produced via a mechanism similar to eqs. 1-9 are toxic to organisms and plants (19-21) and may present a threat to the biosphere, if their concentrations were to increase from present levels to concentrations in the range of 5-50 nM. Schwarzenbach et al. (22) have detected chlorinated acetic acids in rainwater in Switzerland. Since several chloroacetic acids are used in the pharmaceutical industry, they are detectable at trace levels in some surface waters (23). Chlorinated and brominated acetic acids are also present in many municipal water supplies as by-products of chlorination (24-26). Laboratory research to date has indicated that the di- and trihalo acetic acids in the aqueous phase are resistant to chemical degradation (27) and are expected to be stable in the troposphere because their UV absorbance falls off rapidly at $\lambda \geq 250$ nm and therefore their direct photolytic decomposition is negligible. Hu et al. (28) have determined that gas-to-water exchange of halogenated acetic acids is limited only by gas-phase diffusion to water droplet surfaces.

In this paper, we present results of experiments that probe the coupled processes of photoreduction of iron oxide polymorphs and photooxidation of halogenated acetic acids. Our principal experimental objectives were to determine the kinetics and mechanisms of photoreduction {Fe(III) ----> Fe(II)} in a series of iron oxide polymorphs as a function of the physicochemical properties of the electron donor and wavelength. Results of experiments with synthetic iron oxide polymorphs are compared to the photoreduction of

ambient aerosol particles in the presence of halogenated acetic acids. Implications of these reaction pathways for tropospheric chemistry are discussed.

Experimental

Ferrihydrite (am-$Fe_2O_3 \bullet 3H_2O$) was prepared using the method described by Schwertmann and Cornell (29). Fresh iron hydroxide colloids were prepared at a frequency of once every 10 days to avoid complications that arise from the slow transformation of ferrihydrite to goethite (30). This transformation was monitored with a Scintag PAD-5 X-Ray Diffractometer with an automated $\theta/2\theta$ goniometer by following the appearance of distinct X-ray diffraction peaks of goethite. Goethite was prepared according to Scott (31), lepidocrocite was prepared using a method by Sorensen and Thorling (32) and hematite was prepared according to Schwertmann and Cornell (29). All of the iron phases were washed several times with 18 MΩ Milli-Q water to remove residual ionic species. The identity of the iron phases was determined by X-ray diffraction analysis as described above. The particle size distribution of the different iron phases was determined by Photon Correlation Spectroscopy (PCS) with a sub-micron particle-size analyzer (Malvern 4700 M/SM). In addition, the size and the shape of the crystals were determined by TEM (Phillips 430 {300 kV} Analytical Electron Microscope).

The photoreduction of ferrihydrite in the presence of fluoroacetate was carried out in the presence of 3-atom % $H_2{}^{18}O$. After two hours of irradiation, an aliquot was withdrawn, filtered, dried and redissolved in ethyl ether. After isolation in ethyl ether, the glycolic acid was derivatized by diazomethane to yield the methyl ester of 2-methoxyacetic acid. The ^{18}O-labeled methyl ester of 2-methoxyacetic acid was then quantified by GC-MS (HP GC 5880 Series II, MS Engine 5989A).

A 0.1 L photochemical reaction cell (14) was mixed vigorously with a magnetic stirrer. The cell had a flat window with an area of 8.5 cm^2 on one side for direct illumination. The vessel was open to the atmosphere in order to simulate conditions similar to those found in a cloud droplet or haze aerosol particle. The wavelengths of irradiation obtained from a 450 W Xenon lamp (Oriel Corp. Model 66021) were controlled by the use of a filter with a window of 325 to 800 nm or by the use of a monochromator with a bandwidth of 6.5 nm. The pH and ionic strength were kept constant by the presence of the electron donors at concentrations of 6 mM or by perchloric acid when lower concentrations of electron donors were used. When the added electron donors also served as the buffers, the pH increase was limited to 0.05 to 0.1 pH units during the course of the reaction. The halogenated acetic acids (Table 1) employed in this study have pK_a's ranging from 0.2 to 3.0. Since the experiments were carried out at pH ~ 4, they provided limited buffering capacity. The temperature of the reaction vessel was kept constant at 25 ± 2 °C by fan-driven air cooling. Aliquots were withdrawn with a syringe as a function of time and filtered through 0.2 μm cellulose acetate syringe filters before the addition of Ferrozine (33, 34) (iron(II) measurement), DPKBH (35, 36, 11) (iron(II) and iron(III)) or pH measurement. The concentration of Br^- was measured with an ion-selective electrode (Orion model 94-35 halide electrode). For anoxic control reactions water in the irradiation vessel was purged with N_2 for 60 minutes prior to the experiment and the vessel was kept closed during the irradiation. Experiments with deuterated chloroacetic acid (Cambridge Isotope Laboratories) were performed similarly to the non-labeled chloroacetic acid (i.e., 3 mM chloroacetic acid, ferrihydrite, lepidocrocite, maghemite or hematite suspensions {resulting in 130 μM of Fe_{tot}} at pH ~ 4.25).

Acid	pK_a	[1] Ó*	[2] $\log(K_{Fe(III)\text{-}HA})$
Fluoroacetic	2.59	1.10	2.2
Chloroacetic	2.86	0.94	2.1
Bromoacetic	2.9	0.908	2.1
Iodoacetic	3.18	0.72	2.1
Dichloroacetic	1.26	1.94	1.9
Trichloroacetic	0.64	2.65	0.85 (at 3.0 M $NaClO_4$)
Difluoroacetic	1.22	2.05	-
Trifluoroacetic	0.23	2.61	-

[1] values obtained from Ref. (37, 38) and Ó* are values for the substituents attached to COOH.

[2] values were obtained at 20° and at I = 1.0 except where noted (39, 40).

Table 1: Characteristics of halogenated acetic acids.

The incident photon flux of the light source was measured using Aberchrome 540 {(E)-α-(2,5-dimethyl-3-furylethylidene) (isopropylidene) succinic anhydride} (41) and by digital irradiance measurements. The latter technique was used in related field studies (12) to measure light intensity on a cloudy day at the time of atmospheric water collection. The light intensity of the 450 W Xenon light source is similar to the light intensity measured on a cloudy summer morning between 8 am and 11 am from 380 nm to 750 nm (~15 - 40 x 10^{15} quanta sec^{-1} cm^{-2}).

In most cases, a minimum of three replicate experiments were performed. The iron(II) concentrations during the replicate experiments were averaged and the relative standard deviation (100% x standard deviation / the average) was used as the magnitude of the error bars in the graphs. Initial rates of photoreduction of iron were determined by a linear least-squares fit when the data points formed a straight line from the beginning of the experiment to the end and by a linear least-squares fit of the first three data points in cases where linearity did not persist. Estimation of the halogenated acetic acid concentrations in atmospheric water over the Los Angeles basin were determined with a simple box model as follows:

$$[\{F_3CCOOH\}] = \frac{\frac{m}{M_w \cdot V} \cdot f \cdot \frac{10^3 g}{1 kg}}{LWC} \quad (M) \qquad (10)$$

where f = Fraction of HCFC converted to trifluoroacetic acid, m = Mass of HCFC emitted (g), LWC = Liquid Water Content (g/m^3), M_w = Molecular weight of trifluoroacetic acid (g/mol) and V = volume of air mass (m^3).

In this formula, the fraction of HCFC converted to the halogenated acid was calculated to be 0.03 based on the rate constant of 7 x 10^{-14} cm^3 $molecule^{-1}$ s^{-1} for the

reaction of F_3CCH_2Cl with the hydroxyl radical {estimated from rate constants of related HCFC-123 and HCFC-124 (18)}, a concentration of 10^6 OH radicals cm^{-3} and a period of five days for the reaction with the hydroxyl radical prior to cloud formation. Mass of HCFC emitted was estimated to be 2500 kg during a temperature inversion based on the current emission estimate of CFC 113 (CCl_2FCClF_2) (42), assuming the contribution of the Los Angeles basin to be proportional to its population and assuming an industrial substitution of F_3CCH_2Cl to CFC 113. The molecular weight of trifluoroacetic acid is 114 g/mol. The value of LWC was chosen to be 0.25 g/m^3. This is a typical water content of a marine stratus cloud (43). The volume of air mass was calculated using a simple box model of L. A. basin of 75 by 75 km and an inversion layer at 600 m. Complete mixing of the air mass prior to the formation of clouds was assumed. The Henry coefficient was assumed to large due to the complete dissociation of trifluoroacetic acid at pH values greater than two and therefore not limiting in this calculation. Also, Hu et al. (28) have concluded that gas-to-water exchange of halogenated acetic acids such as trifluoroacetic acid is limited only by gas-phase diffusion to water droplet surfaces.

Aerosol-collection filters used in all experiments were 47 mm Gelman Zeflour Teflon ® filters with a pore size of 1 μm. The filters were cleaned in a 10% HF bath for 24 hours and then in a 10% HCl bath for another 24 hours before sampling (Seastar acids and 18 MΩ Milli-Q water were used). The filters were also rinsed 4 times with 18 MΩ Milli-Q water between the baths and again after the final bath. Aerosol samples were collected on the roof of the Millikan Library of the California Institute of Technology on 9 filters from 11:30 am on 9/1/92 to 1:30 PM on 9/10/92 (218 hr) with a pumping rate of 10 L $min.^{-1}$. After the collection each filter had an aerosol mass of ~ 6.5 mg. One filter was used for each photoreduction experiment. Each filter was sonicated inside the reaction vessel for 90 minutes with ~ 100 g of 18 MΩ Milli-Q water in order to suspend the aerosol into solution

with ~ 70 % mass removal efficiency. After the sonication the filter was removed from the reaction vessel and the photoreduction experiment was initiated.

Results

Relative Effects of Electron Donor on Observed Photoreduction Rates

Figure 1a shows the trends of photochemical reduction of ferrihydrite. Other iron oxyhydroxides show similar behavior and therefore are not plotted; the rates for am-$Fe_2O_3 \cdot 3H_2O$, γ-FeOOH, α-FeOOH, α-Fe_2O_3, γ-Fe_2O_3 are summarized in Table 2. As can be seen in Figure 1a there are several obvious trends in the photoreduction of iron oxides in the presence of the halogenated acetic acids. Fluoroacetate reduced iron(III) at the fastest rate followed by chloroacetate and bromoacetate. In addition, after a rapid initial rate of iron(III) photoreduction in the presence of fluoroacetate, the rate of Fe(III) photoreduction decreased significantly. The rate of Fe(III) reduction in the presence of trichloroacetate and dichloroacetate was substantially lower than in the presence of chloroacetate (Figure 1b).

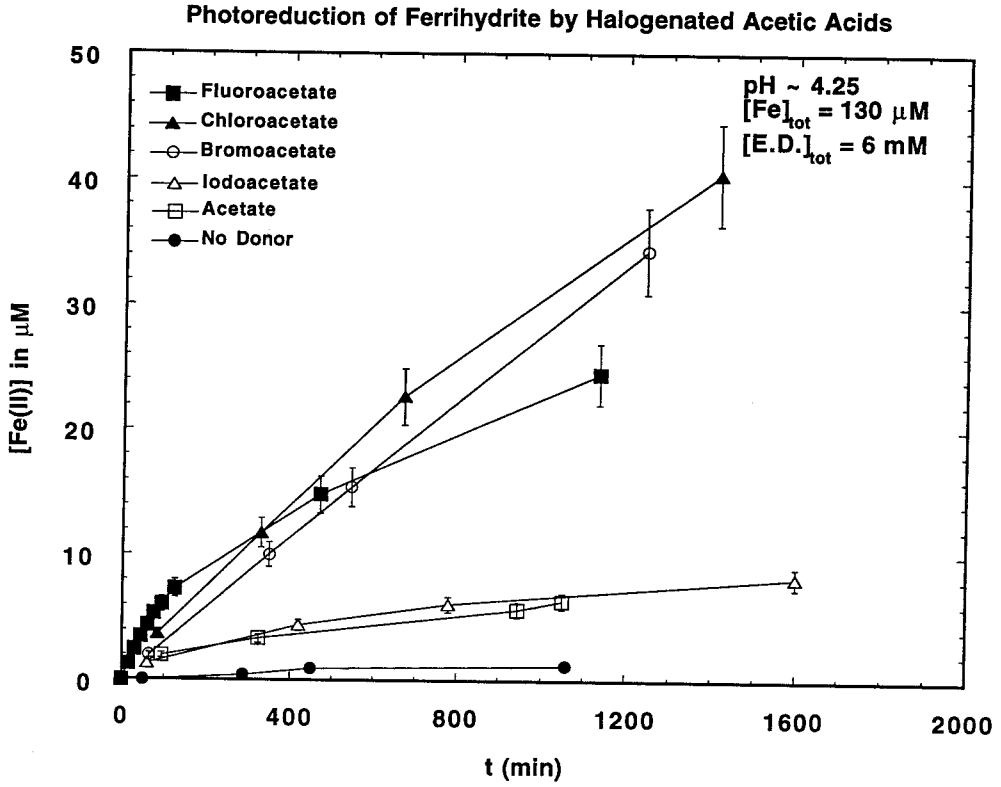

Figure 1a: Photoreductive dissolution of ferrihydrite with a variety of haloacetic acids. $[Fe(III)]_{initial}$ = 130 μM, $[Electron\ Donor]_{initial}$ = 6.0 mM, λ_{irrad} from 320 to 800 nm and pH ~ 4.25-4.30 throughout the experiments.

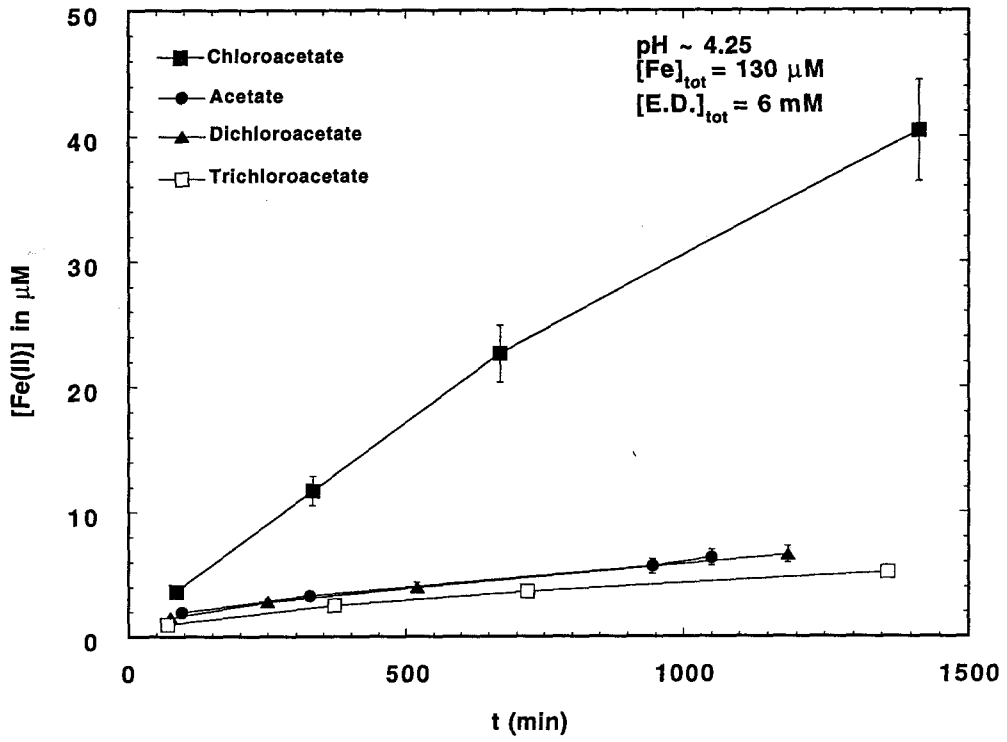

Figure 1b: Photoreductive dissolution of ferrihydrite with a mono-, di-, and trichloroacetic acids. $[Fe(III)]_{initial}$ = 130 μM, $[Electron\ Donor]_{initial}$ = 6.0 mM, λ_{irrad} from 320 to 800 nm and pH ~ 4.25.

	Goethite	Hematite	Lepidocr.	Ferrihydrite	Maghemite	$Fe_{Aer.}$
Fluoroacetate	0.2	14	18	70	39	12
Chloroacetate	0.13	2.3	1.3	35	2.2	10
Bromoacetate	-	1.3	0.8	27	1.0	-
Iodoacetate	-	0.8	0	4.2	0	-
Dichloroacetate	-	0.6	0.7	4.4	1.2	-
Trichloroacetate	-	-	0.5	3.1	0.55	-
Difluoroacetate	-	-	0.7	5.5	-	-
Trifluoroacetate	-	-	-	4.8	1.3	-
No Added Donor*	0.02	0.01	0.2	2.2	0	

* proton-assisted iron oxide dissolution

Table 2: Initial rates (nM/min.) of photoreduction of iron oxyhydroxides with halogenated acetic acids.

Isotope Studies

Insight into the mechanism of electron-transfer was provided by photoreduction experiments with deuterated chloroacetic acid, $CD_2ClCOOH$, that were carried out with lepidocrocite, hematite and ferrihydrite. The deuterium kinetic isotope effect for the observed rate of iron(III) photoreduction (eq. 22 & 23) was found to be 5.5 for ferrihydrite and maghemite and 2 for lepidocrocite and hematite. Experiments with ^{18}O-labeled water were carried out to determine the pathway leading to one of the photooxidation products, glycolate. No ^{18}O-labeled glycolate was detected.

Role of Oxygen

In order to determine the role of oxygen in the mechanism, the determination of the rate of ferrihydrite photoreduction and the rate of Br^- photoproduction were carried out both with deoxygenated water and with water in equilibrium with air. A significantly-reduced rate of iron-induced Br^- photoproduction was observed in a deoxygenated aqueous solution compared to a solution in equilibrium with air (i.e., decrease from 54 nM/min. to 17 nM/min. of bromide production) (Figure 2). However, the rate of iron oxide photoreduction did not change from experiments with a deoxygenated aqueous solution to experiments with a solution in equilibrium with air. Bromoacetate photolyzes without iron oxides to produce Br-, but at a slower rate compared to iron-induced photooxidation (Figure 2).

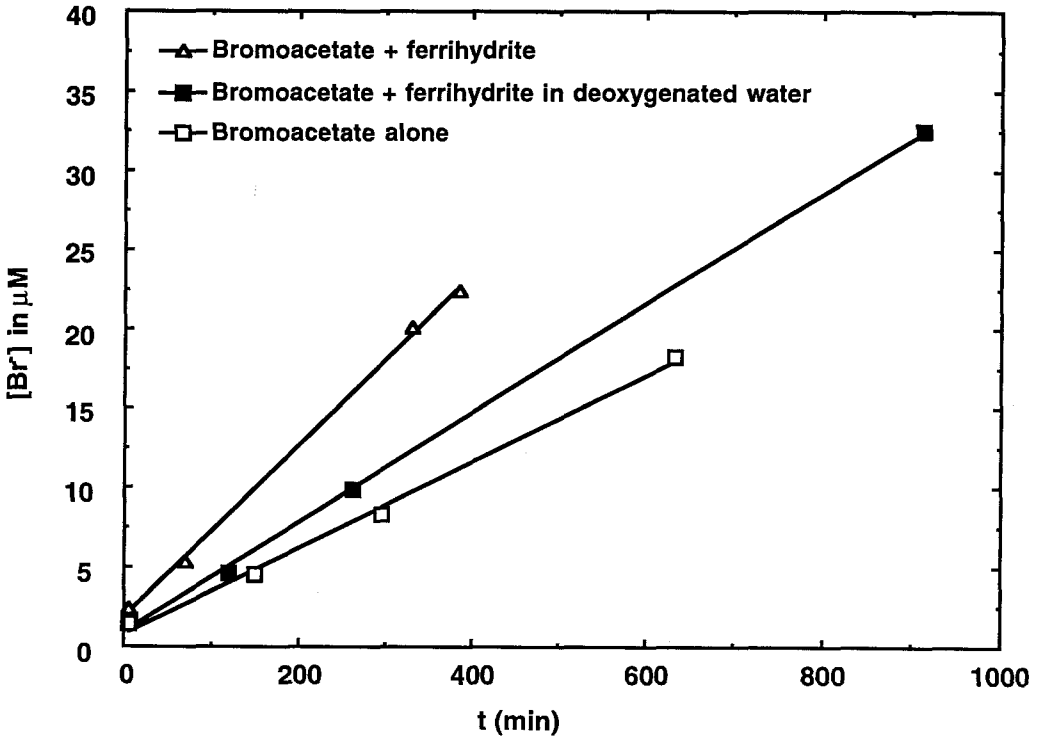

Figure 2: Photoproduction of bromide with ferrihydrite and bromoacetate as the electron donor in deoxygenated and air-equilibrated water and photoproduction of bromide without iron. $[Fe(III)]_{initial}$ = 130 μM, $[Bromoacetate]_{initial}$ = 6.0 mM, $[Bromide]_{initial}$ = 0, λ_{irrad} from 320 to 800 nm and pH ~ 4.25.

Effect of the Wavelength

The wavelength dependency of the photoreduction of ferrihydrite with trifluoroacetate was studied from 325 nm to 400 nm with a bandwidth of 6 nm. The results are presented in Figure 3. The rate of iron photoreduction decreases by a factor of three from 325 nm to 400 nm. The trend of decreasing rate of photoreduction from 325 to 400 nm is consistent with the onset of a bulk-phase O^{2-} to Fe(III) charge-transfer transition common to all of the iron-oxide polymorphs (44, 45). Similar trends have been observed in previous studies of iron oxides (14, 46). The calculated quantum yield at 325 nm using the standard equation described elsewhere (44) is 4×10^{-4}; this value is apparent because the absorbance used in the calculation includes light scattering.

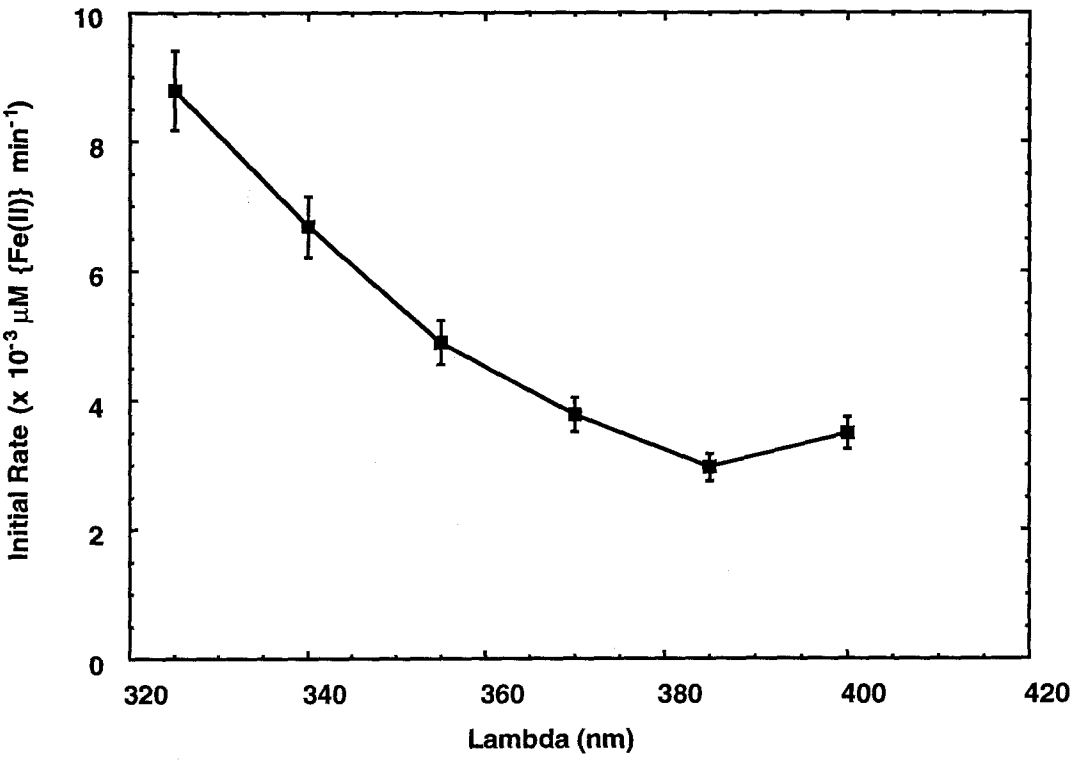

Figure 3: Photoreductive dissolution of ferrihydrite with trifluoroacetate as a function of wavelength. $[Fe(III)]_{initial}$ = 130 µM, $[Electron\ Donor]_{initial}$ = 6.0 mM, bandwidth = 6.5 nm and pH ~ 4.25.

Effect of the Iron Phase

The relative reactivities of the iron oxide polymorphs are shown on the first line in Table 2. The initial photoreduction rates in the presence of fluoroacetate at pH = 4.25 for ferrihydrite, lepidocrocite, hematite, goethite and maghemite are compared; the order of reactivity is ferrihydrite > γ-Fe_2O_3 > γ-FeOOH ≥ α-Fe_2O_3 > α-FeOOH. The observed order of reactivity is similar to the order observed with formate (14).

Comparison between Synthetic Iron Oxyhydroxides and Natural Iron-Containing Aerosols

Preliminary results indicate that the photochemical behavior of natural iron-containing aerosol suspensions (iron content ~ 4%) in the presence of halogenated acetic acids leads to significant iron reduction and photooxidation of the acetic acids. This is illustrated by the experiments of ambient iron-containing aerosols with fluoroacetate and chloroacetate as shown in Figure 4. In these experiments the initial rates of photoreduction were found to be similar to those for formate as the electron donor (14). Control experiments were carried out to test the possibility that organic compounds originating from the ambient aerosol were contributing to Fe(III) reduction in addition to fluoroacetate and chloroacetate. They showed that the initial rate of iron(III) photoreduction was smaller, when no additional electron donor was introduced to the reaction vessel (pH at 4.2 maintained by perchloric acid).

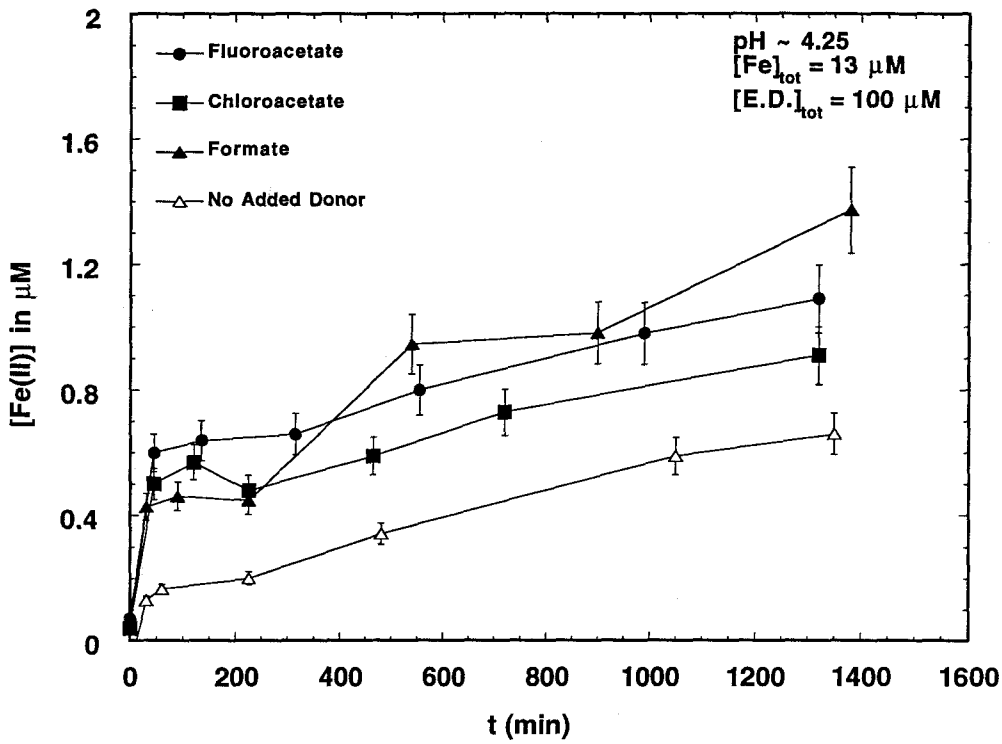

Figure 4: Photoreductive dissolution of ambient iron-containing aerosols in the presence of fluoroacetate, chloroacetate, formate and no donor. $[Fe(III)]_{initial}$ ~ 13 μM, $[Electron\ Donor]_{initial}$ = 100 μM, λ_{irrad} from 320 to 390 nm and pH ~ 4.25.

Concentration of Trifluoroacetic Acid in Atmospheric Water

The box model of the Los Angeles basin described earlier was used to estimate the concentration of trifluoroacetic acid in atmospheric water over the Los Angeles basin. The resulting concentration of trifluoroacetate is ~ 1 μM based upon the aforementioned values for the different variables in the calculation.

Effect of Ambient Competing Ligands

Photoreduction experiments of ferrihydrite (at 40 μM of total iron) were carried out in the presence of 200 μM of acetate (known to reduce iron oxides at a much lower rate (14) compared to chloroacetate) and 100 μM of chloroacetate at pH ~ 4.25. Acetate and ferrihydrite were allowed to equilibrate for 60 minutes in the stirred reaction vessel prior to the addition of chloroacetate and the start of the irradiation. No change in the rate of ferrihydrite photoreduction was observed compared to the case with ferrihydrite and chloroacetate as the sole electron donor.

Discussion

The difference in the rate of iron photoreduction between chloroacetate and bromoacetate can be attributed to the greater electronegativity of chlorine than bromine. Due to its greater electronegativity, chlorine will withdraw more electron density away from the adjacent carbon atom than will bromine or iodine, thus stabilizing a radical formed from an H-atom abstraction by a surficial • OH radical. Stabilization of a free radical intermediate is suggested by the LFER of Figure 5 in which $\log(k_{photoreduction})$ is plotted against the Taft parameter, σ^*, for ferrihydrite, maghemite and lepidocrocite. The relative stability of the surface complexes of chloroacetate and bromoacetate with >FeOH sites

cannot explain the observed differences in photoreduction rates {i. e., $10^{2.1}$ for chloroacetate and $10^{2.1}$ (estimated from Cu^{2+} binding constants) for bromoacetate (39) }. Also, the similarity of pK_a's of chloroacetic and bromoacetic acid (2.86 & 2.90) indicates that both are dissociated approximately to the same extent at a given pH.

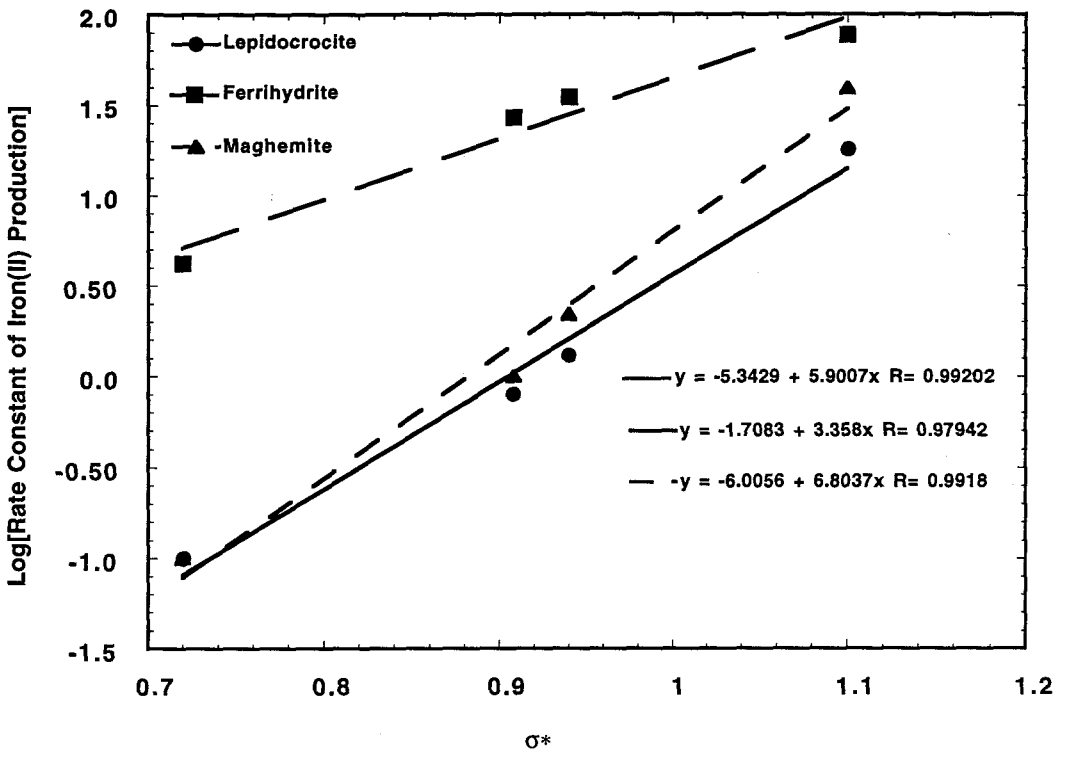

Figure 5: LFER relationship between $\log[k_{photoreduction}]$ and σ^* for the photoreduction of ferrihydrite, lepidocrocite and maghemite with fluoro-, chloro-, bromo-, and iodoacetate.

The continuous decrease in the rate of ferrihydrite photoreduction in the presence of fluoroacetate (Figure 1a) can be explained by the buildup of fluoride in the reaction vessel (F^- is an expected product based on the production of bromide in the case of bromoacetate and the concurrent production of glycolate as observed by GC-MS). Fluoride forms strong complexes with iron(III) (39), it blocks many of the active surface sites and slows down the photoreduction of surficial iron. This observed trend is in contrast to chloroacetate and bromoacetate, whose photooxidation results in the buildup of chloride and bromide in the system, but since chloride and bromide form very weak complexes with iron(III) (39), the rate of iron photoreduction remains relatively constant throughout the experiment. Similar trends were observed for the other iron oxyhydroxides.

Stumm and co-workers (52) proposed the following mechanism for the reductive dissolution of iron oxides by carboxylic acids:

$$>Fe(III)OH + XCH_2CO_2^- + H^+ \overset{K}{\rightleftharpoons} >Fe(III)O_2CCH_2X + H_2O \quad (11)$$

$$>Fe(III)O_2CCH_2X \overset{k}{\underset{h\nu}{\rightleftharpoons}} >Fe(II)O_2CCH_2X \quad (12)$$

$$>Fe(II)O_2CCH_2X \longrightarrow >Fe(II) + {}^{\bullet}CH_2X + CO_2 \quad (13)$$

$$>Fe(II) \xrightarrow{rds} Fe(II)_{aq} + > \quad (14)$$

where the rate-determining step is the detachment of surface Fe(II) from the crystal lattice and they (46) express the rate of the Fe(II) production as

$$\frac{d[Fe(II)]}{dt} = 2.3\ L\ I_{o\lambda}\varepsilon_{\lambda}\frac{2k_{13}}{k_{-12} + k_{13}}[> Fe(III)O_2CCH_2X] \qquad (15)$$

where L is the pathlength, $I_{o\lambda}$ is the incident light intensity and ε_{λ} is the molar absorptivity.

A value of 5.5 for the kinetic isotope effect in the case of ferrihydrite and maghemite indicates that the transition state has a higher degree of bond breaking (i.e., the hydrogen atom is bound about equally to two interacting species in the transition state{the surface OH radical and the carbon of the chloroacetic acid }), while the lower value of 2 indicates that the transition state in the case of lepidocrocite and hematite does not have a high degree of bond breaking and is either product-like or reactant-like. These results are consistent with the fact that the hydrogen atom abstraction is the rate-determining step and explain the lower reactivity of dichloroacetate, since in the case of dichloroacetate, there is only one hydrogen atom available for abstraction.

Since no ^{18}O-labeled glycolate was detected, the attack on the acetate radical by "vicinal water" and not bulk $H_2{}^*O$ water is suggested. "Vicinal water" is the ordered water layer immediately adjacent to solid surfaces (47). Since ferrihydrite is a very porous iron oxide, the amount of the "vicinal water" is relatively high compared to other iron oxides (47). We can conclude from our results that the rate of the attack of the acetate radical by a water molecule is faster than the rate of exchange of water molecules between vicinal and bulk water.

The experiments with deoxygenated water indicate that dissolved O_2 does not have an effect in the mechanism of iron(III) photoreduction, but plays a role in the photoproduction of Br^- (Figure 2). In addition, the rate of iron(II) production is very similar (within experimental error) to the net rate of production of Br^- (the difference

between bromoacetate + ferrihydrite rate and bromoacetate alone rate in Figure 2). This indicates that for every Fe^{2+} produced there is one Br^- produced and, therefore, the product of bromoacetate photodegradation, glycolate, does not participate in the photoreduction of iron. This is most likely due to the fact that bromoacetate is present at much higher concentration than glycolate (6 mM vs. 5-20 μM) and because glycolate and bromoacetate have similar constants for iron complexation {log(K) = 2.9 vs. log(K) = 2.1 for bromoacetate}(39).

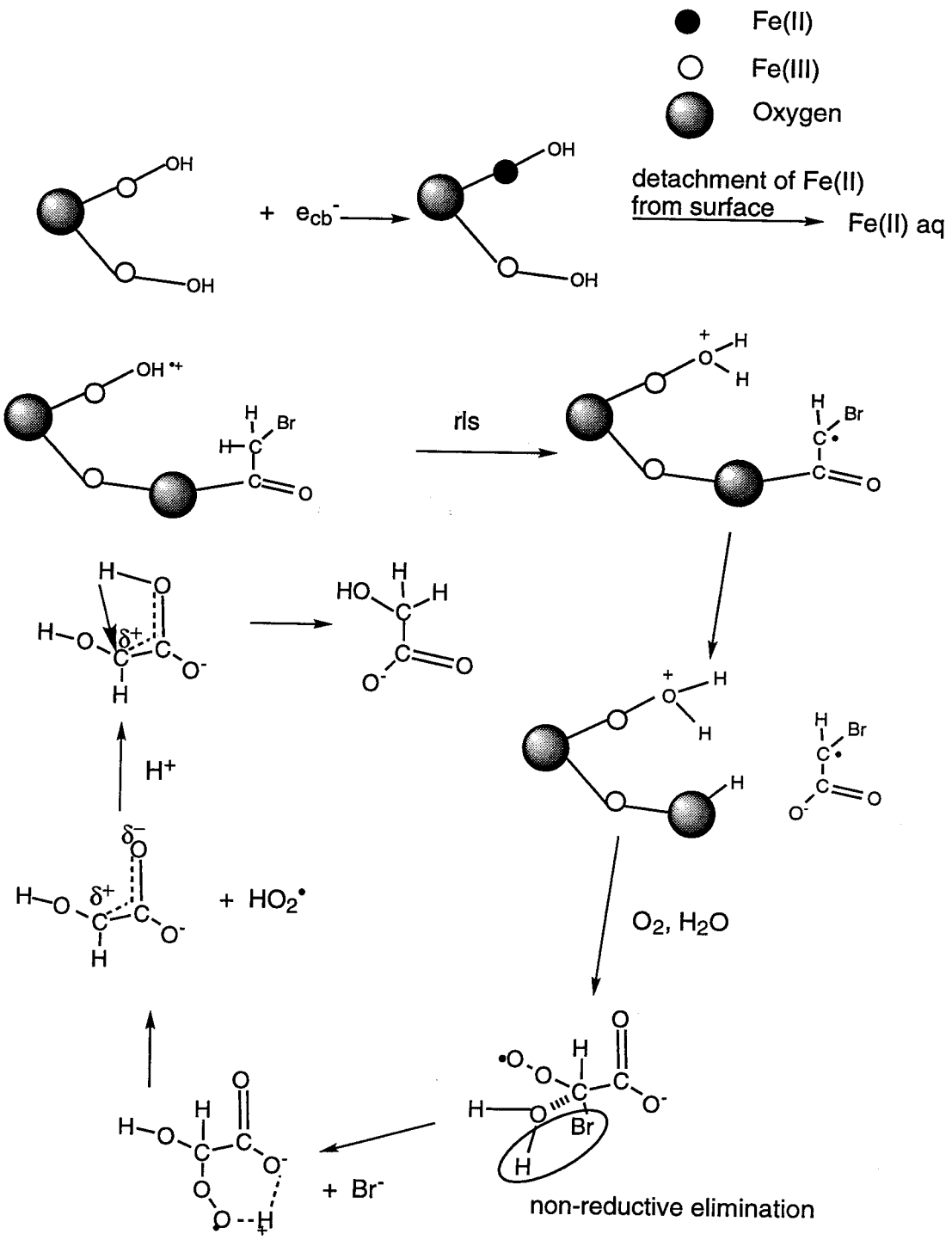

Figure 6: Proposed mechanism for the photoreduction of iron oxides and the concomitant photooxidation of haloacetic acid (i.e., bromoacetate as a specific example).

Based on the observed LFER of Fig. 5, the deuterium kinetic isotope effect, the reduced rate of halide photoproduction in deoxygenated water, and the identification of bromide and glycolate as the products, the mechanism in Figure 6 is proposed to account for the fate of the electron donors and the photoreduction of surficial iron(III). Based on this general reaction mechanism (48, 49), the following stepwise mechanism can be written:

Formation of Fe(III)-Bromoacetate Surface Complex

$$>Fe(III)OH + CH_2BrCO_2^- + H^+ \underset{k_{-14}}{\overset{k_{14}}{\rightleftharpoons}} >Fe(III)O_2CCH_2Br + H_2O \quad (16)$$

Photophysical Excitation of Bulk Iron Oxide Polymorph

$$Fe_2O_3 \xrightarrow{h\nu \leq 400\ nm} h^+_{vb} + e^-_{cb} \quad (17)$$

Direct Band-Gap Recombination

$$h^+_{vb} + e^-_{cb} \xrightarrow{fast} Fe_2O_3 + h\nu\ (\text{or heat}) \qquad (50\ ns) \qquad (18)$$

Conduction-Band Electron Transfer to a Surface-Trap

$$>Fe(III)OH + e^-_{cb} \rightleftharpoons >Fe(II)OH^- \quad (50 - 100\ ns) \quad (19)$$

Valence-Band Hole Transfer to a Surface Trap

$$>Fe(III)OH + h^+_{vb} \rightleftharpoons >Fe(III)OH^{\bullet +} \quad (50 - 100\ ns) \quad (20)$$

Tunneling of the Surface Trapped Electron

$$> Fe(III)OH^{\bullet +} + > Fe(II)OH^{-} \longrightarrow 2 > Fe(III)OH \qquad (21)$$

Creation of a Surface Haloacetate Radical

$$> Fe(III)OH^{\bullet +} + > Fe(III)OOCCH_2Br \xrightarrow{rds} > Fe(III)OH_2^{+} + > Fe(III)OOC\dot{C}HBr \qquad (22)$$

$$> Fe(III)OOCC\dot{H}Br + > Fe(II)OH^{-} \xrightarrow[fast,\ H_2O]{} 2 > Fe(III)OH + BrCH_2CO_2^{-} \qquad (23)$$

$$> Fe(III)OOC\dot{C}HBr + H_2O \longrightarrow > Fe(III)OH_2^{+} + Br\dot{C}HCO_2^{-} \qquad (24)$$

$$> Fe(II)OH^{-} + 6H_2O \longrightarrow > + Fe(H_2O)_6^{2+} \qquad (25)$$

$$O_2C\dot{C}HBr + O_2 \xrightarrow{fast} \qquad (26)$$

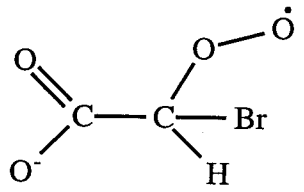

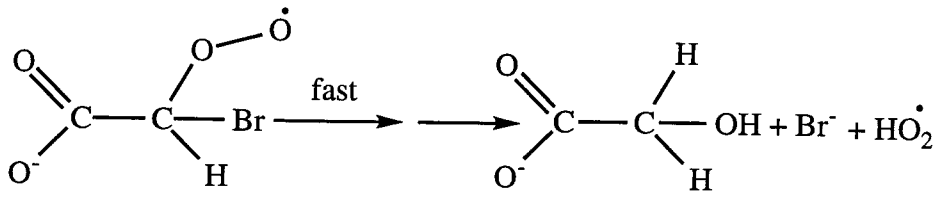

The rate of the formation of surface bromoacetate radical can be written as

$$\frac{d[> Fe(III)O_2C\dot{C}HBr]}{dt} = k_{22}[> Fe(III)OH^{\bullet+}]\,[> Fe(III)O_2CCH_2Br] \qquad (28)$$

Using a steady-state analysis on the concentration of the surficial $Fe(III)OH^{\bullet+}$ gives

$$\frac{d[> Fe(III)OH^{\bullet+}]}{dt} = k_{20}[> Fe(III)OH]\,[h^+_{vb}] - k_{-20}[> Fe(III)OH^{\bullet+}] - k_{22}[> Fe(III)OH^{\bullet+}]\,[> Fe(III)O_2CCH_2Br] = 0 \qquad (29)$$

Rearranging eq. 29 yields

$$(k_{-20} + k_{22}\,[>FeO_2CCH_2Br])\,[Fe(III)OH^{\bullet+}] = k_{20}\,[>Fe(III)OH]\,[h_{vb}^+] \qquad (30)$$

Eq. 30 can be rearranged further to give an expression for $>Fe(III)OH^{\bullet+}$

$$[> Fe(III)OH^{\bullet+}] = \frac{k_{20}[> Fe(III)OH]\,[h^+_{vb}]}{k_{-20} + k_{22}[> Fe(III)OOCCH_2Br]} \qquad (31)$$

Using a steady-state analysis on the concentration of the valence-band holes, $[h_{vb}^+]$, gives

$$\frac{d[h^+_{vb}]}{dt} = I_{abs}\phi_{17} - k_{18}\,[h^+_{vb}]\,[e^-_{cb}] - k_{20}[> Fe(III)OH][h^+_{vb}] + k_{-20}[> Fe(III)OH^{\bullet+}] = 0 \qquad (32)$$

If we assume $[h_{vb}^+] = [e_{cb}^-]$, then we can write

$$I_{abs}\,\phi_{17} - k_{18}[h_{vb}^+]^2 - k_{20}[>Fe(III)OH][h_{vb}^+] + k_{-20}[>Fe(III)OH^{\bullet+}] = 0 \qquad (33)$$

For the limiting case of $I_0 \dashrightarrow \infty$ (high light intensity)

$$[h^+_{vb}] = \sqrt{\frac{I_{abs}\phi_{17}}{k_{18}}} \qquad (34)$$

and for I_0 ---> 0 (low light intensity)

$$[h^+_{vb}] = \frac{I_{abs}\phi_{17} + k_{-20}[> Fe(III)OH^{\bullet+}]}{k_{20}[> Fe(III)OH]} \qquad (35)$$

if k_{-20} [>Fe(III)OH$^{\bullet+}$] << I_{abs} ϕ_{17}, then

$$[h^+_{vb}] \cong \frac{I_{abs}\phi_{17}}{k_{20}[> Fe(III)OH]} \qquad (36)$$

$$\nu = \frac{d[> Fe(III)O_2C\dot{C}HBr]}{dt} = k_{22}[> Fe(III)OH^{\bullet+}][> Fe(III)O_2CCH_2Br] \qquad (37)$$

Substituting eqs. 31 & 36 to the above yields

$$\nu = \frac{k_{22}I_{abs}\phi_{17}[> Fe(III)O_2CCH_2Br]}{k_{-20} + k_{22}[> Fe(III)O_2CCH_2Br]} \qquad (38)$$

We define the quantum yield for Fe(III) photoreduction as the ratio of the rate of Fe(II) production to the rate of photon absorption as follows

$$\phi_0 \equiv \frac{\nu}{I_{abs}} \qquad (39)$$

Substitution of eq. 38 into eq. 39 yields

$$\phi_0 = \frac{k_{22}\, k^{-1}_{-20}\, \phi_{17}[> Fe(III)O_2CCH_2Br]}{1 + k_{22}\, k^{-1}_{-20}[> Fe(III)O_2CCH_2Br]} \qquad (40)$$

if we assume $\phi_{17} \approx 1$ and $K' = \frac{k_{22}}{k_{-20}}$, then we can reduce eq. 40 to the simple form as follows:

$$\phi_0 = \frac{K'[>Fe(III)O_2CCH_2Br]}{1 + K'[>Fe(III)O_2CCH_2Br]} \quad (41)$$

For a given set of conditions in which the total reactive surface area is held constant and the bulk solution concentration of $XCH_2CO_2^-$ is also constant and that K' $[>Fe(III)O_2CCH_2Br] << 1$, we see that eq. 38 reduces to a pseudo zero-order expression

$$\frac{d[Fe(II)]}{dt} = k' \quad (42)$$

where $k' = K' [>Fe(III)O_2CCH_2Br] I_{abs}$

During the initial stages of photoreduction (i.e., $t < 500$ min.), the rate of production of Fe^{2+} is linear and the slopes of the lines in Figs. 1a and 1b yield values of k'. When deuterated chloroacetic acid, $ClCD_2CO_2H$, is substituted as an electron donor we see that $k_H'/k_D' = 5.5$ in the case of ferrihydrite and maghemite and 2 in the case of hematite and lepidocrocite. The general mechanism of eqs. 16-25 should also be applicable to ferrihydrite, especially in light of recent reports of the semiconducting characteristics of ferrihydrite (bernalite) that has the perovskite crystal structure (50, 51).

The comparison of the rate expression obtained in this study to the expression obtained by Sulzberger and co-workers (46) and Stumm and co-workers (52) illustrates the differences between the two proposed mechanisms. The rate-determining step found in our study appears to be the abstraction of hydrogen atom from the surface-bound haloacetate radical in contrast to the detachment of surface Fe(II) from the crystal lattice as proposed by

Sulzberger and co-workers. Furthermore, valence-band hole transfer to a surface trap is a precursor step to the rate-determining step (rds) in our system. Finally, the chromophore in our system appears to be the bulk iron oxide polymorph and not the Fe(III)-haloacetate surface complex as proposed by Sulzberger and co-workers (46) and Stumm and co-workers (52). These differences indicate that the mechanism of iron oxide-carboxylate photochemistry is dependent on the chemical nature of the electron donor and the iron oxide and that one mechanism cannot be extended readily to other systems.

Experiments with varying concentrations of the iron oxide were carried out to determine whether the observed rate of iron photoreduction (eq. 42) is directly proportional to the concentration of the surficial Fe(III)OH. The observed results with lepidocrocite, hematite and ferrihydrite in the presence of chloroacetate as the electron donor indicate that the kinetics involved are first order with respect to the surficial Fe(III)OH, since the rate of iron photoreduction doubled with the doubling of the concentration of total iron (up to ~ 130 μM) for all three iron oxides (Figure 7a). Above a concentration of 130 μM of total iron, the rate leveled off (most likely due to increased light scattering of the iron oxide suspension). The rate of iron(III) photoreduction is plotted against the concentration of chloroacetate in Figure 7b. The dependence follows a Langmuir adsorption isotherm, so the concentration of $>Fe(III)O_2CCH_2Br$ (using the Langmuir equation) for ferrihydrite under the experimental conditions of 6 mM of bromoacetate is 1.8×10^{-5} M assuming a surface area of 250 m^2/g for ferrihydrite. Similar calculations can be carried out for the other haloacetates. The dependence of the rate of lepidocrocite photoreduction with chloroacetate on the absorbed light intensity is plotted in Figure 7c. The rate does not decrease in a square root like fashion (see eq. 34) from a linear trend at high light intensity, even though that would be expected due to the increasing contribution of the band gap recombination (eq. 18) for the fate of valence-band holes and conduction-band electrons. The observed linearity is most likely due to the relatively low light intensity used (the

relative light intensity of 1 in Figure 7c corresponds to an absolute intensity of 2.1×10^{16} photons s^{-1} cm^{-2}) in the experiments, such that the reaction in eq. 18 is not contributing significantly to the overall mechanism.

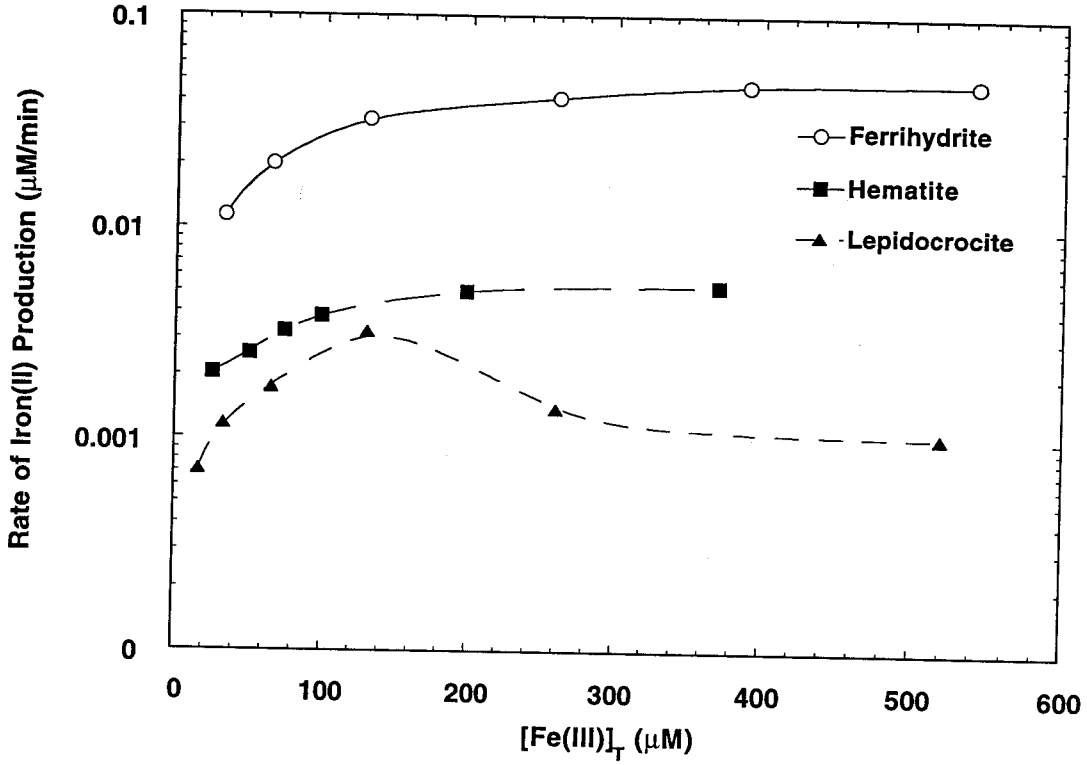

Figure 7a: The dependence of the rate of iron photoreduction on the concentration of iron oxide for hematite, lepidocrocite and ferrihydrite in the presence of chloroacetate. The concentration of $iron_{tot}$ was varied, the concentration of chloroacetate was 3.0 mM and the pH ~ 4.25.

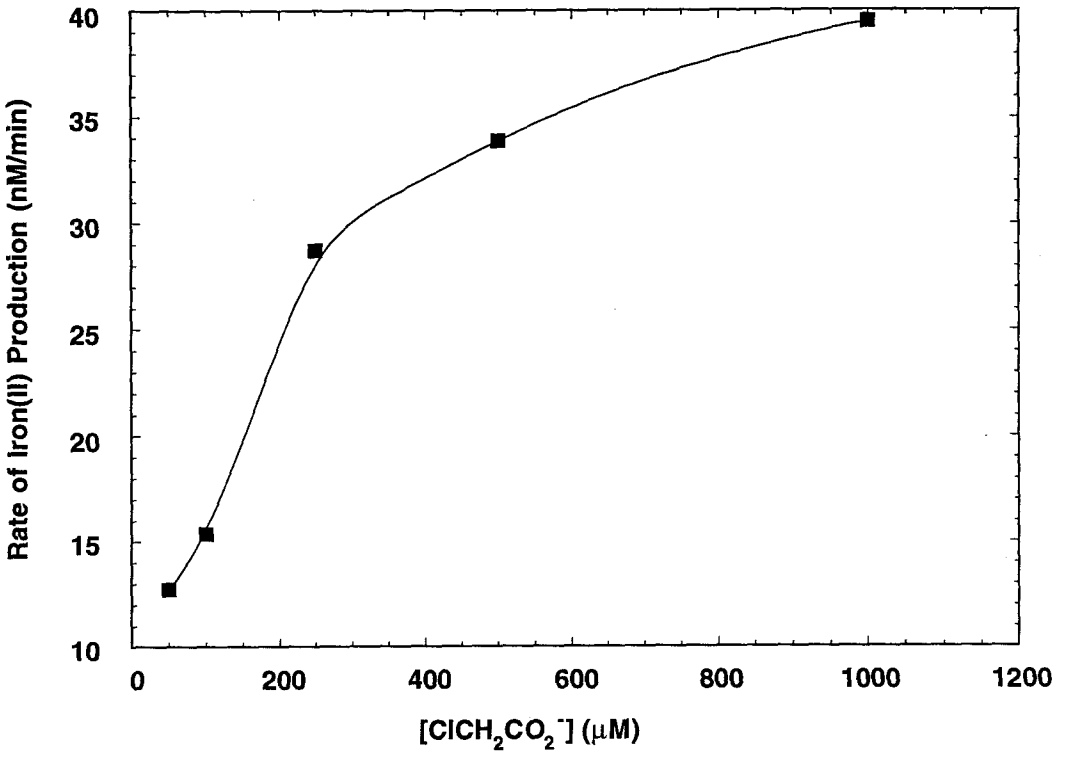

Figure 7b: The dependence of the rate of ferrihydrite photoreduction on the concentration of chloroacetate. The concentration of $iron_{tot}$ was 130 μM and the pH ~ 4.25.

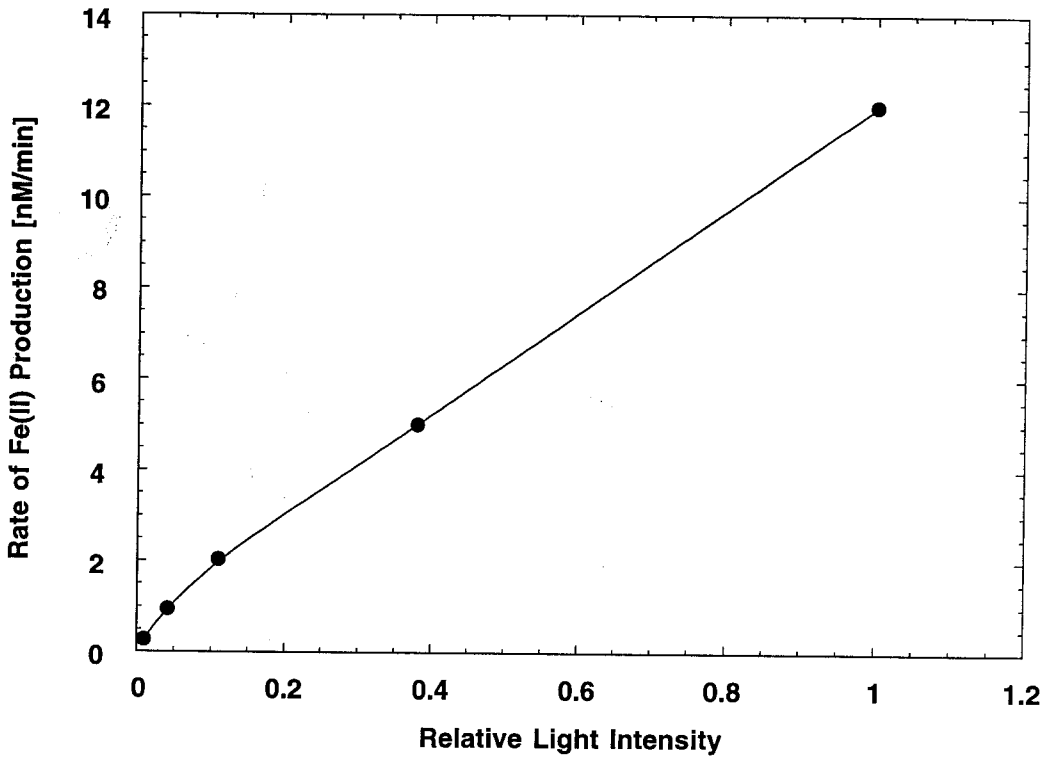

Figure 7c: The dependence of the rate of iron photoreduction on the absorbed light intensity in the case of lepidocrocite and chloroacetate as the electron donor. The concentration of $iron_{tot}$ was 810 μM and the concentration of chloroacetate was 3.0 mM and the pH ~ 4.25.

Trihaloacetates, unlike the mono- and dihaloacetates, are most likely photooxidized by a photo-Kolbe mechanism to yield $CF_3^{\bullet}$ radicals, which then react with the O_2 to produce $CF_3O_2^{\bullet}$ radicals as follows :

$$H^+ + CF_3CO_2^- + >Fe^{III}OH \rightleftharpoons >Fe^{III}O_2CCF_3 + H_2O \quad (43)$$

$$>Fe^{III}O_2CCF_3 \xrightarrow{h\nu} >Fe^{II} + CF_3^{\bullet} + CO_2 \quad (44)$$

$$>Fe^{II} \rightleftharpoons > + Fe^{2+} \quad (45)$$

$$CF_3^{\bullet} + O_2 \longrightarrow CF_3O_2^{\bullet} \quad (46)$$

$$2\ CF_3O_2^{\bullet} \longrightarrow CF_3OOCF_3 + O_2 \quad (47)$$

$$2\ CF_3O_2^{\bullet} \longrightarrow CF_3OF + FCFO + O_2 \quad (48)$$

$$FCFO + H_2O \longrightarrow 2HF + CO_2 \quad (49)$$

Evidence for this mechanism includes the observed decrease of the rate of iron(III) photoreduction due to the buildup of F^- similar to the trends observed with fluoroacetate.

The observed order of reactivity of the iron oxides (first line in Table 2) is an indication of the importance in the strength of Fe-O bond in the different iron phases; there appears to be a weak correlation between photochemical reactivity and the calculated {>FeOH} concentrations (14). Photochemical reactivity (Table 2) correlates relatively well with the surface area of each iron oxide (Table 3), if goethite is not included. The reason for the nonlinearity with goethite is not known. Ferrihydrite has a weakly-defined structure (50, 51, 53) and thus bonding between iron and oxygen in ferrihydrite is weaker than in

the other iron oxyhydroxide polymorphs. Our results are consistent with the results of Leland and Bard (45) for the photooxidation of sulfite and oxalate in the presence of a variety of iron oxide polymorphs. Furthermore, the difference in the pK_{a1} values (Table 3) (and therefore the ratio of >FeOH and $>FeOH_2^+$ surface groups) does not seem to be an important factor in the photoreactivity, since goethite has a much slower reactivity compared to lepidocrocite (Table 2), even though their pK_{a1} values are very similar.

Iron Oxide	pK_{a1}^s	pK_{a2}^s	pK_{zpc}	Surface Area[1] (m^2/g)	Aveg. Particle Size[2] (nm)	E_g^*(eV)	$\lambda(O^{2-} \rightarrow Fe^{3+})$ (nm)
Hematite	6.7	10.3	8.3	30	60	2.02	380
Goethite	6.2	9.0	7.5	40	1500	2.10	~ 340
Lepidocrocite	6.0	8.0	7.1	80	1300	2.06	~ 340
Ferrihydrite	7.3	8.9	8.0	250	370	-	~ 285
Maghemite	-	-	-	130	350	-	-

[1] from Refs. 29 and 31

[2] from Photon Correlation Spectroscopy

Table 3: Surface Ionization Constants, pK_{zpc}'s, Surface Areas, Average Particle Sizes, $O^{2-} \rightarrow Fe^{III}$ Band-Gap Energies (E_g^*) and Onset of $O^{2-} \rightarrow Fe^{III}$ Charge Transition for the Studied Iron Oxides.[31, 45, 54, 55]

The results with both acetate and chloroacetate present as electron donors indicate that in the presence of a competing ligand (i.e., acetate) with only a slightly larger stability constant (the stability constant of iron(III)-acetate complex is $10^{3.4}$ (39), which is approximately ten times larger than the corresponding constant for iron(III)-chloroacetate), the rate of photoreduction of ferrihydrite by chloroacetate was not affected. However, ligands with a much larger stability constant with iron, such as oxalate, may affect the rate of iron photoreduction and the rate of concomitant photooxidation of haloacetates.

Implications for Atmospheric Chemistry

The photoreduction experiments of a variety of iron phases in the presence of halogenated acetic acids give us insight into the fate of these acids in the lower atmosphere. The results clearly indicate that halogenated acetic acids can be oxidized photochemically by iron oxide polymorphs in contrast to their previously reported nonreactivity (27). Fluoroacetic acid reduces iron at the fastest rate and trihaloacetic acids seem to be less reactive than dihalo- and monohaloacetic acids. The mechanism we propose based on ^{18}O-labeling experiments, an LFER analysis and kinetic isotope effects with deuterated chloroacetic acid seems to be consistent with the observed trends of decreasing reactivity: fluoroacetic acid > chloroacetic acid > bromoacetic acid > iodoacetic acid and monochloroacetic acid > dichloroacetic acid. The experimental results show that the principal chromophore in these systems is the bulk iron-oxide phase and not the surface complex (supported by the kinetic isotope effect), which has been hypothesized to be the chromophore in some other systems involving iron oxides (46, 52). Similar results observed for synthetic and naturally-occurring Fe particles suggest coupling of the redox chemistry of iron and halogenated acetic acids in atmospheric water and in other natural water systems. Concentrations of ~ 1 μM of trifluoroacetic acid are predicted to be present in cloudwater over the Los Angeles basin. This concentration is comparable to the

concentration of iron found in atmospheric cloud and fogwater collected over the Los Angeles basin (56, 57).

Since the halogenated acetic acids act as such powerful reducing agents, they will affect the role of iron in the redox chemistry of sulfur and other trace metals such as copper and chromium. For example, if higher concentrations of Fe(II) are present due to the photoreduction of Fe(III) by halogenated acetic acids and other carboxylic acids studied earlier by Pehkonen et al. (14), the redox cycle involving S(IV) oxidation, which depends on Fe(III), could be retarded. Similarly, the oxidation of Cu(I) to Cu(II) (17) will not take place as readily with lower concentrations of Fe(III) relative to the total Fe concentrations. However, the reduction of Cr(VI) to Cr(III) should take place more readily with higher concentrations of Fe(II) relative to the total Fe concentrations (16).

Acknowledgments

The authors wish to thank Prof. J. Morgan and Scot T. Martin for helpful discussions and Mr. Sam Webb for his help in the photoreduction experiments. Support for this research has been provided by a grant from the National Science Foundation, Division of Atmospheric Sciences, Atmospheric Chemistry Section (ATM 9015775).

References

1. Taylor, S. R.; McLennan, S. M. "The Continental Crust: Its Composition and Evolution," Blackwell Scientific Publications: London, **1985**, 9.

2. Jacob, D. J.; Hoffmann, M. R. *J. Geophys. Res.*, **1983**, *88*, 6611.

3. Martin, L. R.; Hill, H. W. *Atmos. Environ.*, **1987**, *21*, 1487.

4. Hoffmann, M. R.; Jacob, D. J. In "Kinetics and Mechanism of the Catalytic Oxidation of Dissolved SO_2 in Atmospheric Droplets: Free Radical, Polar and Photoassisted Pathways," Calvert, J. G., Ed., Butterworth Publishers: Boston-London, **1984**, 101.

5. Weschler, C. J.; Mandich, M. L.; Graedel, T. E. *J. Geophys. Res.*, **1986**, *91*, 5189.

6. Graedel, T. E.; Mandich, M. L.; Weschler, C. J. *J. Geophys. Res.*, **1986**, *91*, 5205.

7. Conklin, M. H.; Hoffmann, M. R. *Environ. Sci. Technol.*, **1988**, *22*, 899.

8. Jacob, D. J.; Gottlieb, E. W.; Prather, M. J. *J. Geophys. Res.*, **1989**, *94*, 12975.

9. Martin, L. R.; Hill, M. W.; Tai, A. F.; Good, T. W. *J. Geophys. Res.*, **1991**, *96*, 3085.

10. Zuo, Y.; Hoigné, J. *Environ. Sci. Technol.*, **1992**, *26*, 1014.

11. Pehkonen, S. O.; Erel, Y.; Hoffmann, M. R. *Environ. Sci. Technol.*, **1992**, *26*, 1731.

12. Erel, Y.; Pehkonen, S. O.; Hoffmann, M. R. *J. Geophys. Res.*, **1993**, *98*, 18423.

13. Siefert, R. L.; Pehkonen, S. O.; Erel, Y.; Hoffmann, M. R. *Geochimica et Cosmochimica Acta,* **1994,** in press.

14. Pehkonen, S. O.; Siefert, R. L.; Erel, Y.; Webb, S.; Hoffmann, M. R. *Environ. Sci. Technol.*, **1993**, *27*, 2056.

15. Faust, B. C. *Environ. Sci. Technol.*, **1994**, *28*, 216A.

16. Kieber, R. J.; Helz, G. R. *Environ. Sci. Technol.*, **1992**, *26*, 307.

17. Sedlak, D. L.; Hoigne, J. *Atmos. Environ. A.*, **1993**, *27*, 2173.

18. Hampson, R. F.; Kurylo, M. J.; Sander, S. P. "Evaluated Rate Constants for Selected HCFC's and HFC's with OH and $O(^1D)$," World Meteorological Organization Global Research and Monitoring Project, Report No. 20, Scientific Assessment of Stratospheric Ozone: 1989, Volume II, Appendix: Alternative Fluorocarbon Environmental Acceptability Study Report.

19. Mead, R. J.; Moulden, D. L.; Twigg, L. E. *Aus. J. Biol. Sci.,* **1985**, *38*, 139.

20. Wu, T. J.; Mcarthur, N. H.; Harms, P. G. *Ann. New York Ac. Sci.,* **1991**, *633*, 626.

21. Clarke, D. D. *Neurochem. Res.,* **1991**, *16*, 1055.

22. Schwarzenbach, R. P. et al. *Env. Sci. Technol.,* **1994**, in press.

23. Helgeson, H. C. *App. Geochem.,* **1992**, *7*, 291.

24. Rook, J. J. *Environ. Sci. Technol.,* **1977**, *11*, 478.

25. Miller, J. W.; Uden, P. C. *Environ. Sci. Technol.,* **1983**, *17*, 150.

26. Christman, R. F.; Horwood, D. L.; Millington, D. S.; Johnson, J. D.; Stevens, A. A. *Environ. Sci. Technol.,* **1983**, *17*, 625.

27. Wine, P. H.; Chameides, W.L. Report to AFEAS, **1989**.

28. Hu, J. H.; Shorter, J. A.; Davidovits, P.; Worsnop, D. R.; Zahniser, M. S.; Kolb, C. E. *J. Phys. Chem.,* **1993**, *97*, 11037.

29. Schwertmann, U.; Cornell, R. M. "Iron Oxides in the Laboratory," VCH: Weinheim, Germany, **1991**, 91.

30. Dzombak, D. A. "Adsorption of Metals on Hydrous Ferric Oxides," Ph.D. thesis, Massachusetts Institute of Technology, **1986**, 123.

31. Scott, M. J. "Kinetics of Adsorption and Redox Processes on Iron and Manganese Oxides: Reactions of As(III) and Se(IV) at Goethite and Birnessite Surfaces," Ph. D. thesis, California Institute of Technology, **1991**, 67.

32. Sorenson, J.; Thorling, L. *Geochimica et Cosmochimica Acta,* **1991**, *55*, 1289.

33. Stookey, L. L. *Anal. Chem.,* **1970**, *42*, 119.

34. Carter, P. *Anal. Biochem.,* **1971**, *40*, 450.

35. Garcia-Vargas, M.; Belizon, M.; Hernandez-Artiga, M. P.; Martinez, C.; Perez-Bustamante, J. A. *A. Spectroscopy,* **1986**, *40*, 1058.

36. Zatar, N. A.; Abu-Zuhri, A. Z.; Al-Nuri, M. A.; Mahmoud, F. M.; Abu-Obaid, A. A. *Spec. Letters,* **1989**, *22*, 1203.

37. Schwarzenbach, R. P.; Gschwend, P. M.; Imboden, D. M. "Environmental Organic Chemistry," Wiley: New York, **1992**, 356.

38. Perrin, D. D.; Dempsey, B.; Serjeant, E. P. "pKa Prediction for Organic Acids and Bases," Chapman and Hall: London, **1981**, 34.

39. Smith, R. M.; Martell, A. E. "Critical Stability Constants," Plenum: New York, **1976**, 23.

40. Perrin, D. D. "Stability Constants of Metal-Ion Complexes- Part B Organic Ligands," Pergamon Press: New York, **1979**, 125.

41. Heller, H. G.; Langan, J. R. *J. C. S. Perkin I,* **1981**, *1*, 341.

42. Fisher, D. A.; Midgley, P. M. *Atmos. Environ.,* **1993**, *27A*, 271.

43. Collett, J. L.; Daube, B. C.; Hoffmann, M. R. *Tellus B,* **1991**, *43*, 390.

44. Faust, B. C.; Hoffmann, M. R. *Environ. Sci. Technol.,* **1986,** *20*, 943.

45. Leland, J. K.; Bard, A. J. *J. Phys. Chem.,* **1987**, *91*, 5076.

46. Siffert, C.; Sulzberger, B. *Langmuir,* **1991,** *7*, 1627.

47. Schwarzenbach, R. P.; Gschwend, P. M.; Imboden, D. M. "Environmental Organic Chemistry," Wiley: New York, **1992**, 289.

48. Hoffman, A. J.; Carraway, E. R.; Hoffmann, M. R. *Environ. Sci. Technol.,* **1994**, *28*, 776.

49. Carraway, E. R.; Hoffman, A. J.; Hoffmann, M. R. *Environ. Sci. Technol.,* **1994**, *28*, 786.

50. Birch, W. D.; Pring, A.; Reller, A.; Schmalle, H. W. *Naturwissen,* **1992**, *79*, 509.

51. Birch, W. D.; Pring, A.; Reller, A.; Schmalle, H. W. *Am. Min.eral.,* **1993**, *78*, 827.

52. Stumm, W.; Sulzberger, B. *Geochim. Cosmochim. A.,* **1992**, *56*, 3233.

53. Schwertmann, U.; Cornell, R. M. "Iron Oxides in the Laboratory," VCH: Weinheim, Germany, **1991**, 6.

54. Dzombak, D. A.; Morel, F. M. M. "Surface Complexation Modeling- Hydrous Ferric Oxide," John Wiley & Sons: New York, **1990**, 323.

55. James, R. O.; Parks, G. A. "Characterization of Aqueous Colloids by Their Electrical Double-Layer and Intrinsic Surface Chemical Properties in Surface and Colloid Science," Ed., Matijevic, E., Plenum: New York, **1982**, 185.

56. Jacob, D. J.; Waldman, J. M.; Munger, J. W.; Hofmann, M. R. *Env. Sci. Technol.,* **1985**, *19*, 730.

57. Erel, Y.; Pehkonen, S. O.; Hoffmann, M. R. H. *J. Geophys. Res.,* **1993**, *98*, 18423.

Chapter 8

Epilogue

In the preceding chapters, research was presented which demonstrates that the redox chemistry of iron in the atmosphere is coupled to the redox chemistry of a variety of other species. The combination of field research and laboratory kinetic studies have indicated that iron oxides can catalyze the oxidation of not only reduced sulfur species but of a variety of organic compounds such as oxalic acid, formic acid, acetic acid and halogenated acetic acids. Halogenated acetic acids are especially interesting in light of their previously reported nonreactivity (1) and the expected increase in the concentration of trifluoroacetic acid as a result of the OH radical gas phase destruction of HCFC's. A new spectrophotometric reagent, DPKBH, that can measure both Fe(III) and Fe(II) in the aqueous phase was developed and thoroughly investigated in terms of its stability constants with Fe(II) and Fe(III), the structure of the DPKBH-Fe complex (by FTIR) and analytical interferences that may cause changes in the oxidation state of iron when measured using DPKBH (2, 3). Laboratory studies of the kinetics and mechanism of iron oxide photoreduction and the concomitant photooxidation of halogenated acetic acids, formic, acetic and oxalic acid were carried out (4). It was discovered that the stability of the iron oxide and the strength of Fe-O bonding in the iron oxide is more important than the reactive surface area in determining the rate of iron oxide photoreduction. The mechanism in the case of the monohaloacetic acids was deduced by the use of deuterium primary kinetic isotope effect, an LFER relationship and by the use of ^{18}O-labeled water to follow the production of one of the photooxidation products. It was found that the rate-determining step of the iron oxide photoreduction is the abstraction of hydrogen from the surficial OH group by the surface-bound haloacetate radical.

The field studies of the redox chemistry of iron in clouds and fogs revealed a strong correlation between the reduced oxidation state of iron and the presence of organic electron donors such as acetic acid and formic acid (5). Additionally, the current study of iron in atmospheric water has heightened the importance of clean, contamination-free techniques in

measuring the speciation of metals in any aquatic environment (6). The field studies also indicated that a significant fraction of the iron present in the samples is in the particulate form (larger than 0.025 μm). This finding has implications for the importance of heterogeneous photochemistry in controlling the redox cycling of iron in atmospheric water. Additionally, related studies carried out by a fellow graduate student, Ron Siefert, on the aerosol chemistry of iron have indicated that iron in aerosols is a very effective catalyst for the aqueous phase photoproduction of hydrogen peroxide (7).

Some unanswered questions still remain in the redox chemistry of iron in the atmosphere. Since the knowledge of kinetic rate constants is so sparse, a model that would be able include the vast array of important chemical reactions in predicting the redox behavior of iron is lacking. Some kinetic rate constants have been recently measured both during the course of this study and by other researchers and now provide a small but sensible database to begin this type of modeling. A model consisting of thermodynamics only has been used to carry out speciation calculations of Fe(II) and Fe(III) in cloudwater in this study. It has been shown that Fe-oxalato complexes dominate the speciation of Fe(III) and that Fe(II) exist mainly in the hexaaqua complex as well as a small fraction as the ferrous sulfate species.

Another interesting, but challenging aspect of the redox chemistry of iron deals with the interactions of iron with other transition metals such as copper, manganese and chromium. These metals have important catalytic roles in many aquatic environments including atmospheric water. There has been speculation and some preliminary research indicating that these metals indeed interact in ways that may enhance or decrease the role of any one of them existing in isolation from the others (8, 9). However, these studies have so far mostly ignored the role of heterogeneous chemistry and therefore may be misleading. In light of these considerations, the knowledge of the ways these metals interact and affect

the speciation of each other and other aquatic chemicals is vitally important. Currently, the next generation of students is beginning to work on these scientific questions. The transformations of iron in the atmosphere have very significant implications to the capability of phytoplankton to utilize iron when atmospheric iron is deposited to the ocean. If iron undergoes transformations from oxides such as soil-derived hematite to less stable iron oxides such as ferrihydrite or even reduced Fe(II) (10, 11, 12), then the phytoplankton uptake of iron is greatly enhanced relative to hematite. This finding would contribute to the current scientific knowledge and aid in the debate of the exact role of iron in controlling the growth of oceanic phytoplankton.

References

1. Wine, P. H.; Chameides, W.L. Report to AFEAS, **1989**.

2. Pehkonen, S. O.; Erel, Y.; Hoffmann, M. R. *Env. Sci. Technol.*, **1992**, *26*, 1731.

3. Suarez-Iha, M.; Pehkonen, S. O.; Hoffmann, M. R. *Env. Sci. Technol.*, **1994**, in press.

4. Pehkonen, S. O.; Siefert, R. L.; Erel, Y.; Webb, S.; Hoffmann, M. R. *Env. Sci. Technol.*, **1993**, *27*, 2056.

5. Erel, Y.; Pehkonen, S. O.; Hoffmann, M. R. *J. Geophys. Res.*, **1993**, *98*, 18423.

6. Patterson, C. C.; Settle, D. M. *National Bureau of Standards, Special Publication,* **1976**, *422*, 321.

7. Siefert, R. L.; Pehkonen, S. O.; Erel, Y.; Hoffmann, M. R. *Geochim. Cosmochim. Acta*, **1994**, in press.

8. Kieber, R. J.; Helz, G. R. *Environ. Sci. Technol.*, **1992**, *26*, 307.

9. Sedlak, D. L.; Hoigne, J. *Atmos. Environ. A.*, **1993**, *27*, 2173.

10. Zhuang, G.; Yi, Z.; Duce, R. A.; Brown, P. R. *Global Biogeochemical Cycles,* **1992**, *6*, 161.

11. Zhuang, G.; Yi, Z.; Duce, R. A.; Brown, P. R. *Nature,* **1992**, *355*, 537.

12. Zhu, X. R.; Prospero, J. M.; Savoie, D. L.; Millero, F. J.; Zika, R. G.; Saltzman, E. S. *J. Geophys. Res. A.,* **1993**, *98*, 9039.